Insights of Taste Masking from Molecular Interactions and Microstructures of Microspheres

Insights of Taste Masking from Molecular Interactions and Microstructure of Microspheres

Zhen Guo

Submitted for the Degree of

Doctor of Philosophy

Institute of Cancer Therapeutics,

Faculty of Life Sciences,

University of Bradford

2017

Abstract

Zhen Guo

Insights of Taste Masking from Molecular Interactions and Microstructures of Microspheres

Keywords: Taste Masking, Cyclodextrin, Lipid Microspheres, Kinetics, Synchrotron Radiation, Surface Plasmon Resonance Imaging, High Performance Affinity Chromatography

The effects of taste masking are determined by interactions between drug and excipients as well as the microstructures of the particulate drug delivery systems (DDS). Cyclodextrin (CD) is a widely used taste masking agent, to which the relationship between kinetic parameters (K_a and K_d) of a drug and taste masking remains unexplored, which is investigated for the first time in this study. A data base of the kinetic parameters for drug-CD was established by Surface Plasmon Resonance Imaging (SPRi) and High Performance Affinity Chromatography (HPAC). Combined with the electronic tongue, K_a and K_d based models for the taste masking effect of HP-β-CD were successfully established and applied to the prediction of taste masking effects. Paracetamol was used as a model drug for taste masking formulation optimization. As well as drug release the microstructure of solid DDS has considerable influence on drug taste. The microstructure of lipid microspheres and the molecular distribution of drug and excipients in lipid microspheres were investigated by Synchrotron radiation-based micro-computed tomography (SR-μCT) and Synchrotron radiation-based Fourier-transform infrared spectromicroscopy (SR-

FTIR), respectively. The results demonstrated that the polymeric formulation components as well as shape and particle size of the drug were the key factors to taste masking of paracetamol by inhibiting bust release thereby reducing the interaction intensity of the bitterness. The FTIR absorption spectra confirmed the deposition and formation of chitosan and gelatin films on the drug microsphere surface by layer-by-layer coating. In conclusion, this research demonstrates the molecular kinetic basis of CD taste-masking as well as microstructural basis of particle systems for bitter taste masking.

Acknowledgements/Dedications

First of all, I wish to thank Prof. Jiwen Zhang and Prof. Laurence Patterson who identified a great topic to challenge of taste-masking as part of UK-China cooperation project. I have a great supervisor team from University of Bradford and Shanghai Institute of Materia Medica, Chinese Academy of Sciences. I would like to give my sincere gratitude to Prof. Laurence Patterson, Prof. Jiwen Zhang and Dr. Qun Shao for their extraordinary patience and consistent encouragement, the greatest help and inspiration of new ideas. It is their encouragements that draw my attention to this topic for children and an area with limited methodology. Without their strong support, this thesis could not be fulfilled. My heartfelt thanks also go to Prof. Peter York, for his help as well as enlightening communications with him from which I have benefited a great deal.

I wish to acknowledge my colleagues Mr. Xianzhen Yin, Mr. Tao Guo, Ms. Caifen Wang, Dr. Vikaramjeet Singh, Ms. Xiaohong Ren and post-graduates in SIMM, Ms. Li Wu, Ms. Xiaonan Xu, Mr. Longwei Fang, Ms. Jing Feng, Ms. Xue Li for their invaluable assistance, collaboration, contribution to this multidisciplinary research.

Finally, in particular, I would like to express my gratitude to my family for their support, assistance and love.

Table of Contents

List of Figures

List of Tables

Glossary

API - active pharmaceutical ingredient

BATA - brief-access taste aversion

BSA - bovine serum albumin

CA - cellulose acetate

CD - Cyclodextrin

ChemFET - chemical modified field effect technology

CPA - aftertaste sensor output

CTA - conditioned taste aversion

D - Euclidean distance

DDS-drug delivery systems

DMAP - dimethyl amino pyridine

DSC - differential scanning calorimetry

EMG - exponentially modified Gaussian

FET - field effect technology

GPCR - G-Protein Coupled Receptor

HM - plate height of the non-retained substance

$H_{M,C}$ - conventional non-retained substances

$H_{M,T}$ - theoretical non-retained substances

HPAC - High Performance Affinity Chromatography

HP-β-CD - hydroxypropyl-β-CD

H_R - plate height of the retained solute

HSA - human serum albumin

IP3 - inositol 1,4,5-trisphosphate

K - binding equilibrium constant

K_a - association constant

K_d - dissociation constant

LBL - Layer-by-layer

MCC - microcrystalline cellulose

NLC - nonlinear chromatography

PBI - propagation-based imaging

PBST - phosphate buffered saline

PCA - principal component analysis

PLCβ2 - phospholipase C β2

QCM - Quartz crystal microbalance

ROIs - Oval regions of interest

SEM - scanning electron microscopy

SIP - surface initiated polymerization

SPHT - sphericity

SPRi - Surface Plasmon Resonance Imaging

SR-μCT - Synchrotron radiation-based micro computed tomography

SR-FTIR - Synchrotron radiation-based Fourier-transform infrared spectromicroscopy

SSRF - Shanghai Synchrotron Radiation Facility

TAS2Rs - bitter taste receptors

TIE-Hom - Transport of Intensity equation

t_M - retention time of the peak for the non-retained substance

TRPM5 - transient receptor potential channel 5

XRD - x-ray diffraction

λ - correction factor

σ_M^2 - variance of the peak for the non-retained substance

Chapter 1 Introduction

The taste of an active pharmaceutical ingredient (API) plays a critical role in orally administered medicines. APIs may taste bitter and/or irritate the mouth and throat and thus are unpleasant not only to children but also to many adults. Undesirable taste is one of the top factors influencing the patient compliance. Therefore, research on the bitter taste mechanism, flavouring and taste masking technologies are of significant interest especially in paediatric medicines.

Bitter tasting compounds can be amino acids and peptides, esters and lactones, phenols and polyphenols, flavonoids and terpenes, methylxanthines, sulfimides (notably saccharin), and organic and inorganic salts [1]. The fact that such structurally diverse compounds can elicit a single bitter taste suggests that multiple mechanisms are responsible for the perception and transduction of bitterness [2, 3]. Some of these mechanisms may be common to the perception of both bitter and sweet taste. Small changes in chemical structure can convert bitter compounds to intensely sweet or vice versa. For example, L-tryptophan is bitter but D-tryptophan is sweet. Bitter and sweet taste in solution can enhance or suppress each other, with the interplay between bitter and sweet occurring at the neuronal level [4]. The ability to perceive some bitter tastes varies greatly across individuals.

On a cellular level, the various tastants are recognized by taste receptor cells, which are within the oral cavity assembled to taste buds consisting of about 100 cells. Four cell types can be distinguished based on their morphological and physiological characteristic: type-I cells serve a glial-like function, type-II cells express, strictly separated in distinct subsets, taste receptor proteins specific for sweet, umami, and bitter tastants, type-III cells are the only cell type within the taste bud capable of forming synapses with afferent nerve fibers and express sour taste receptors and, finally, type-IV cells are precursor cells able to differentiate throughout an individual's lifetime [5].

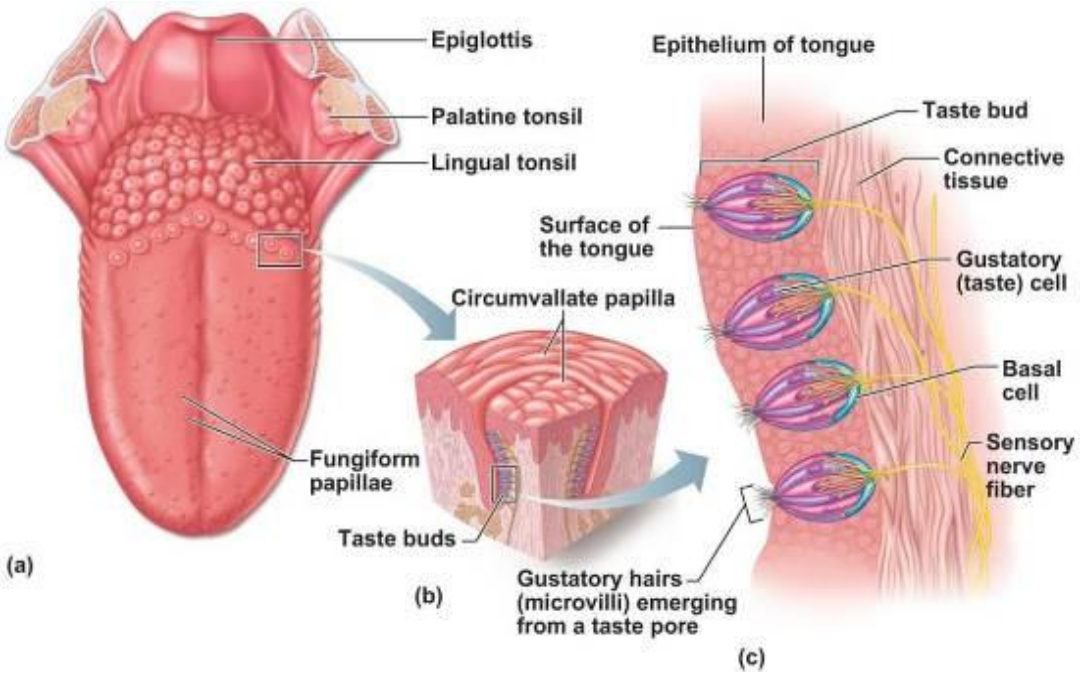

Figure 1 Taste buds located in the tongue (https://sites.google.com/a/bcssd.com/painter/anatomy-physiology/07-special-senses)

Taste transduction begins, when a stimulus comes into contact with a taste receptor cell. Whereas each taste bud may contain 75-150 epithelial cells, only a few are exposed at the taste pore at any one time [2]. Most taste buds are clustered in fungiform, foliate, and circumvallate papillae on the tongue surface, though some can also be found on the soft palate, epiglottis, and pharynx. As a result, taste sensation can differ with the proportion of taste buds that are stimulated, depending on whether the stimulus is swallowed or not [6].

Taste stimuli can influence the receptor cells in a variety of ways. One of the most important pathways involves a G-Protein Coupled Receptor (GPCR) that stimulates enzyme-activated inositol-1,4,5-trisphosphate (IP3), leading to a release of calcium from cell stores (Figure 2).

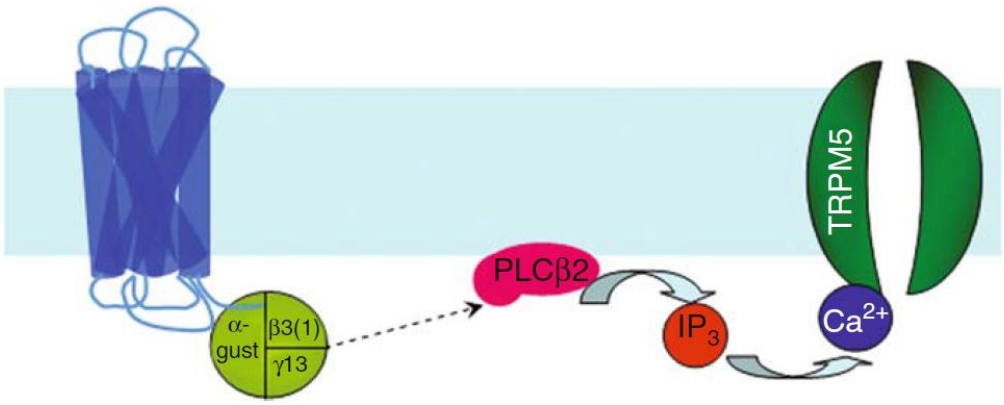

Figure 2 The bitter taste signal transduction cascade. Bitter taste receptors are G-protein-coupled receptors. Activation of TAS2Rs results in the activation of the heterotrimeric G-protein complex α-gustducin (α-gust), 3 or β1, and γ13. The βγ-subunits activate phospholipase C β2, (PLCβ2) resulting in the production of inositol 1,4,5-trisphosphate (IP3). The IP3-mediated increase of intracellular calcium activates transient receptor potential channel 5 (TRPM5) [7]

The number of different bitter taste receptors in humans (hTas2Rs) is estimated to be at least 25 [8]. The bitter taste receptor genes are organized in the genome in clusters and are genetically linked to loci that influence bitter perception in humans (and mice) [9]. The hTas2Rs are expressed in all taste buds of circumvallate and foliate papillae, and in palate taste buds. Whereas, hTas2Rs are rarely expressed in fungiform papillae, those fungiform taste buds that do express T2Rs have a full repertoire of different receptors, suggesting that each cell may recognize multiple bitter tastants. The limited number of bitter taste receptors detects an enormous number of structurally different bitter compounds [10]. It is therefore necessary that a given taste receptor responds to more than one substance, implying that the TAS2Rs are broadly tuned which increases the number of agonists stimulating a bitter taste receptor. Besides, hTas2Rs receptors are highly specialized. The human bitter taste receptor (hTas2R-4), which was the first human receptor to be deorphanized responded only to denatonium and 6-n-propylthiouracil, whereas a mouse receptor (MTas2R-5) responded only to cycloheximide [11]. Moreover, the bitter taste receptor genes of mammals not only lead to variability of bitter taste perception across species, but also show a considerable degree of intraspecies variability observed in mouse strains [12] and humans [13-19].

Different taste masking technologies have been used to address the problem of patient compliance, including coating, granulation, sweeteners,

microencapsulation, taste suppressants and potentiators, solid dispersions, ion exchange resins, viscosity enhancers, inclusion formation, pH modifiers and adsorbates [20].

(a) Coating

Coating is one of the most efficient and commonly used taste masking technologies. Here, it is classified based on the type of coating material, coating solvent system, and the number of coating layers. Hydrophobic polymers, lipids, sweeteners and hydrophilic polymers can be used as coating materials, either alone or in combination, as a single or multi-layer coat, to achieve the taste masking by aqueous or organic based coating process [21, 22]. However, film coating may reduce the onset of action of the drug by retarding disintegration of the tablet and therefore the release of drug is affected. And usually high coating weight is demanded to achieve a satisfactory taste, especially for particle coating.

(b) Granulation

Mixture of bitter medicaments and sweeteners, hydrophobic polymers, lipids or waxes can be processed by dry, wet and melt granulation techniques to prepare taste masked oral solid or liquid dosage forms [23-25]. Taste masked pharmaceutical granules, which can be formulated as dry syrup, suspension, conventional chewable or dispersible tablet are described. For example,

granulation of erythromycin with alginic acid was shown to enhance the mouth feel and acceptance of the bitter medicament [24].

Granulation is a relatively inexpensive rapid operation and an easily scalable taste masking technology. Low melting point waxes such as glycerol palmitostearate, glyceryl behenate and hydrogenated castor oil are commonly used ingredients in granulation to achieve taste masking effects. Both pH dependent and independent water insoluble polymers, especially, the swelling polymers such as microcrystalline cellulose (MCC) and polycarbophil have been employed. A swelling matrix phenomenon can reduce the overall diffusion of the bitter active compound. Thus, swellable polymers can give a better taste masking in granulation compared to non-swellable polymers. However, during granulation, particle coating may remain incomplete, as a result of which, suppression of bitterness may be incomplete.

(c) Sweeteners

Sweeteners are commonly used in combination with other taste masking technologies. They can be mixed with bitter taste medicaments to improve the taste of the core material which is prepared for further coating or may be added to the coating liquids [26, 27]. But sweeteners for taste masking are not often successful for strongly bitter or water soluble bitter drugs.

(d) Microencapsulation

Microencapsulation is a valuable technique applicable to protect the materials from volatilizing, oxidation as well as to mask their unpleasant taste [28]. Microencapsulation processes are commonly based on the principle of solvent extraction or evaporation. However, modifications of other techniques such as phase separation (coacervation) and spray drying are also utilized for microencapsulation [29]. Spray congealing is another method of microencapsulation [30-33]. Low encapsulation efficiency and environmental concerns due to use of organic solvents are the main limitations for microencapsulation technology.

(e) Taste suppressants and potentiators

In general, the hydrophobic nature of bitter substances contributes greatly to their interaction with the bitter taste receptor sites. Lipoproteins are universal bitter taste blockers. Studies using animal models show that lipoproteins composed of phosphatidic acid and β-lactoglobulin inhibit the taste nerve responses to bitter substances without affecting those due to the sugars, amino acids, salts or acids [34].

Potentiators increase the perception of the sweeteners taste and mask the unpleasant taste. Potentiators such as thaumatine, neohesperidine dihydrochalcone (NHDC) and glycyrrhizin can increase the perception of sodium or calcium saccharinates, saccharin, aspartyl-phenyl-alanine, acesulfame, cyclamates, and stevioside. Thaumatine was used with sugar alcohols to achieve the taste masking of bromhexine [35].

(f) Solid dispersions

Specific interactions between poorly soluble drugs and hydrophilic polymers can increase the drug solubility ; likewise specific interactions between the drug and the hydrophobic polymers can decrease the solubility of a drug [36].

Solid dispersion was prepared from a solution of quinolone and the natural hydrophobic polymer shellac by solvent evaporation [37]. Solid dispersion of cephalosporins and cellulosic or methacrylic polymer was formulated to mask the unpleasant taste of the medicament. Additional excipients such as meglumine and magnesium silicate were added to increase the efficiency of taste masking [38]. Hydrophobic polymers and long chain fatty acids have been used to achieve the taste masking by solid dispersion. However, this approach usually requires a higher concentration of excipients compared to the other taste masking techniques.

(g) Ion exchange resins

Ion exchange resins are high molecular weight polymers with cationic and anionic functional groups. Resins form insoluble resinates with oppositely charged drugs maintains the low concentration of free drug in a suspension through weak ionic bonding. Chlorpheniramine maleate:Indion-234 (cation exchange resins) inclusion of ratio 1:2 was used to mask the bitter taste of Chlorpheniramine maleate [39-42]. But this method is not effective for acid drugs and delayed onset of action.

(h) Viscosity enhancers

Suspending coated particles or microcapsules may not be efficient enough to achieve the taste masking of highly bitter medicaments in liquid oral suspensions. Usage of viscosity enhancers in these cases would retard the migration of dissolved medicament from the surface of the solid particle to the suspending medium. Additionally, they can also decrease the contact between the bitter medicament and the taste receptors, thus improving the overall taste masking efficiency [43]. At the same time, viscosity enhancers could prolong bitter aftertaste because of increased viscosity.

(i) Complex formation

Inclusion agents have been utilized to mask the objectionable taste of drugs. The mechanism of taste masking by inclusion formation has two theoretical possibilities. Either the cyclodextrins includes the bitter tasting molecule to inhibit its interaction with the taste buds, or it interacts with the gatekeeper proteins (GPCRs) of the taste buds [44-48]. However, whether the cyclodextrins can mask unpleasant taste of drug is dependent on the physicochemical properties of drug; additionally this approach requires cyclodextrin pre-inclusion formation of the drug before dosage form development.

(j) pH modifiers

Agents that can modify pH are capable of generating a specific pH microenvironment in aqueous media that can facilitate *in situ* precipitation of the

bitter drug substance in saliva thereby reducing the overall taste sensation for liquid dosage forms, e.g. suspensions. L-arginine maintains alkaline pH of the suspending vehicle to promote *in situ* precipitation of des-quinolone in saliva [49]. As for pH independent drugs, pH modifiers could not precipitate drugs for taste masking.

(k) Adsorbates

Adsorbates are commonly used with other taste masking technologies. The drug may be adsorbed or/and entrapped in the matrix of the porous component, which may result in a delayed release of the bitter active during the transit through the oral cavity thereby achieving taste masking. Kashid et al developed a taste masked pharmaceutical composition suitable for oral solid dosage form comprising adsorbate of unpleasant tasting active pharmaceutical agents and water insoluble polymer. In this technique, the active ingredient was blended with an adsorbent such as magnesium aluminium silicate to achieve the taste masking of bitter drug. The resultant blend was further granulated with water insoluble polymer to strengthen the taste masking without affecting the release of drug [50]. However, a higher concentration of adsorbates is needed, which is not beneficial to the final formulations.

Although, various technologies have been developed to address the unpleasant taste of drugs, taste masking of pharmaceuticals can still be a challenge due to their limitations described above. Properties such as solubility, viscosity, pH,

coating weight and amount of excipient of drugs and excipients are often investigated empirically to design a taste masking formulation. Few studies attempt to predict whether the interactions level between API and their taste masking ingredients will result in bitter taste masking. As for cyclodextrins, the ring structure can have 6 (α-cyclodextrins), 7 (β-cyclodextrins), 8 (γ-cyclodextrins) or more glucopyranose units connected by α-glycosidic bonds. A historical voyage from the discovery of these compounds in 1891 up to their present applications has been recently reported[51]. Due to the chair conformation of the glucopyranose units in the CD rings, they have the shape of a truncated cone or torus with the primary and secondary hydroxyl groups orientated to the narrow rim and to the wider edge of the cone, respectively. The CDs present then a hydrophilic external surface and a relatively lipophilic cavity in which guest molecules can be hosted. Ono and others measured the effects of parent CDs as well as the β-CD derivatives on the bitterness of a range of antihistaminic drugs. They showed that the level of bitterness suppression was correlated with the CD/drug binding coefficient K. A higher value of K means a lower free bitterant concentration and hence less bitter taste [46]. However, a few exceptions have been reported to the relationship between binding and bitterness reduction. Despite formation of a CD-caffeine inclusion [52], Gaudette and Pickering hardly observed any suppression of caffeine bitterness. Homoeriodictyol sodium salt reduced the bitterness of high and low caffeine by 15% and 43%, respectively. Meanwhile, the β-CD did not

significantly affect bitterness ratings, although interestingly, it trend towards an increase in bitterness [53]. In another example, the bitterness of propantheline and oxyphenonium bromide was more effectively suppressed by α- and γ-CDs than by β-CD [54] even the affinity of oxyphenonium bromide for CDs increased in the sequence β > γ > α [55]. Therefore, other factors might influence the taste masking of CDs for drugs.

Approaches to evaluate and characterize taste masked products have resulted in the development of a number of quantitative/semi-quantitative methodologies:

(a) Human taste panel test

The human taste panel test is the main method used to establish the overall palatability and acceptability of a drug product to a patient towards the end of the development of an orally administered medicine. However its uses are restricted by ethical and safety concerns especially when testing drugs with limited toxicity data [56, 57].

(b) Electronic taste sensors

There are several electronic sensors in the food and beverages industry using different measurement principles such as voltammetry, potentiometry, impedance, optical techniques and mass change [57]. The most commonly used in the pharmaceutical industry for taste evaluation is an electronic taste sensing system (electronic tongue). According to the definition of the IUPAC (International Union of Pure and Applied Chemistry) technical report, the

electronic tongue represents a multisensory system, which consists of a number of low selectivity sensors and uses advanced mathematical procedures for signal processing based on pattern recognition (PARC) and/or multivariate analysis [58]. Compared to the enormous amount of chemically different bitter substances, the number of electrodes (i.e., sensors) is limited. Thus, electronic tongues need to be cross-selective, which means not specific for a particular substance but universal to various bitter substances [59]. However, for a particular target, sensors with unique selectivity may be more useful [60]. With the development in selectivity and sensitivity, the electronic tongue becomes a promising instrument in bitterness evaluation and is an ideal alternative due to the lack of safety issues compared with human panel tests [61, 62]. Several are available including (i) SA401, SA402/TS-5000z (Insent, Atsugi-Chi, Japan) based on lipid membrane sensors; and (ii) a-Astree e-sensor (Alpha M.O.S., Toulouse, France) based on chemical modified field effect technology (ChemFET) with polymeric sensors. The Insent electronic sensor has detectors (exact composition is undisclosed by the manufacturer) assigned to a specific taste with partial cross-selectivity (e.g., AAE for umami, CT0 for saltiness, CA0 for sourness, AE1 for astringency and AC0, AN0 and C00 for bitterness). The α-Astree electronic taste sensing system (Figure 3) is a potentiometric based system with a seven-sensor probe and an Ag/AgCl reference electrode. The seven-sensor probe can differ in composition of different sensors [63]. These sensors operate in a cross-selective way and not assigned to a specific taste

quality or gustatory feeling. The underlying sensor technology is based on ChemFET, similar to the ion selective field effect technology (FET) technology, but sensors are coated with specific materials. These ChemFET sensors are composed of two highly conducting semiconductor regions surrounded with an insulator: a source and a drain. A sensitive layer (coated membrane) is deposited between the source and the drain. The type and composition of materials in the layer is not disclosed, but they are able to form specific interactions, like hydrogen bonds and van der Waals interactions with the chemical substances measured.

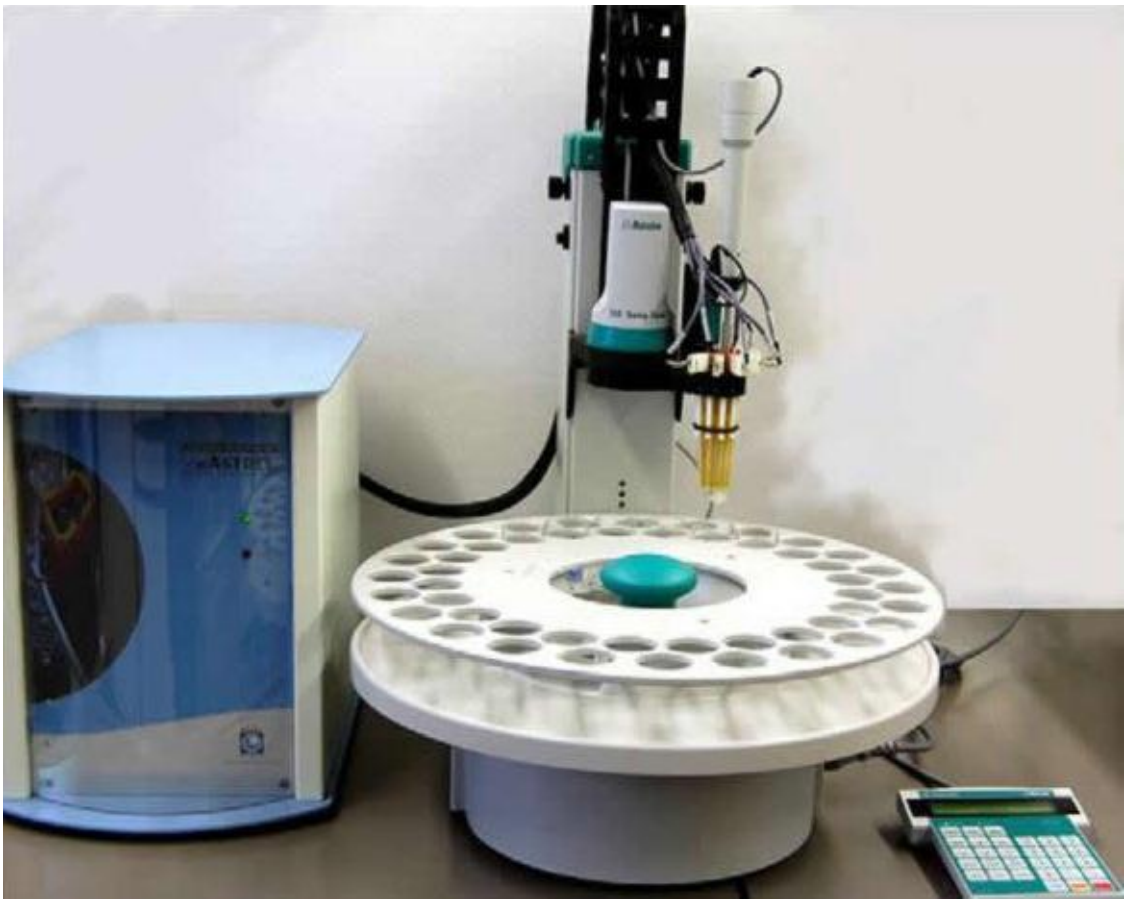

Figure 3 Commercially available electronic tongues: α-Astree2 (AlphaMOS, Toulouse, France).

Data from sensor response (relative value mV or aftertaste sensor output (CPA), Euclidean distances) can be correlated directly with human taste panel data. Good correlation between taste data obtained using electronic sensor (Insent and Astree) and human taste data can be achieved [64-66].

(c) Drug release and dissolution test

The measurement of the amount of drug released or dissolved in simulated oral cavity conditions can give an idea about the drug taste. The drug molecules must be dissolved in order to interact with the taste receptors in the (human) taste buds. Dissolution and release of APIs from a taste masking formulation is widely used to predict or quantify the *in vitro* effect of the taste masking technique. The most common choice as a medium is phosphate buffer (pH 6.8) as described in pharmacopeias [67-71]. Phosphate buffer with pH values in the range 5.6–8.0 has also been employed [72, 73]. Release into water (pH 1.5 and 6.8) has also been used as a dissolution media in the evaluation of polymeric microparticles, where 'tap water' was used to simulate intake conditions [74]. This was coupled with different taste masking evaluation methods such as human taste testing panels [75, 76]. The most common bias in these studies are: (i) the use of larger dissolution medium far exceeding normal human saliva volume; (ii) uncontrolled pH for example, use of water as dissolution medium; and (iii) filtration of sample and/or online analytical method are not used.

(d) Animal models for taste evaluation

Some animal models are designed to measure the taste quality of a compound defined as the sense by which the qualities and flavour of a substance are distinguished by the taste buds (e.g., bitter, salty, sweet, umami and sour): these models are classified as ‘taste discrimination experiments’. Alternatively, studies of ‘taste-guided’ behaviour can assess the palatability of tastants defined by the overall appreciation of a substance by organoleptic properties such as vision, smell, taste, aftertaste and mouth feel (e.g., good or bad taste and aversiveness). Animal models such as the conditioned taste aversion (CTA), the operant taste discrimination, the high-throughput taste assessment model using 96-well plates, two bottle taste preference test and the brief-access taste aversion (BATA) model have shown promising results for identifying bitter-tasting compounds [77].

In the CTA models, the rats are presented with a reference taste (conditioned stimuli), which becomes associated with an aversive stimulus such as peritoneal injections of lithium chloride (LiCl). As a consequence, when the rat is exposed to novel compounds with a similar taste they will avoid it as a function of their similarity to the conditioned stimuli [78]. The operant taste discrimination model is an animal model where rats are trained to perform a specific behavioural task such as pressing a lever after having tasted a certain compound and an alternative task after sampling another tastant that can be distinguished from the first one [79]. When a novel tastant is presented to the animal, it will perform the task learnt depending on the degree of similarity of the

new compound to the two compounds learnt. In the high-throughput taste-assessment model, rats are trained to sample different tastants in a standard 96-well plate, and then perform an operant discrimination task: pressing levers to deliver food pellets [77]. In this method, taste quality is assessed by the taste-discrimination component, whereas palatability is evaluated by the licks recorded from the 96-well plate. In the two-bottle taste preference experiment, animals have free access in their cage to two different bottles, one containing a taste solution and the other containing water or a different taste solution. This test is usually 48 h in duration to assess a single concentration. After 24 h, the relative positions of the two bottles are counterbalanced because rodents can have pronounced side preferences. The volume missing from each bottle is measured and a preference ratio of tastant to water then calculated [80]. In the BATA model, rodents, most often mice or rats, are mildly water deprived for a period of 16–24 h to motivate them to drink. The rodents are then put into an apparatus called a lickometer, which records the number of licks that the rodents make to different concentrations of the compound under test samples presented in several sipper tubes. Animals only have a very short period of time (between 5 and 10 s) to sample a solution. Typically, a high number of licks indicate a pleasant taste whereas when licks are nearly completely suppressed it indicates an unpleasant taste.

However, these methods are not able to directly investigate the fine microstructures or molecular distribution of taste masking products within a

formulation before and after release of the API/taste masking ingredients. Therefore, a quantitative method to correlate the detailed structural information with the drug release behaviour will provide mechanism and novel knowledge for taste masking technologies.

With respect to the challenges of taste masking the focus of the present investigation was on the molecular basis and microstructure basis of bitter taste suppression:

(1) To investigate the molecular basis of bitter taste suppression Surface Plasmon Resonance Imaging (SPRi) and High Performance Affinity Chromatography (HPAC) where used to construct a database of K_a and K_d values determined from the inclusion of bitter drugs with hydroxypropyl-β-CD (HP-β-CD) and correlating this with bitter taste masking data from electronic tongue measurements. Principal component analysis (PCA) from electronic-tongue data was used to quantitate the relationship between bitter taste masking by HP-β-CD. Specifically, the Euclidean distance (D) between each drug and its corresponding HP-β-CD inclusion complex as measured by the electronic tongue taste sensor apparatus. In this way a model based on molecular kinetic parameters and D (using SPSS, a software package used for statistical analysis acquired from IBM) was established to investigate the relationship between host-guest kinetics of CD-drug interactions and taste masking. Furthermore, a kinetic model of CD-drug inclusion was applied for producing a formulation with optimal taste masking properties.

(2) To investigate the formulation microstructure basis of bitter taste supression Synchrotron Radiation-based Micro Computed Tomography (SR-μCT) was utilized to investigate the relationship of the fine microstructure of formulated microspheres and mechanism of taste masking. The formulation approach adopted was the technique of layer-by-layer coating onto lipid microspheres for taste masking and Synchrotron Radiation-based Fourier-transform Infrared (SR-FTIR) used to determine the distribution of the formulation components on the cross section of microspheres and film coating. Thus the SR-μCT and SR-FTIR provided a deep understanding of the nature of the fine microstructure of taste masking formulations and their structural assembly in microspheres. This approach facilitated rational design and manufacturing of taste masking products.

Chapter 2 Relationship between Host-Guest Kinetic of Drug-CD Interactions and Taste Masking

Inclusion agents have been utilized to mask the objectionable taste of drugs. Cyclodextrin (CD), a cyclic oligosaccharide derived enzymatically from starch hydrolysylates, is an inclusion agent for food and drugs which has been approved by the FDA [81, 82]. The best-characterized forms are α-CD and β-CD consisting of six and seven D-glucose units, respectively. α-CD and β-CD are widely accepted ingredients for taste masking with relatively good solubility in water [83-85]. The CD molecule possesses a tapered cone structure with an inner diameter of 5-10 Å which can accept a wide range of molecules into a hydrophobic cavity to form a thermodynamically stable inclusion [86]. Amphiphilic molecules can be partially entrapped by CDs with the hydrophobic moiety within the cone cavity and the hydrophilic portion excluded and hence within the solvent phase. The bitter taste could be suppressed if the molecular component of the bitter tasting drug is partially or totally concealed within the CD cavity. The binding affinity of CD to a given compound is usually represented by a binding equilibrium coefficient (K). The K values for drugs and small molecules have been reported to be relatively weak in the range of 10^{-3}-10^{-6} M^{-1} [87, 88]. In a study of aromatic compounds, Astray et al. showed K was lower for α-CD than for β-CD (i.e., the larger diameter cone could bind more

efficiently) and increased linearly with logP (i.e., more hydrophobic compounds were bound more readily) [89]. The effect of parent CDs and β-CD derivatives on a range of antihistamines showed bitter taste suppression was correlated with the drug/CD binding coefficient K. [46]. However, some exceptions have been reported to the expected relationship between binding and bitterness reduction. Despite the formation of a strong CD-caffeine inclusion [52], poor suppression of caffeine bitterness by CD inclusion was observed [53]. In another example, the bitterness of propantheline and oxyphenonium bromide was effectively suppressed by α-CD and γ-CD more than β-CD [54]. The affinity of oxyphenonium bromide for CDs increased in the sequence β > γ > α [55]. Therefore, other factors might also influence the taste masking capability of drugs by CDs, such as the host-guest kinetics of the association (K_a) and dissociation (K_d) processes, which is the basis for the inclusion formation [86, 90, 91].

$$\mathrm{D} + \mathrm{CD} \underset{k_\mathrm{d}}{\overset{k_\mathrm{a}}{\rightleftharpoons}} \mathrm{D-CD} \tag{1}$$

$$K = \frac{K_a}{K_d} \tag{2}$$

where, K_a was the association rate constant and K_d was the disassociation rate constant.

Additionally, besides formation of CD inclusion, bitterness might be suppressed if molecular groups responsible for the bitterness could be competitively bound by groups outside the CD ring with bitter receptor on taste bud. Therefore, the

relationship between taste masking effects and host-guest interaction between CDs and drugs should be investigated more deeply.

However, the quantitative measurement of kinetics constants has proved challenging [92-94] due to short relaxation time (< 1 s) and high time of resolution which is difficult to achieve [95]. The use of fluorescence correlation spectroscopy, capillary electrophoresis, isothermal titration calorimetry, NMR spectroscopy and high performance affinity chromatography to determine kinetics constants is limited due to the poor reproducibility and/or labour intensive procedures [96-98]. Recently, we have reported high-throughput methodology based on the conjugation of small molecule microarray and SPRi for the measurement of drug-CD kinetic constants [99].

Surface plasmon resonance is a charge-density oscillation that may exist at the interface of two media with dielectric constants of opposite signs, for instance, a metal and a dielectric. The charge density wave is associated with an electromagnetic wave, the field vectors of which reach their maxima at the interface and decay evanescently into both media. This surface plasma wave (SPW) is a TM-polarized wave (magnetic vector is perpendicular to the direction of propagation of the SPW and parallel to the plane of interface) [100]. SPR transduction belongs to the class of refractometric sensing devices, which use evanescent waves to investigate surface phenomena. Changes in refractive index at the sensing surfaces due to analyte binding influence the resonant angle and this shift is used to generate a real-time signal. In contrast to

scanning angle SPR, SPRi systems are generally based on intensity modulation, measuring the reflectivity of monochromatic incident p-polarised light at a fixed angle. SPRi offers two main advances over conventional SPR: the ability to visualise the entire biochip surface in real time and the chance to monitor up to hundreds of molecular interactions continuously and simultaneously in a multi-array format of molecular probes formed as circular or square spots. It is also possible to control the quality of the spotted array by viewing the surface image to accurately select the measurement area. The ability to immobilise many receptors (up to hundreds) on the surface and to monitor the kinetic parameters of biospecific interactions simultaneously, in a real-time and label-free microarray format, is a tantalising opportunity. Spots (currently from 50_m^2 up to 1 cm^2) can be created both manually or by automatic spotters [101].

Using a SPRi database, K_a and K_d values, determined from the inclusion of 13 bitter drugs with HP-β-CD, were correlated with bitter taste masking data from the electronic tongue (model/manufacturer). An electronic-tongue was used to quantitate the bitter taste masking by HP-β-CD, specifically the Euclidean distance (D) between drugs and its corresponding HP-β-CD inclusion based on the PCA of the electronic tongue taste sensor data. In this way a model based on K_a, K_d and D by SPSS software was established. The reliability of the established model was verified by 10-fold cross-validation and then used to predict the extent of taste masking of 44 bitter drugs by HP-β-CD.

2.1 Modelling and Prediction of Taste Masking by Host-Guest Kinetic of Drug-CD Interactions Measured by SPRi

A variety of bio-interactions have been reported on SPRi for measuring protein-ligand interaction and protein–protein binding [102-105]. The performance and efficiency of SPRi are mainly dependent upon the surface chemistry. A small-molecule microarray screening platform based on a surface with high sensitivity and immobilization capacity which is able to detect weak interactions in the micromolar range [97]. The photo-cross-linked technique with surface initiated polymerization (SIP) chemistry proved to be highly efficient for screening of thousands of molecules on a single platform.

2.1.1 Materials

Caffeine, Chloramphenicol and Norethindrone with purity of 99.0%, Metoprolol tartrate salt and Ofloxacin with purity of 98.0% were purchased from Shanghai Suobio Bioscience & Technology Co. Ltd., China. Theophylline, Ethosuximide and Orphenadrine hydrochloride with purity of 98.0% were purchased from Tokyo Chemical Industry Co. Ltd., Shanghai. Theobromine and Penicillamine with purity of 99.0% was supplied by Sinopharm Chemical Reagent Co., Ltd., China. Propranolol hydrochloride with purity of 100% was provided by National Institute for Food and Drug Control, China. Cortisone with the purity of 99.0% was purchased from Merck Co., Inc., USA. Nortriptyline hydrochloride with

purity of 98% was obtained from Sigma-Aldrich Co. LLC. HP-β-CD (degree of substitution = 4.5, substituent groups per glucopyranose unit) was obtained from Shijiazhuang Pharmaceutical Group Co., Ltd., China.

2.1.2 Methods

2.1.2.1 Kinetic constants determination by SPRi

The SIP surface was prepared according to our previously published work [106]. In brief, a mixed self-assembled (SAM) solution was prepared by initiators ω-mercaptoundecyl bromoisobutyrate ($BrC(CH_3)_2COO(CH_2)_{11}SH$) and EG3-thiol in a 1:99 ratio. The sensor chips CM5, purchased from GE Healthcare UK Ltd.(Buckinghamshire, England), were immersed in this mixture (1 mM total concentration) for 16 hours at room temperature, and then thoroughly washed by ethanol and Milli-Q water and dried in a nitrogen stream. The polymerization solution was prepared by 64 mg Bipy, 10 mL 0.04 M $CuCl_2$, 2.6 g HEMA, 7.2 g OEGMA, 20 mL Milli-Q water and 20 mL methanol. After 30 min deoxygenation, 10 mL of Ascorbic acid (0.04 M) were added to the solution and the chips were immersed in this solution for 16 hours at room temperature under an atmosphere of nitrogen. After being thoroughly washed with methanol and Milli-Q water, the chip were incubated in a DMF solution containing 0.1 M N,N'-disuccinimidyl carbonate and 0.1 M dimethyl amino pyridine (DMAP) for 16 hours for acidification [107].

The photo-cross-linker moiety (3-trifluoromethylene-diazarine) was synthesized according to a previously reported protocol by Kanoh et al [108]. PEG and SIP assembled slides were activated by a freshly prepared aqueous mixture (1:1) of EDC/NHS solution for 20 minutes. Slides were then incubated with a 100 mM base added (500mM diisopropylethylamine) solution (DMF) of photo-cross-linker (20 mL), covered with cover slips and placed in the dark for 4 hours at room temperature. Slides were then extensively washed with DMF for 30 minutes and blocked with a 1 M solution of ethanolamine in DMF. After washing with DMF and ethanol (10 minutes) and drying with N_2, the slides were ready for printing. Stock solutions (10 mM) in 100% DMSO were spotted in multiplex using a Genetix QArray 2 spotter (produced 300 mm features) and left for complete evaporation of DMSO (under vacuum) at room temperature for 2 h. After printing, the slides were exposed to UV irradiation 2.4 J cm^{-2} (365 nm) in a UV chamber (Amersham life science). The slides were subsequently washed with DMSO, DMF, ACN, ethanol, phosphate buffered saline (PBST) and finally with distilled water for 30 minutes (ultrasonically), respectively, to remove non-covalently bound compounds. Dried slides were assembled with a flow cell and then mounted on the SPRi instrument for measurement.

All the experiments were carried out using the PlexArray® HT system (Plexera, LLC) which is based on surface plasmon resonance imaging [109]. All samples were injected at the rate of 2 $\mu L \cdot s^{-1}$ and 25 ^{o}C. Oval regions of interest (ROIs) were set as a 9 pixel × 7 pixel area in imaging area. ROIs of bovine serum

albumin (BSA) were used as controls for the measurement of specific signals. CDs solutions in PBST containing Tween 20 (0.05%), pH 7.4 were used as analytes with an association and dissociation flow rate of 2 $\mu L \cdot s^{-1}$ at different concentrations by serial dilution. A solution of glycine·HCl (pH 4.2, 0.05M) was used to regenerate the surface and remove bound proteins from the small molecules enabling the sensor chip to be reused for additional analyte injections.

HP-β-CD solutions were flowed at multiple concentrations (0.25, 0.5 and 1 mM) over a small molecule microarray containing 485 compounds on a single slide as described previously [99]. The average value of the kinetic constants was calculated by using Plexera SPRi data module software. Detailed kinetic parameters including K_a, K_d and K of 485 drugs against HP-β-CD were calculated (see Appendix), 57 of which were recorded as bitter drugs as per United States Pharmacopoeia 36 (2013). 13 drugs were selected as a test set in accordance with the range of K_a and K_d values which uniformly distributed and covered as many other bitter drugs as possible, for the current research purpose (Table 1).

Table 1 The K_a, K_d and K determined by SPRi for thirteen model bitter drugs as test set

Drugs	K_a (1/Ms)	K_d (1/s)	K (1/M)
Caffeine	72.1	3.43E-05	2.10E+06
Chloramphenicol	3310	1.23E-04	2.69E+07
Cortisone	574	1.74E-06	3.30E+08
Ethosuximide	2280	2.30E-05	9.91E+07
Metoprolol	1520	2.31E-05	6.58E+07
Norethindrone	502	1.27E-05	3.95E+07
Nortriptyline	2370	1.00E-04	2.37E+07
Ofloxacin	530	5.47E-05	9.69E+06
Orphenadrine	1520	6.38E-05	2.38E+07
Penicillamine	3900	8.29E-05	4.70E+07
Propranolol	512	9.83E-05	5.21E+06
Theobromine	3420	4.57E-05	7.48E+07
Theophylline	273	6.03E-05	4.53E+06

2.1.2.2 Electronic tongue test

13 bitter drugs were selected for testing bitterness using an automated electronic tongue (α-Astree electronic tongue gustatory system (Alpha M.O.S., Toulouse, France)). Seven specific sensors, i.e., ZZ, AB, GA, BB, CA, DA, and JE, were used. Each sensor is configured in a silicon transistor and has a specific organic membrane that interacts with ionic, neutral, and chemical compounds present in the sample solution in a specific manner. Any interaction at the membrane interface is detected by the sensor and converted into an electronic signal. The potentiometric difference between each of the seven sensors and the Ag/AgCl reference electrode at ambient temperature was measured for each compound with a data acquisition time for each sample of 120 s. The electronic tongue approach has been shown to provide data which correlate well with results from a human taste panel study [110-112].

Samples measurements were replicated at least eight times and the mean values and standard deviation were determined from the last three measurements. The first three replicate measurements of the test solution were for sensor training purposes. Following each analysis, the sensors were rinsed in deionized water for 10 s to prevent cross-contamination between samples or carry-over residues from previous samples.

Drugs were dissolved with deionized water to a concentration of 1 mM. The hydrophobic drugs were dissolved into ethanol (1 mL) followed by dilution with

deionized water in volumetric flasks (100 mL) to the same concentration. The taste and odour of ethanol at the concentration of 0.01 g/L was not discriminated from deionized water [113]. The drug-HP-β-CD inclusion solution was mixed and prepared at 1:1 molar ratio. The solutions were filtered through a Millipore filter paper (0.45-μm) to prevent particulate damage to the α-Astree sensors. Taste analysis of drug-HP-β-CD inclusion was carried out by electronic tongue.

The signals of the sensors after each assay were integrated into a data matrix that was computed by multidimensional statistic tools. Taste maps of tested samples based on PCA were generated using all sensors. PCA [114] is a well-established statistical method for dimensionality reduction and has been widely applied in data compression, image processing, exploratory data analysis, pattern recognition, and time series prediction [115]. PCA involves a matrix analysis technique called eigenvalue decomposition. The decomposition produces eigenvalues and eigenvectors representing the amount of variation accounted for by the principal component and the weights for the original variables, respectively. The main objective is to transform a set of correlated high dimensional variables to a set of uncorrelated lower dimensional variables (principal components). Therefore, PCA was utilized to convert the seven-dimensional data set obtained from seven different taste sensors to two-dimensional data for the ease of data analysis. Essentially, this approach summarizes the information contained in the database into individual principle

components, which are linear combinations of the original variables. For every sample analysis, the two principle components with the most informative results were used to create the PCA map. In the PCA maps, data points of the samples were compared using the calculated distance between them. The distances between the drug and drug-HP-β-CD inclusion represented the difference or the similarity between the taste of drug and that of drug-HP-β-CD inclusion, which indicated the magnitude of the taste masking effect of CD on specific drugs. If the distance of the sensor output value between drug and drug-HP-β-CD inclusion is small, the taste of the drug sample resembles that of the drug-HP-β-CD inclusion indicating poor taste masking effect.

2.1.2.3 Modeling

Based on K_a and K_d of each drug measured by SPRi, 12 derivative parameters (K_a, K_d, K_a^2, K_a^3, K_aK_d, $K_a^2K_d$, $K_aK_d^2$, $K_a^3K_d$, $K_aK_d^3$, K_d^2, K_d^3, K_a/K_d) were calculated as independent variables. Before undertaking the modeling process, these parameters were normalized (divided by maximum value) in consideration of the difference of dimension and units between K_a and K_d. Euclidean distance between drug and corresponding drug-HP-β-CD inclusion were used as dependent variables for modeling.

In addition, data from the 13 bitter tasting model compounds were used to construct a statistical model of kinetic parameters versus taste-masking using SPSS statistics software (version 19.0). Independent variable reduction and

model construction were carried out by stepwise linear optimization of the regression line fit as determined by R^2 and P values.

2.1.2.4 Cross-validation and prediction

In order to check if the model was sensitive to the presented data sets and correctly predict the outcome using other data sets, a 10-fold cross validation technique was used to evaluate how the results of the statistical analysis would generalize to an independent data set. The data set was divided into 10 folds and one of the 10 subsets was used as the test set, whilst the other 9 subsets were put together to form a training set. This technique has a lower variance compared to other methods and can be used to check if the model is over-fitting.

The established model was used to predict CD-drug kinetic values for another 44 bitter drugs in the established SPRi database. The K_a and K_d values of the 44 drugs provided data for the developed equation to calculate the predicted distances.

2.1.3 Results and discussion

2.1.3.1 Taste evaluation by the electronic tongue

The relative standard deviations of the three measurements taken for each sample were less than 2%, indicating high accuracy and repeatability of the sensor data. The taste sensor data generated from the electronic tongue was analyzed using PCA and based on the statistical analysis for the determination

of Euclidean distance between drug and its corresponding HP-β-CD inclusion. The PCA map (Figure 4) with two-dimensional data represented almost 100% of information on its two axes without any loss.

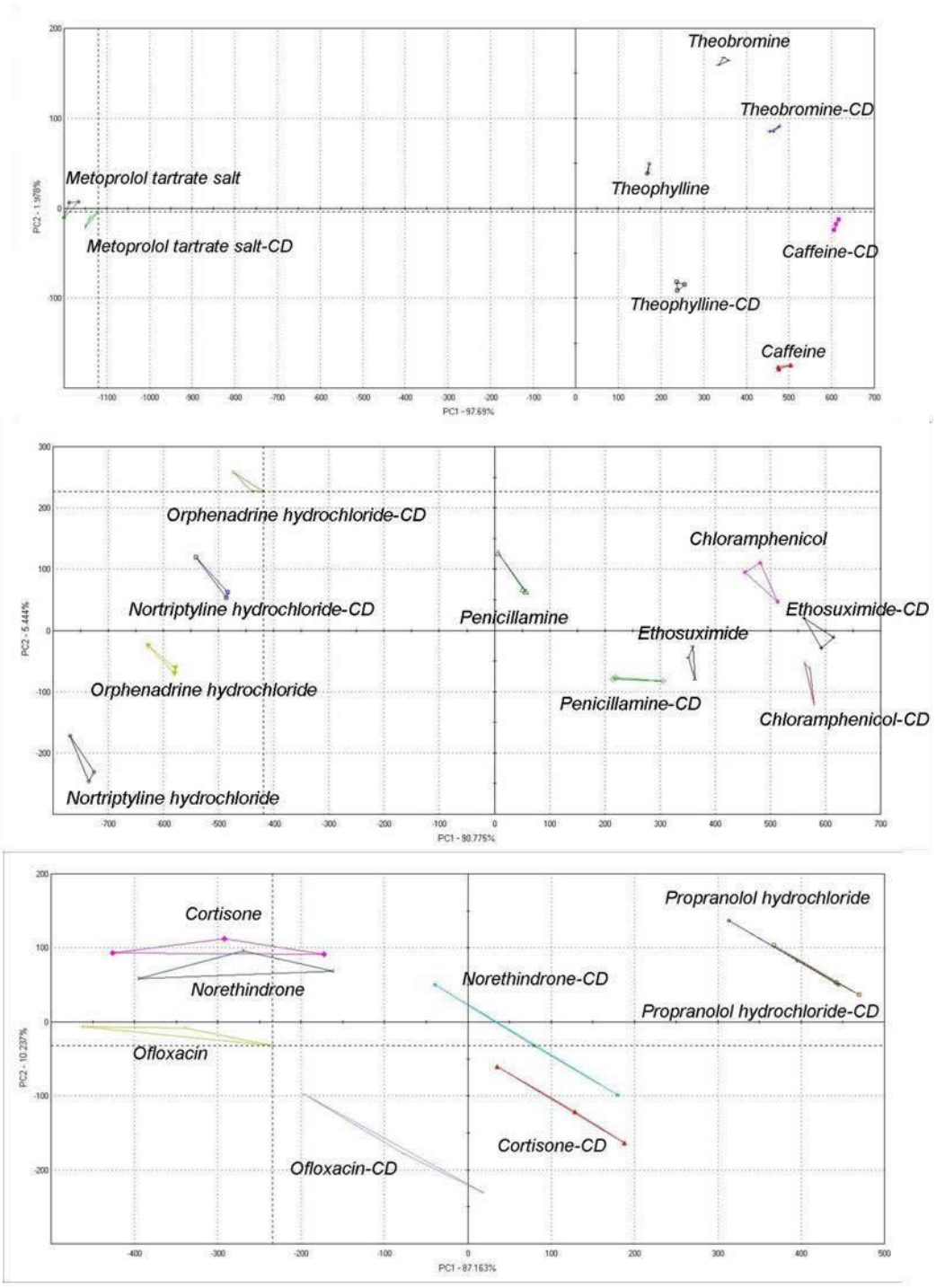

Figure 4 PCA map of bitter drugs and corresponding drugs-HP-β-CD inclusions

The bitter taste intensities of 13 drugs were different from each other. Therefore, the Euclidean distance is indicative of how close/far the taste of two samples is relative to each other. In other words, the degree of taste masking of a drug by CD is greater when a longer Euclidean distance is measured between the drug and its corresponding HP-β-CD inclusion. After adding HP-β-CD, the locations of all HP-β-CD-drugs moved to the right compared with drugs. The further HP-β-CD-drugs moved the better taste-masking effects should be obtained. The Euclidean distances for each sample pair are shown in Table 2. Among the 13 drugs, the distance of norethindrone was the shortest, demonstrating that its taste was relatively the most difficult to be masked by HP-β-CD. It is believed that large molecular size of norethindrone (7.2 Å, shortest linear dimension of the three dimensional molecule) makes it difficult to fit into the hydrophobic cavity (6-6.5 Å) of HP-β-CD. Although the molecular weight of nortriptyline (263.38) is similar to norethindrone (304.47), the hydrophobic branched alkylamino side chain, which might be responsible for the bitterness in nortriptyline structure [116], is of a size and lipophilicity that makes it able to fit into the hydrophobic region of HP-β-CD. Based on this data, the taste masking effect of nortriptyline-HP-β-CD inclusion was the best amongst the 13 tested model drugs.

Table 2 Taste masking effect (Distance) of thirteen model bitter drugs

Samples	Solubility (mg/mL)	Distance
Caffeine	58	143
Chloramphenicol	1.1	253
Cortisone	0.14	46
Ethosuximide	41	279
Metoprolol	11	112
Norethindrone	0.030	43
Nortriptyline	0.066	385
Ofloxacin	0.069	76
Orphenadrine	0.30	335
Penicillamine	31	217
Propranolol	0.47	58
Theobromine	9.7	185
Theophylline	13	128

2.1.3.2 Modeling

By stepwise regression for independent variable reduction, it was found that 6 parameters derived from the K_a and K_d measured by SPRi exhibited marked influence on the taste masking effects of CD-drug inclusions, K_a^3, K_d, K_aK_d, K_d^3, K_a^2 and K_a/K_d were identified from twelve pre-set kinetic parameters. It is well known that the K (K_a/K_d) is one of the important factors for taste masking effects [89]. However, besides K, other parameters also contribute to the taste masking effects.

Based on the six selected parameters, a multiple-linear regression model was established, as given in Eq. 3 with R^2=0.96 and P$\leqslant$0.05.

$$D = 6.902E^{-5}K_a^{\ 2} - 2.266E^{-8}K_a^{\ 3} + 5.272E^{-8}\frac{K_a}{K_d} + 2.589E^{6}K_d + 1394 * K_aK_d - 3.004E^{14}K_d^{\ 3} \quad (3)$$

It is generally recognized that K_a and K_d should have positive and negative correlation with taste masking effects, respectively, since K_a reflects the rate of drug binding/inclusion and K_d reflects the rate of release of drug which is then available for bitter taste receptor binding. However, both of K_a^3 and K_d^3 showed a negative correlation with Euclidean distance, while other derived parameters had a positive correlation with taste masking effects, thus indicating a relationship involving additional factors between taste masking effect and kinetic parameters of drug-HP-β-CD. A three dimensional model for distance as a function of K_a and K_d was developed and is illustrated in Figure 5.

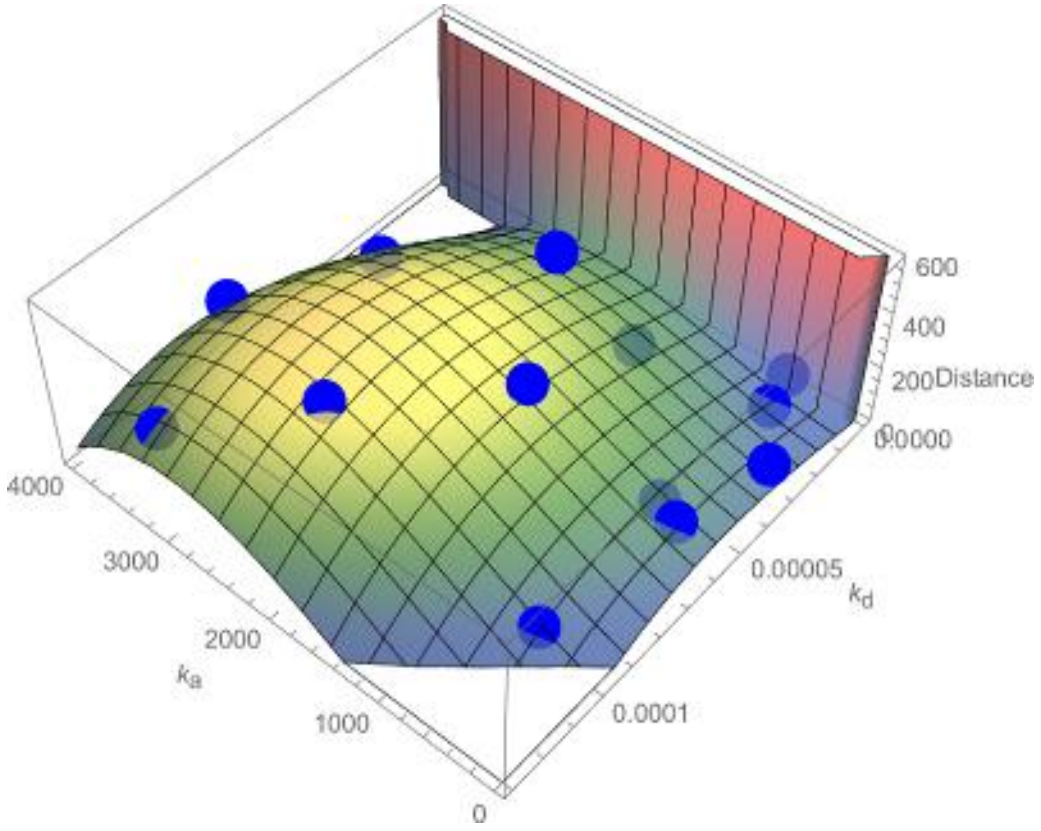

Figure 5 Three dimensional model constructed based on thirteen model bitter drugs (blue balls) for relationship between K_a, K_d measured by SPRi and taste masking effects of HP-β-CD on bitter drugs as measured by the electronic tongue

From this model, it can be observed that the Euclidean distance data measured from electronic tongue evaluation of bitter tasting drugs rapidly increased when K_d was closed to zero, which indicated a strong drug-CD inclusion. Therefore, concentration of free bitter drug in the solution was too low to be measured. Additionally, in the three dimensional graph white zone of $K_a < 1000$ and $K_d > 0.0001$, the Euclidean distance decreased to zero, which demonstrated that drugs located in this area did not form an effective drug-HP-β-CD inclusion to mask bitter taste. However, electronic tongue distance measurement rose to an

apogee then fell as K_a progressed from 0 to 4000. A similar trend in Euclidean distance rise and fall was observed as K_d progressed from 0 to 0.0001.

Nevertheless, the model produced good correlations between taste masking effects and kinetic parameters of HP-β-CD, even with the relatively small number of test samples. However, the range of K_a and K_d covered by 13 model drugs represented more than 80% of drugs in the data base enabling good coverage of molecules that could undergo kinetic analysis to determine whether drug-HP-β-CD interactions predict bitter taste masking.

2.1.3.3 Cross-validation and prediction

This procedure was continued thirteen times, and one of the samples was considered as the test set at each time point. The cross-validation result was evaluated by correlation coefficient, which was calculated by Eq.4,

$$\rho XY = \frac{Cov(X,Y)}{\sqrt{D(X)}\sqrt{D(Y)}} \quad (4)$$

where X was the predicted distance and Y was the determined distance. Cov(X,Y) was covariance of predicted distance and determined distance. D(X) and D(Y) were variance of predicted distance and determined distance, respectively.

The correlation of determined Euclidean distance (Y) as a function of predicted distance (X) of each drug was calculated by 10-fold cross-validation (Figure 6). It is well known that two sets of data strongly correlate with each other when the

correlation coefficient is about 0.8 to 1. A strong correlation was obtained as given in Eq. 5 with a correlation coefficient of 0.84, P<0.05 (bivariate correlated analyse by SPSS).

$$Y = 0.8737X + 26.24 \quad (5)$$

The slope of Eq.5 was close to 1 with an X/Y axis intercept close to zero, indicating that the established model possessed only small systematic errors and was sufficiently accurate to enable its application to predict the taste masking effect of HP-β-CD on the wider data base of bitter drugs.

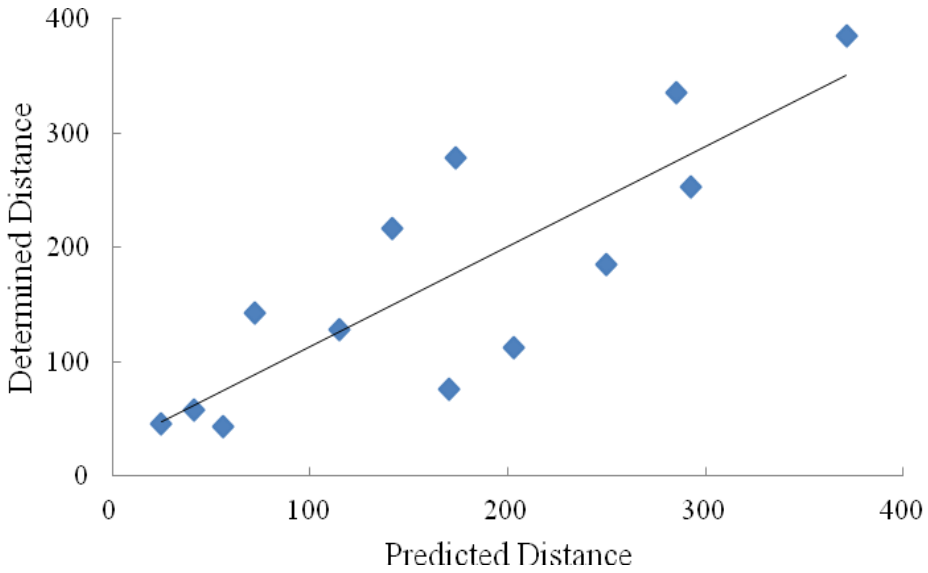

Figure 6 The correlation-ship of predicted distance versus determined distance for constructed model by 10-fold cross-validation

Using Eq.3 the predicted distance of the additional 44 bitter drugs was calculated. The predicted Euclidean distances of 29 bitter drugs were circa 20-300 (Table 3), illustrating that various degrees of taste-masking levels will be achieved using HP-β-CD.

Among the 29 drugs demonstrating predicted Euclidean distance above zero (Table 3), 8 drug-CD inclusions were confirmed to be bitter taste masked through inclusion with β-CD or HP-β-CD. It appears that bitterness of drugs with predicted distances larger than 100 were more likely to be masked by drug-CD inclusion. Although the reported drug-CD inclusions were of β-CD or HP-β-CD, the SPRi signal responses for each drug against β-CD and HP-β-CD were of the same order of magnitude and showed very similar trends of signal responses. This is possibly due to the same inner cavity and that the change in functional groups affects the interaction profile to a little extent [99]. Thus, the taste masking effects of these two chemical types of CDs also follow similar patterns (i.e. they resembled each other). The bitter taste of primaquine with predicted distance of 303, was effectively masked, which is in accordance with a literature report that the bitter taste of primaquine was completely inhibited by β-CD [117]. The alkyldiamino functionality of primaquine responsible for generating bitterness has a molecular size and lipophilicity predicted to undergo inclusion with β-CD. The bitterness of famtodine (predicted distance, 169) was partially masked by drug-CD inclusion and more effectively masked when forming a ternary complex with β-CD and HPMC [118]. The linear structure of famotidine incorporating sulfamoylpropanimidamide and diaminomethylidene functionality would likely lead to partial exposure of a bitter tasting moiety regardless of how famotidine was included within β-CD. Another similar example is seen for HP-β-CD inclusion in the 1:1 M ratio with 0.09% sodium

saccharin as optimum in masking the bitter taste of lidocaine [76, 119], with a predicted distance of 168. Of the additional 44 bitter drugs, the predicted distances of 15 drugs were zero or negative, indicating that not only is HP-β-CD ineffective for taste masking, but also there is possibly an inherent error in the model. For example, it was recommended by the FDA that the palatability of medicines containing chloroquine, an anti-malarial drug with strong bitterness, should be improved [120]. However, to date, there is no published literature or patent showing that the bitterness of chloroquine could be effectively masked by CD. It can be hypothesized that steric hinderance due to the halogen group of chlorobenzene interferes with the formation of chloroquine inclusion with CD or that the alkylamino side chain is not part of the CD-chlroquine inclusion complex allowing the tertiary amine to participate in bitter taste.

Table 3 Predicted distance of bitter drugs, for which the reported ones of taste masking by CD show tendency to have large predicted distance of taste masking by HP-β-CD

Drugs	K_a (1/Ms)	K_d (1/s)	Predicted Distance	If Reported by Literature or Patented	Taste Masking Effect
Dapsone	61	9.04E-05	20	No	/
Prilocaine	434	2.92E-06	28	No	/
Antazoline	151	1.92E-05	54	No	/
Sparfloxacin	15.8	7.98E-05	56	No	/
Prednisolone	200	2.06E-05	60	Yes [121]	Better than PEG 6000
Vancomycin	242	2.87E-05	81	Yes [122]	No details

Drugs	K_a (1/Ms)	K_d (1/s)	Predicted Distance	If Reported by Literature or Patented	Taste Masking Effect
Dicyclomine	39.3	7.05E-05	56	No	/
Bumetanide	636	5.73E-07	60	No	/
Hydroxychloroquine	303	3.10E-05	91	No	/
Antipyrine	88	5.07E-05	99	No	/
Carisoprodol	449	3.05E-05	102	No	/
Tramadol	238	6.78E-05	108	No	/
Pyridostigmine	497	3.37E-05	114	Yes [76]	Acceptable taste masking effect
Trifluoperazine	490	3.55E-05	117	No	/

Drugs	K_a (1/Ms)	K_d (1/s)	Predicted Distance	If Reported by Literature or Patented	Taste Masking Effect
Cefoperazone	357	6.94E-05	122	No	/
Cefuroxime	1070	1.70E-05	122	Yes [123]	Taste-masked by multi-components with CD
Sulfamethizole	395	7.18E-05	124	No	/
Propafenone	621	8.44E-05	133	No	/
Pentobarbital	1140	2.52E-05	159	No	/
Digoxin	1090	2.68E-05	159	No	/
Lidocaine	2260	1.31E-04	168	Yes [76, 119]	Partially masked
Famotidine	899	8.93E-05	169	Yes [118]	Partially masked

Drugs	K_a (1/Ms)	K_d (1/s)	Predicted Distance	If Reported by Literature or Patented	Taste Masking Effect
Chlorpropamide	2720	1.97E-05	185	No	/
Praziquantel	1310	2.78E-05	186	No	/
Tetracaine	2040	2.56E-05	233	No	/
Isoniazid	2390	2.71E-05	244	No	/
Cetirizine	1790	3.16E-05	245	Yes [124]	Better than maltodextrins
Papaverine	1820	3.13E-05	246	No	/
Primaquine	1790	4.76E-05	303	Yes [117]	Completely masked

2.2 Modelling and Prediction of Taste Masking by Host-Guest Kinetic of Drug-CD Interactions Measured by HPAC

With advantages of rapid speed, high precision and ease of automation, HPAC is another technique to measure the kinetics of interactions with weak to moderate affinities. Since 1980s, Hage's group has employed chromatographic techniques based on HPAC to study the kinetics of drug-human serum albumin (HSA) and antibody-antigen interactions [125-136].

In chromatography, peak width increases in proportion to the square root of the distance that the peak has migrated. Mathematically, this is equivalent to saying that the square of the standard deviation is equal to a constant time the distance travelled. The height equivalent to a theoretical plate, as discussed above, is defined as the proportionality constant relating the standard deviation and the distance travelled. Thus, the defining equation of the height equivalent to a theoretical plate is as follows,

$$HETP = \sigma^2/L \quad (6)$$

in which σ is the standard deviation and L the distance travelled. The use of the plate height is superior to the use of peak width in evaluating various chromatographic systems, because it is constant for the chromatographic run, and it is nearly constant from solute to solute. In a previous study [137], a modified peak profiling HPAC method based on the correction of the plate

height for the non-retained substance was established to determine the dissociation rate constant of paracetamol and sertraline-CD supramolecules. The apparent dissociation rate constants were estimated for paracetamol and sertraline respectively with multiple flow rates, which were in good agreement with the magnitude of the rate constants for other drugs determined by capillary electrophoresis reported in the literature [97]. The multianalyte approach was further developed to simultaneously measure the K_d values of three drugs through one injection based on the investigation of the dependence of drug-CD kinetics on the mobile phase composition (including the ion strength, the pH and the addition of the organic solvents) [138, 139]. It was demonstrated that for both of the single and multiple flow rate peak profiling methods, the K_d values of paracetamol, phenacetin and S-flurbiprofen determined by the multianalyte approach were statistically equivalent with that of the single compound analysis ($p>0.05$).

The peak profiling method is a useful chromatographic tool to study the kinetics of drug/macromolecule reversible reactions. The theoretical derivation for this approach was first reported in 1975 by Denizot and Delaage [140]. In the peak profiling method, the retention times and variances were measured on an affinity column for both a retained solute and a non-retained substance using linear zonal elution. Initially, the peak profiling method was carried out at a single flow rate and the K_d was estimated as follows.

$$K_d = \frac{2{t_M}^2(t_R - t_M)}{{\sigma_R}^2{t_M}^2 - {\sigma_M}^2{t_R}^2} \quad (7)$$

where, t_R and σ_R^2 are the retention time and variance of the peak for the retained solute on an affinity column, while t_M and σ_M^2 are the retention time and variance of the peak for the non-retained substance on the same affinity column. In Eq. 7, it was assumed that all sources of band broadening other than stationary phase mass transfer were either negligible or the same for the retained and non-retained species.

A modified form of the peak profiling method at multiple flow rates was further developed [127-130], as shown in Eq. 8.

$$H_R - H_M = \frac{2uk}{K_d(1+k)^2} \quad (8)$$

where, H_R is the plate height of the retained solute on an affinity column, and H_M is the plate height of the non-retained substance on the same column. The term k is the retention factor for the retained solute on the affinity column. The term u is the linear velocity of the mobile phase. The value of K_d can be determined by plotting (H_R-H_M) versus (uk)/(1+k)^2, which would result in a linear relationship with a slope inversely related to K_d.

As described in previous studies [137-139], plate heights for theoretical non-retained substances on the CD column could not be determined directly with conventional non-retained substances due to the extensive inclusion of a wide variety of ions and molecules by CDs, even the usual so-called non-retained void volume indicators. Thus, a correction of plate heights for conventional non-retained substances ($H_{M,C}$) has been made to estimate plate heights for theoretical non-retained substances ($H_{M,T}$) (Eq. 9), and then the K_d of drugs on β-CD columns could be determined according to Eq. 8.

$$H_{\mathrm{M,T}} = A_{\mathrm{C}} + \frac{B_{\mathrm{C}}}{\lambda \cdot u} + C_{\mathrm{sm,T}} \cdot u \tag{9}$$

where, λ is the correction factor, A_C and B_C are the A-term and B-term for the conventional non-retained substance, respectively. The λ can be calculated from the ratio of the B-term for the theoretical non-retained substance and that for the conventional non-retained substance, $C_{sm,T}$ is the stagnant mobile phase mass transfer related C-term for the theoretical non-retained substance.

For the comprehensive determination of K_a, K_d and K values by chromatography, K can be efficiently measured by the peak fitting method in zonal elution with high sample concentrations according to Hage's report [141]. As shown in Eq. 10, the nonlinear chromatography (NLC) model derived from impulse input solution can be used to calculate K values.

$$\mathrm{y} = \frac{\mathrm{a}_0}{\mathrm{a}_3}(1-\mathrm{e}^{-\frac{\mathrm{a}_3}{\mathrm{a}_2}})\left[\frac{\sqrt{\frac{\mathrm{a}_1}{\mathrm{x}}}\mathrm{I}_1\left(\frac{2\sqrt{\mathrm{a}_1\mathrm{x}}}{\mathrm{a}_2}\right)\mathrm{e}-\mathrm{x}^{-\frac{\mathrm{a}_1}{\mathrm{a}_2}}}{1-\mathrm{T}\left(\frac{\mathrm{a}_1}{\mathrm{a}_2},\frac{\mathrm{x}}{\mathrm{a}_2}\right)(1-\mathrm{e}^{-\frac{\mathrm{a}_3}{\mathrm{a}_2}})}\right] \tag{10}$$

where, y was the intensity of signal, x was the retention time, and T was a switching function, and I_1 was a modified Bessel function. The fitted NLC parameters (a_0, a_1, a_2 and a_3) were collected for each chromatography profile and used for the calculation of the K according to the Eq. 11:

$$K = \frac{a_3}{C_0} \tag{11}$$

where, C_0 was the concentration of the solute injected multiplied by the width of the injection pulse (as a fraction of column dead volume). The K_a values were then calculated with K and K_d according to Eq. 2.

2.2.1 Materials

Caffeine, Chloramphenicol and Norethindrone with purity of 99.0%, Metoprolol tartrate salt and Ofloxacin with purity of 98.0% were purchased from Shanghai Suobio Bioscience & Technology Co. Ltd., China. Theophylline, Ethosuximide and Orphenadrine hydrochloride with purity of 98.0% were purchased from Tokyo Chemical Industry Co. Ltd., Shanghai. Theobromine and Penicillamine with purity of 99.0% was supplied by Sinopharm Chemical Reagent Co., Ltd., China. Propranolol hydrochloride with purity of 100% was provided by National Institute for Food and Drug Control, China. Cortisone with the purity of 99.0% was purchased from Merck Co., Inc., USA. Nortriptyline hydrochloride with purity of 98% was obtained from Sigma-Aldrich Co. LLC.

The HP-β-CD bonded column (Astec Cyclobond^{TM} Chiral HPLC Column, 15 cm×4.6 mm, 5 μm) were purchased from Sigma (St. Louis, MO). Ammonium acetate and acetonitrile (HPLC grade) were purchased from Sigma (USA) and J&K (China). Water was purified on a Milli-Q system (USA). The chromatographic system used consisted of a binary pump(G1311C), an autosampler (G1329B) and a diode-array detector (G4212B) (Agilent, Palo Alto, USA). The columns were maintained at 25 ºC with a temperature controller (G1316A) (Agilent, Palo Alto, USA). Chromatographic data were acquired using the workstation of Chemstation Rev.B.04.03 (Agilent, Palo Alto, USA). The

chromatograms were then analyzed using Peakfit 4.12 software (Jandel Scientific Software, San Rafael, CA).

2.2.2 Methods

2.2.2.1 Determination of K_d by peak profiling method using HPAC

For the determination of K_d of fourteen drugs separately, the studies were performed on the Sigma HP-β-CD column (150×4.6 mm, 5 μm) at 25 ºC. Uracil was used as the conventional non-retained substance. In order to enable the elution of drugs in reasonable time period, 35% of acetonitrile was added into the mobile phase of NH_4Ac (10 mM, pH = 6.80). All samples were prepared with the mobile phase. The flow rate was 0.4, 0.6, 0.8 and 1.0 $mL \cdot min^{-1}$. The peak profiling experiments were performed by injecting 10 μL sample, in which the concentration of caffeine, chloramphenicol, cortisone, ethosuximide, metoprolol tartrate salt, norethindrone, nortriptyline hydrochloride, ofloxacin, orphenadrine hydrochloride, penicillamine, propranolol hydrochloride, theobromine, theophylline, and uracil was shown in Table 4. The concentrations of sample were adjusted according to the response difference to confirm the linear elution under the above mentioned methods. All experiments were performed in triplicate under each set of test conditions.

The retention time (i.e., first statistical moment) and variance (second statistical moment) of each chromatographic peak were obtained by using Peakfit 4.12 software with an exponentially modified Gaussian (EMG) fit and the linear progressive baseline plus residual options of this program. Then the data were analyzed according to the published method [142-145].

2.2.2.2 Determination of K by peak fitting method with HPAC

For the determination of K by the peak fitting method, sample of 10 µL was injected and the UV detector was applied to measure K with the flow rate of 1.0 $mL \bullet min^{-1}$, the elution condition of drugs was same as the method mentioned before (see section 2.2.2.1) for the determination of K_d. And the concentration of drugs was also listed in Table 4. Low drug concentration benefits K_d determination since linear elution should be carried out and high drug concentration benefits K determination because all ligands could be occupied. The a_3 (distortion parameter) of each chromatographic peak could be obtained by using Peakfit 4.12 software with nonlinear chromatography (NLC) fit and the linear progressive baseline plus residual options of this program. Then the data were analyzed according to the published method [137].

Table 4 The injected concentration of drugs for determination of K and K_d

Drugs	Drug concentration used for K_d determination (μg/mL)	Drug concentration used for K determination(mg/mL)
Theophylline	0.96	0.96
Theobromine	0.91	0.18
Paracetamol	1.00	1.00
Caffeine	1.09	1.09
Metoprolol	10.86	5.06
Norethindrone	5.70	5.03
Nortriptyline	5.24	5.05
Ethosuximide	47.60	5.38
Orphenadrine	48.80	5.30
Cortisone	1.00	2.01
Chloramphenicol	0.97	1.53
Ofloxacin	9.05	0.36
Penicillamine	105.60	5.63
Propranolol	1.04	5.61
Uracil	1.034	-

2.2.2.3 Modeling of drug/CD kinetic parameters with bitter taste as determined using the electronic tongue

The electronic tongue test was as described in section 2.1.2.2.

Based on the experimentally determined K_a and K_d for each drug shown in Table 4, 12 derivative parameters (K_a, K_d, K_a^2, K_a^3, K_aK_d, $K_a^2K_d$, $K_aK_d^2$, $K_a^3K_d$, $K_aK_d^3$, K_d^2, K_d^3, K_a/K_d) were calculated as independent variables. Before undertaking the modeling process, these parameters were normalized (divided by maximum value) in consideration of the difference of dimension and units between K_a and K_d. Euclidean distance between drug and corresponding drug-HP-β-CD inclusion were used as dependent variables for modeling.

In addition, data from the 10 bitter tasting model compounds were used to construct a statistical model of kinetic parameters versus taste-masking using SPSS statistics software (version 19.0). Independent variable reduction and model construction were carried out by stepwise linear optimization of the regression line fit as determined by R^2 and P values.

2.2.2.4 Cross-validation

In order to find out if the model was sensitive to the presented data sets or they could properly predict using other data sets, 10-fold cross validation technique was applied.

For the model in this research, this procedure continued ten times, and at each time one of the samples was considered as the test set. The cross-validation result was evaluated by correlation coefficient, which was calculated by Eq.4 (see section 2.1.3.3).

2.2.3 Results and discussion

2.2.3.1 The determination of K_d and K by peak profiling and peak fitting method

As described previously [137-139], the plate height values of test drugs (H_R) and uracil ($H_{M,C}$) on the HP-β-CD column at flow rates of 0.4, 0.6, 0.8 and 1.0 mL•min^{-1} were calculated (as shown in Figure 7). The linear trend between H_R and u in Figure 7 indicated the main contribution of stationary mass transfer on the peak broadening of orphenadrine hydrochloride, nortriptyline hydrochloride, norethindrone and ethosuximide ($R \geqslant 0.9885$). However, the contribution of the B-term on the peak broadening of uracil was found to be more important than that of drugs. This finding was reinforced by the observations that the B-term of uracil was larger than that of drugs. As stated previously, this observation is thought to be due to the extensive and weak non-specific interactions of CD with the small molecules and the significant diffusion of uracil.

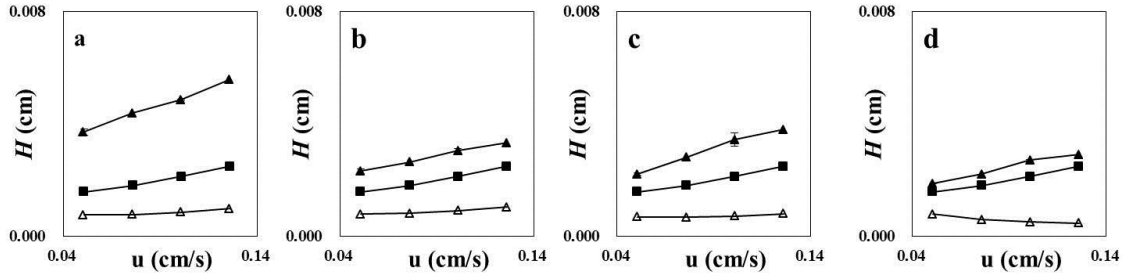

Figure 7 Typical peak profiling results for four test drugs and uracil on HP-β-CD column by single compound analysis (a: orphenadrine, b: nortriptyline hydrochloride, c: norethindrone, d: ethosuximide) (■: plate heights for uracil ($H_{M,C}$), ▲: plate heights for drugs (H_R), △: plate heights for theoretical non-retained substance ($H_{M,T}$))

As expected, the stationary phase mass transfer (C-term) for uracil was also the dominant parameter in the Van Deemter equations, confirming the binding

kinetic broadening. Similar with findings described previously, it was also suggested that $H_{M,T}$ with no C-term contribution, could not be equivalent with the C-term dominated $H_{M,C}$. Thus, it was necessary to perform a correction to obtain the real plate height for the theoretically non-retained substance.

Unlike the interaction of drugs with HSA, the cavity of CDs can include a wide variety of ions and molecules, even the so-called non-retained void volume indicators, such as sodium nitrate, citric acid and uracil. In addition, the interaction of solutes with CDs is usually weak ($K_a<10^5$ M^{-1}). The contributions of the C-term to the total plate height for the drug-CD combination were consistently found to be smaller than that for drug-HSA system. As a result, the differences of the longitudinal diffusion and stagnant mobile phase mass transfer between the retained drug and the conventional non-retained substances should not be neglected. Thus, plate heights for the theoretically non-retained substance were corrected and then the K_d values could be calculated.

The data for test drugs on the HP-β-CD column were analyzed using the multiple flow rates peak profiling method based on the above mentioned theory, with the correction of the plate height for the theoretical non-retained substance. When plots of (H_R-H_M) versus $(uk)/(1+k)^2$ were processed, linear fits were observed for the fourteen drugs, the slopes of these plots were then used to estimate the K_d under the above mentioned conditions. The data for orphenadrine, nortriptyline, norethindrone and ethosuximide on HP-β-CD column were also analyzed with the multiple flow rates peak profiling method. When plots of (H_R-H_M) versus $(uk)/(1+k)^2$ were processed, linear fits were observed for the four drugs, with corresponding correlation coefficients of 0.989,

0.979, 0.949, 0.966 and intercepts of 0.0010, 0.0011, 0.0006, 0.0002 for orphenadrine, nortriptyline, norethindrone and ethosuximide (as shown in Figure 8). The intercepts were all close to zero, indicating the main contribution of C-term on the peak broadening of the four drugs. The responses were consistent with the linear behaviour that was predicted for (H_R-H_M) versus $(uk)/(1+k)^2$ in Eq. 4. The slopes of these plots were then used to estimate the K_d. The K_d were estimated for orphenadrine 12.56±0.09 s^{-1}, nortriptyline 14.01±1.74 s^{-1}, norethindrone 23.61±0.14 s^{-1} and ethosuximide 9.71±0.27 s^{-1} respectively over the flow rate range of 0.4-1.0 $mL \cdot min^{-1}$. As for the K values of the thirteen drugs, which could be obtained according to the Eq. 11 by peak fitting method (see section 2.2), the K_d and K values determined were as listed in Table 5.

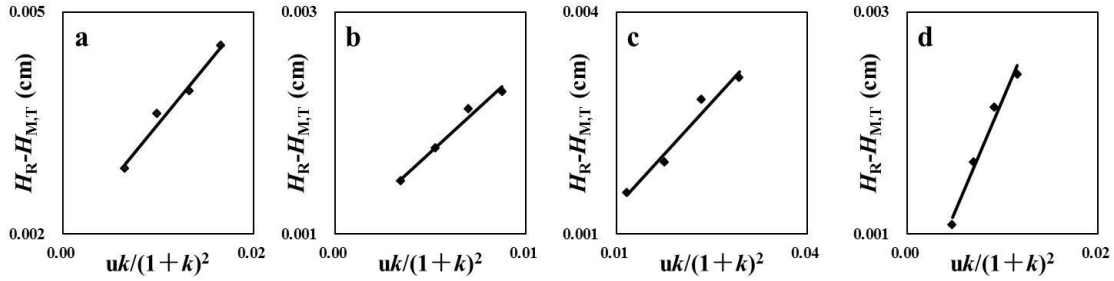

Figure 8 Plots of (H_R-H_M) versus $(uk)/(1+k)^2$ of four drugs on HP-β-CD column by single compound analysis (a, orphenadrine hydrochloride: y = 0.16x + 0.0019, R^2 = 0.979; b, nortriptyline hydrochloride: y = 0.16x + 0.0010, R^2 = 0.978; c, norethindrone: y = 0.09x + 0.0004, R^2 = 0.968; d, ethosuximide: y = 0.20x + 0.0002, R^2 = 0.978)

Table 5 K_d and K values determined by the peak fitting method

Drugs	K(±SD)(M^{-1})	K_d (±SD)(s^{-1})
Theophylline	0.01±0.00	5.26±0.20
Theobromine	0.92±0.00	1.21±0.07
Caffeine	12.00±0.14	1.81±0.68
Metoprolol	40.36±0.34	11.03±0.96
Norethindrone	4.40±0.00	23.61±0.14
Nortriptyline	102.94±12.02	14.01±1.74
Ethosuximide	0.69±0.13	9.71±0.27
Orphenadrine	24.65±0.05	12.56±0.09
Cortisone	5.25±0.04	22.16±1.40
Chloramphenicol	0.41±0.00	11.02±2.55
Ofloxacin	2005.79±1.70	0.12±0.01
Penicillamine	0.29±0.01	1.07±0.06
Propranolol	108.06±0.49	26.11±8.77

See section 2.2.2.2 for detail of methodology used

2.2.3.2 Taste evaluation of test compounds using the electronic tongue

The results of electronic tongue are shown in 2.1.3.1.

2.2.3.3 Modeling

By stepwise regression for independent variable reduction, seven parameters with notable influence on the taste masking effect including K_a^3, K_d, $K_a^2K_d$, $K_a^3K_d$, $K_aK_d^3$, K_d^2 and K_a/K_d were identified from twelve pre-set kinetic parameters. Based on the six selected parameters, a multiple-linear regression model was established, as given in Eq. 12 with R^2=0.98 and P$\leqslant$0.05.

$$D = -3.892E^{-5}K_a^{\,3} + 0.342\frac{K_a}{K_d} + 44.121K_d - 1.462E^{-3}K_a^{\,2}K_d + 5.808E^{-6}K_a^{\,3}K_d - 1.639K_d^{\,2} + 1.805E^{-3}K_aK_d^{\,3} \quad (12)$$

It is conventionally believed that K_a and K_d for drug/macromolecule complexation should have a positive and negative correlation with taste masking respectively. However, both of K_a^3, K_d^2 and $K_a^2K_d$ possessed negative correlation with Euclidian distance, while other parameters had positive correlation with taste masking effects. A three dimensional model for distance as a function of K_a and K_d was depicted (Figure 9).

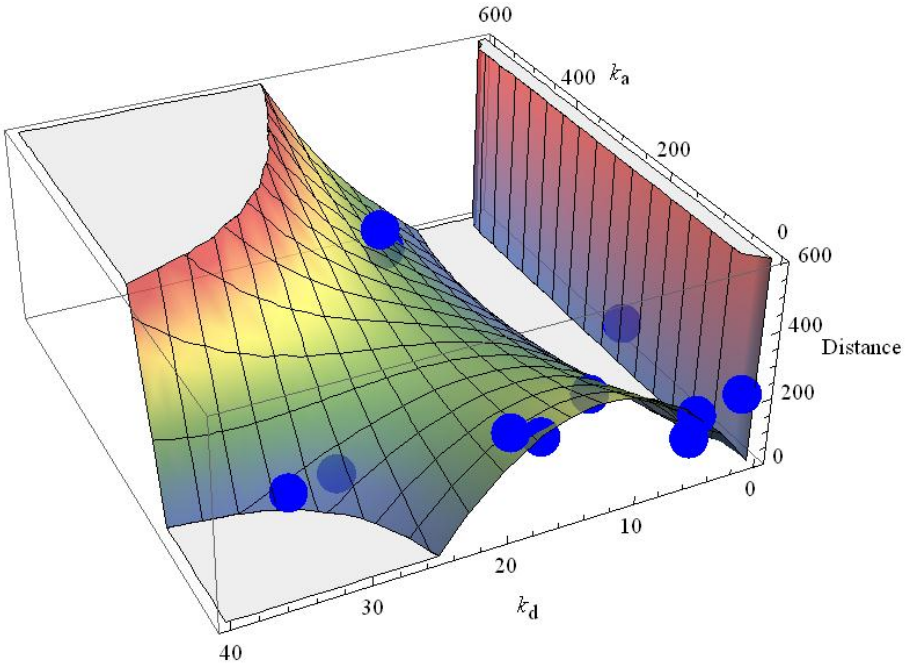

Figure 9 Three dimensional model based on thirteen model bitter drugs data (blue balls) for relationship of K_a, K_d measured by HPAC and taste masking effects (as measured by the electronic tongue) of drug/ HP-β-CD complexation

From this model, it could be observed that the distance rapidly increased when K_d was closed to zero, which implied very strong drug-CD inclusion. Therefore, the concentration of free bitter drug molecules in the solution was too low to be perceived. Additionally, in the white area of $K_a < 100$ and $K_d > 25$, the distance decreased to zero, which demonstrated that drugs in this area could poorly form drug-HP-β-CD inclusion to mask bitter taste. However, distance has been rising as K_a value increased from 0 to 600. Meanwhile, a rise following by a fall of distance could be observed as the K_d value from 0 to 20.

The model produced a good correlation between taste masking and kinetic parameters of drug-HP-β-CD complexation, although the number of test samples was limited. Compared with SPRi method, it is difficult for HPAC to determine kinetic parameters in high-throughput.

2.2.3.4 Cross-validation and prediction

The correlation of determined distance (Y) as a function of predicted distance (X) of each drug was calculated by 10-fold cross-validation (Figure 10). It is well known that two sets of data strongly correlate with each other when the correlation coefficient is about 0.8 to 1. A good correlation was obtained as given in Eq. 13 with correlation coefficient of 0.82, P<0.05 (bivariate correlated analyse by SPSS).

$$Y = 0.6054X + 70.06 \quad (13)$$

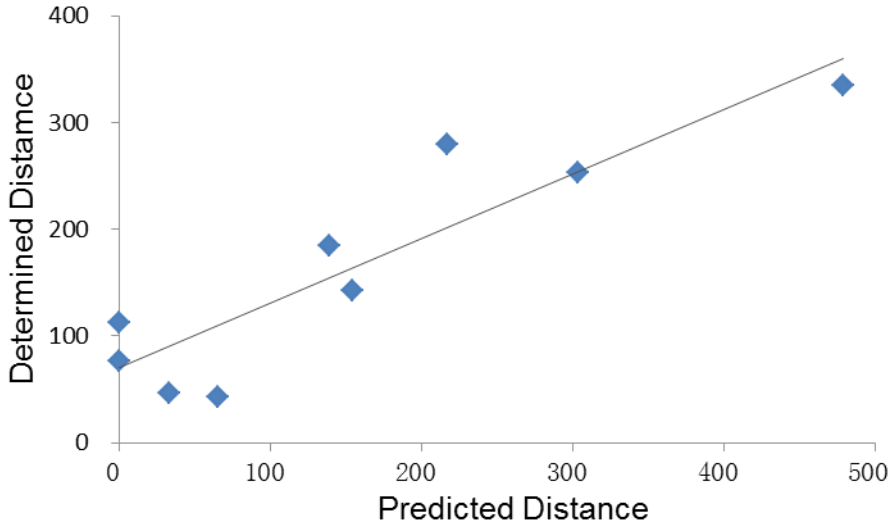

Figure 10 The correlation-ship of predicted distance versus determined distance for constructed model by 10-fold cross-validation

2.3 Comparison of Kinetic Parameters Obtained by SPRi and HPAC on Taste masking Models

From the three dimensional models established by SPRi and HPAC methods, it could be observed that the general tendencies of the two models was almost the same (Figure 11). The distance rapidly increases when K_d is closed to zero, because K (K_a/K_d) exerts a positive influence for both models and K_d is the denominator in this relationship. Also, in the white area (see Figure 11) K_a is a small value and K_d is in big value, the distance decreases to zero. This demonstrates that drugs in this region are poorly complexed by HP-β-CD and hence the drug-HP-β-CD inclusion complex is likely to rapidly dissociate to release free drug.

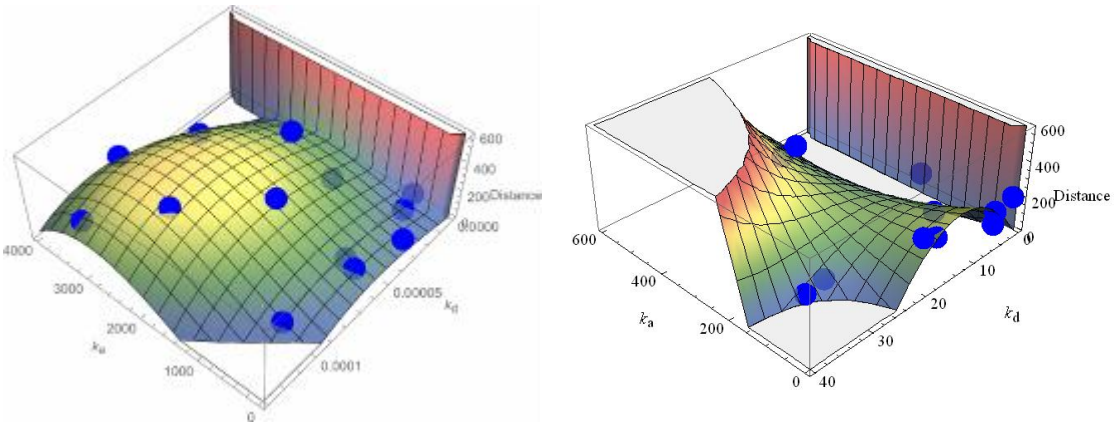

Model based on SPRi Model based on HPAC

Figure 11 Comparison of two models relating K_a and K_d for drug-CD reversible complexation measured by SPRi or HPAC and taste masking measured using the electronic tongue

However, the SPRi model data, e-tongue Euclidean distance rises to a crest followed by a gradual reduction as CD/drug K_a and K_d values increase. By

comparison, the HPAC model showed that e-tongue Euclidean distance increases linearly with CD/drug K_a and K_d. This difference might be caused by the distribution of K_a values obtained by two methods. K_a values of most of drugs based on HPAC measurement are very similar, all exhibiting small values (less than 110 M^{-1} except ofloxacin is about 2005 M^{-1}). In contrast the distribution of K_a value based on SPRi is more uniform (within three orders of magnitude). Although the correlation coefficients for both models was>0.8, the larger coefficient of SPRi method and smaller intercept indicate that the systematic error for the model based on SPRi is smaller than that based on HPAC. Additionally, compared with SPRi based model an obvious area with distance of zero could be seen in HPAC based model even K_d is small and K_a is with large value which might be also caused by systematic error. Firstly, in SPRi, drug molecules are immobilized over the sensor surface and CDs are used as the mobile phase, which is totally reversed in HPAC, where the drugs are used as a mobile phase and CDs are modified and fixed onto the surface. In other words, chemical groups specifically responsible for bitter taste would not necessarily be bound on the microarray. The microarray bound drugs would therefore not necessarily present the correct functionality to the HP-β-CD and hence influence the drug/CD kinetic parameters measured. Photo-cross-linking technique is used to immobilize the drug molecules which allowed one molecule to display in various orientations. Each orientation may have different binding affinity to the specific CD and therefore, the kinetic constant we have obtained from SPRi is probably the average of different multiple orientations. Non-specific binding which is present in all systems might also contribute to the kinetic parameters determined. The taste-masking effect would be influenced by

various factors besides inclusion formation. These include competitive binding of chemical groups responsible for bitter (internal or external binding to CD cavity) as well as the natural sweet intensity of CD. These properties will be revealed by Euclidean distance determination using the Electronic Tongue. In summary, besides drug concentrations present in free and complexed forms, non-specific bindings and other interactions in the SPRi determination should be taken into account.

A further issue concerning the measured drug K_a values using by HPAC and SPRi is that the calculated value may be influenced by the mobile phases employed. Using HPAC, for solubility purposes acetonitrile is the required solvent for drug dissolution, which, per se, has a competitive interaction with HP-β-CD. Acetonitrile will reduce the polarity and enhance elution capability of the mobile phase. As a result, the inclusion of drugs into the cavity of HP-β-CD could be hindered and lead to a reduction in measured K_a. In contrast, for SPRi, drugs were immobilized on the microarray and HP-β-CD dissolved in PBS added, which is at a similar pH and ionic strength similar to that found in the mouth cavity environment. And the drug concentrations varied a lot in HPAC which might lead to greater systematic error than SPRi. Additionally, the flow rates of the two methods are also not the same with flow rate for SPRi being much less than that for HPAC. A lower flow rate will facilitate the association process of drug/HP-β-CD allowing greater ease of discrimination between the interaction of these guest and host molecules.

2.4 Formulation Optimization based on Kinetic Parameters of Drug-CD Inclusion

Paracetamol, a bitter tasting medication used to treat many conditions such as headache, muscle aches, arthritis, backache, toothaches, colds and fevers, was used as a model drug. A number of taste masking methods were tried, including granulation and microencapsulation based on solvent evaporation. Dissolution testing showed granulation and microencapsulation released more than 60% of the paracetamol within 30 seconds. A further formulation of paracetamol lipid microspheres prepared by spray congealing released less than 6% paracetamol within 30 seconds. However, a slightly bitter taste could still be perceived due to the 6% of released drug. Paracetamol lipid microspheres in association with β-CD inclusion were prepared for taste masking. By spraying a fusion mixture of paracetamol, octadecanol and Eudragit into cold air to obtain solid microspheres and sieving, the size distribution and sphericity of microsphere were acceptable (close to 1) as characterized by inverted microscope examination and flowability testing. The dissolution test indicated that the release of paracetamol from lipid microspheres followed zero-order kinetics. Whilst only a small amount (less than 6%) of paracetamol was released from the microspheres within 30 seconds, the bitter taste could still be perceived. Therefore, in order to prevent the released paracetamol impacting on the bitter taste receptors, β-CD was added to complex any paracetamol that was released. However, it was important to minimise the amount of β-CD added to minimise the interference of β-CD on subsequent paractemol formulations. By calculation, the theoretically amount of β-CD required was obtained. The

electronic tongue test was carried out to evaluate taste masking because concentration-dependent methods such as HPLC, could not distinguish free paracetamol from paracetamol in complexation with β-CD.

Paracetamol lipid microsphere with β-CD follows a kinetic model in aqueous solutions including saliva (Figure 12).

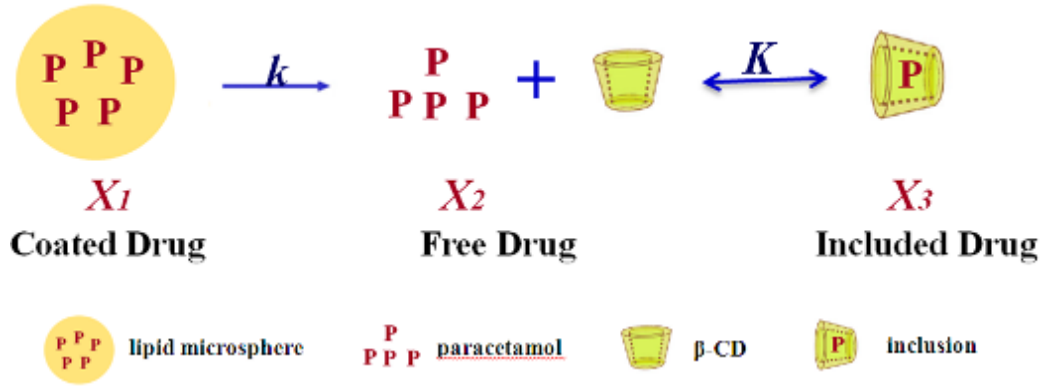

Figure 12 The schematic diagram showing paracetamol distribution behaviour in aqueous media including saliva

The drug in microsphere (X_1) follows first-order kinetics [146]:

$$X_1 = D \cdot e^{-kt} \tag{14}$$

where, D is initial drug dosage in the microsphere and k is the release rate constant.

Free drug in saliva (X_2) is the drug released subtracted from that in β-CD inclusion (X_3):

$$X_2 = D \cdot \left(1 - e^{-kt}\right) - X_3 \tag{15}$$

Assuming β-CD and drug can reach an equilibrium state rapidly, X_3 is mainly determined by the β-CD concentration (Y) and the equilibrium constant between β-CD and drug (K) and X_2:

$$X_3 = KX_2Y \tag{16}$$

Meanwhile, in consideration of drug-CD inclusion formed as 1:1 in molar ratio, Y is decreasing with formation of X_3:

$$Y = Y_0 - X_3 \tag{17}$$

where Y_0 is the initial β-CD concentration.

X_1, X_2, X_3 and Y could be obtained by Mathematica software:

$$X_1 = D \cdot e^{-kt} \tag{14}$$

$$X_2 = \frac{e^{-kt}}{2K}\left(\sqrt{\left(KD + e^{kt} + KY_0e^{kt} - KDe^{kt}\right)^2 + 4KDe^{kt}\left(e^{kt} - 1\right)} + e^{kt}(KD - KY_0 - 1) - KD\right) \tag{18}$$

$$X_3 = \frac{1}{2}\left(Y_0 + D(1 - e^{-kt})\frac{1 - e^{-kt}\sqrt{\left(KD + e^{kt} + KY_0e^{kt} - KDe^{kt}\right)^2 + 4KDe^{kt}\left(e^{kt} - 1\right)}}{K}\right) \tag{19}$$

$$Y = \frac{1}{2}\left(Y_0 + D(e^{-kt} - 1) + \frac{e^{-kt}\sqrt{\left(KD + e^{kt} + KY_0e^{kt} - KDe^{kt}\right)^2 + 4KDe^{kt}\left(e^{kt} - 1\right)} - 1}{K}\right) \tag{20}$$

When $t \to \infty$, following equations could be obtained:

$$\lim_{t\to\infty} X_2 = \frac{K(D - Y_0) - 1 + \sqrt{K^2(D - Y_0)^2 + 2K(D + Y_0) + 1}}{2K} \tag{21}$$

$$\lim_{t\to\infty} X_3 = \frac{K(D + Y_0) + 1 - \sqrt{K^2(D - Y_0)^2 + 2K(D + Y_0) + 1}}{2K} \tag{22}$$

$$\lim_{t\to\infty} Y = \frac{K(Y_0 - D) - 1 + \sqrt{K^2(D - Y_0)^2 + 2K(D + Y_0) + 1}}{2K} \quad (23)$$

D = 0.026462027 M and K = 142.3 M^{-1} [137] when dosage is 20 mg (strength) and saliva volume is 5 mL. $\lim_{t\to\infty} X_2$ (equilibrium concentration of free paracetamol) gradually decreases with increase of Y_0 (concentration of β-CD).

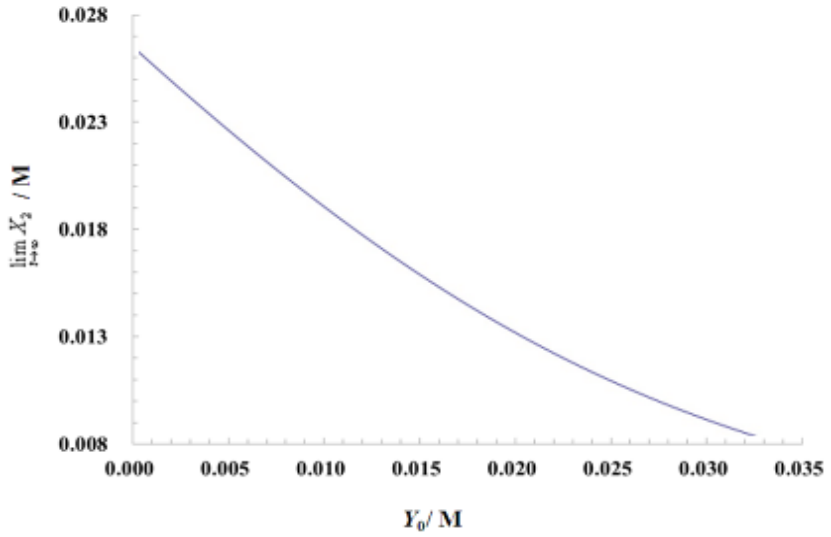

Figure 13 Effects of Y_0 (the concentration of β-CD) as a function of $\lim_{t\to\infty} X_2$ (the equilibrium concentration of free paracetamol)

It is rationalised that a combination of lipid microspheres and β-CD could be used to retard drug release (k) including drug released into saliva. The result of which is a better taste-masking effect i.e. the co-operation of microsphere and β-CD will work in concert to prevent the contact between bitter paracetamol and taste buds.

Since people normally complete the swallowing process within 30 s, it can be estimated that within this time the free concentration of paracetamol should be less than 35 μg/mL since this is the threshold concentration for people to perceive bitter taste of paracetamol [147]. When drug loaded lipid microspheres

equivalent to 20 mg paracetamol is administered, the free paracetamol concentration is 80 μg/mL at 30 s (in 5 mL saliva). By theoretical calculation, K=142.3 M^{-1}, k=0.001270 s^{-1}, D=0.026462027 M at 30 s, from Eq. 18:

$$X_2 = 0.00338235 \cdot (\sqrt{(147.826Y_0 + 0.8926)^2 + 0.607658} - 147.826Y_0 - 0.8926) \quad (24)$$

When $X_2 \leqslant 0.0002315$ M (35 μg/mL), $Y_0 \geqslant 0.02375$ M. Therefore, as the dosage of β-CD is 134.8 mg (6.74:1 with drug in mass ratio), concentration of free drug released could be reduced to 35 μg/mL by inclusion of β-CD.

2.4.1 Materials

Paracetamol (Anhui Fengyuanlikang Pharmaceutical Co. Ltd.); Octadecanol (Hunan Erkang Pharmaceutical Co. Ltd.); Eudragit E100 was selected because it dissolved in aqueous media with pH<5 (pH of saliva between 6.8 and 7.4) (Shanghai Chineway Pharmaceutical Tech. Co. Ltd.); β-CD (Anhui Shanhe Pharmaceutical Co. Ltd.); Sodium phosphate monobasic dehydrate, Sodium hydrogen phosphate, Phosphoric acid (Sinopharm Chemical Reagent Co., Ltd., China.) Electronic contact thermometer (ETS-D5, IKA, German); Inverted phase contrast microscope (TS-100F, Nikon, Japan); Ultra performance liquid chromatography (UPLC) (1290, Agilent, America); Particle sizing systems (Camsizer XP, Retsch, German); α-Astree electronic tongue Ⅱ (Alpha MOS, Toulouse, France); Dissolution apparatus (ZRS-8G, Tianjin Haiyida Co., Ltd, China); Spray gun (W-71, Iwata, Japan); Electrothermal draught drying cabinet (BPG-9140A, Shanghai Yiheng Instruments Co., Ltd, China); Vapour-bathing constant temperature vibrator (Taicang Experimental Equipment Factory, China); Electronic scales (ML203, Mettler Toledo, Switzerland); Electronic

scales (TE601-L, Sartorius, Geman); pH meter (PP-20-P11, Sartorius, Geman); Water purification system (Milli-Q, Millipore Corporation, America)

2.4.2 Methods

2.4.2.1 Preparation of paracetamol lipid microspheres

Paracetamol lipid microspheres were prepared by the addition of an appropriate amount of Eudragit E100, which can only dissolve at pH≤5, into octadecanol at 100^{o}C (Paracetamol:Octadecanol:Eudragit E100 = 30:60:10 w/w). Paracetamol as a micronized powder was gradually added whilst stirring the system at 1000 rpm and 100^{o}C to produce a uniform mixture. The mixture was then immediately poured into the reservoir of a spray gun preheated to 90^{o}C in a drying oven and sprayed such that the air dried microspheres at room temperature (approx 25^{o}C) were collected from stainless steel trays. Batch sizes were between 30-50 g. The solid microspheres were sieved and the fraction size 160-200 mesh (~75-96 μm) was collected for further study as described previously [147].

2.4.2.2 Morphology characterisation of paracetamol lipid microspheres

The morphology of paracetamol lipid microspheres sieved between 160-200 mesh were investigated by inverted phase contrast microscopy.

Examinations of the size distribution, sphericity and symmetry were studied using the Camsizer XT particle sizing systems. In this study, about 100mg of paracetamol lipid microspheres were transported from a hopper to the analyzing area, and then injected by compressed air, which was set at 30 Kpa. The shadows projections of the microspheres were captured by cameras, following

by transforming greyscale images through a multistep algorithm into binary images to determine the exact outlines. All particle size and particle shape parameters, including sphericity and symmetry, could be measured on this basis.

2.4.2.3 ^{1}HNMR characterisation of paracetamol lipid microspheres

Paracetamol, β-CD and a physical mixture of paracetamol with β-CD in an optimized ratio (1:6.74 w/w) were vibrated for 5 min in water (10 mL) at 37 ^{o}C and mixing speed of 50 rpm. Samples (10 mL) were taken, filtered and freeze-drying. The freeze-drying powders were re-dissolved in D_2O and then determined by ^{1}HNMR.

2.4.2.4 Dissolution test on paracetamol lipid microspheres

For the in vitro dissolution test to mimic dissolution in saliva, microspheres containing 20mg of paracetamol (pharmaceutical grade material) particle size fraction 160-200 mesh were assessed in triplicate for each batch of the microspheres prepared using the paddle method according to the Chinese Pharmacopoeia 2010 with a rotation speed of 50 rpm. Distilled water (200 mL) was used as the dissolution medium at 37 ± 0.5 ^{o}C. Aliquots of 2mL solution samples were withdrawn at 10, 30, 60, 90, 120, 180, 240, 300 s and an equal volume of distilled water added to each sample solution immediately after collection. This solution was immediately filtered through a 0.22 μm membrane and analysed by an Agilent 1260 series HPLC system (Agilent Technologies Inc., China). The mobile phase consisted of methanol-phosphate buffer (pH 4.5) (20:80, v/v). Elution was performed at 25 ^{o}C at a flow-rate of 1 mL/min. The wavelength of the detector was set at 254 nm. The dissolution test could not

distinguish free paracetamol from that included in β-CD. Therefore it was difficult to evaluate the taste masking effect of β-CD using the dissolution test. Subsequently, the electronic tongue was used to evaluate taste masking effect of β-CD.

2.4.2.5 Determination of taste masking effects by electronic tongue

A series of paracetamol standard solutions (P1, P2, P3, P4) were prepared by addition of an appropriate amount (0.30, 1.00, 3.00, 10.00 mg) of paracetamol to 80mL of deionized water. Then paracetamol lipid microsphere (M), paracetamol lipid microsphere in association with β-CD at an optimized mass ratio of 1:6.74 (C), and paracetamol-β-CD inclusion at mass ratio of 1: 6.74 (B) equal to 10 mg of paracetamol were transferred into dissolution cups with 100 mL deionized water at paddle speed of 50 rpm. The samples were withdrawn at 30 s and filtered. The assays were determined on an Astree electronic tongue system equipped with an Alpha M.O.S. sensor set #2 (for pharmaceutical analysis) composed of 7 set of sensors (ZZ, AB, BA, BB, CA, DA, JE) on a 13-positions autosampler (using 80 mL-beakers). Acquisition times were fixed at 120 s. The data generated on the Astree system was processed using multidimensional statistics on AlphaSoft V12.3 software. Samples measurements were replicated at least eight times and the values of the last three measurements were used in the data analysis. Average values at 120 s were used to build the taste maps. Astree sensors were washed by deionized water between each sample measurement.

2.4.3 Result and discussion

2.4.3.1 Morphology characterization of paracetamol lipid microspheres

Size distribution analysis indicated that the mean diameter of the microspheres was 97.6 μm (Figure 14). The morphology of paracetamol lipid microsphere showed particles with good sphericity (i.e., sphericity (SPHT) of 0.949 and symmetry factor of 0.953, which were both close to 1) [148]. Generally, particles with regular shape and smooth surface have smaller surface area as well as slower dissolution rate than the rough particles, which is likely to influence the taste masking performance.

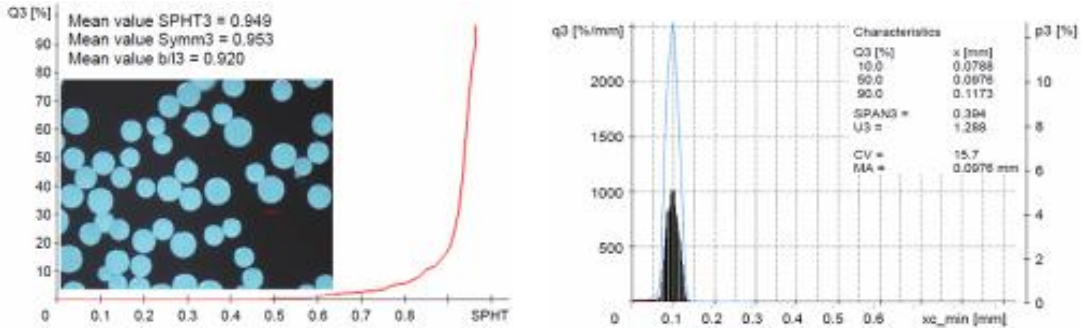

Figure 14 Morphology of microspheres. 2D micrograph, morphology features (left), and the size distribution (right) of paracetamol lipid microspheres

2.4.3.2 ^{1}HNMR characterization of paracetamol lipid microspheres

As could be seen in the ^{1}H NMR spectra, there were two characteristic peaks for paracetamol: the H-2, H-6 doublets at 7.12 ppm and the CH_3 singlet at 2.01 ppm. All the characteristic chemical shift values of paracetamol in the physical mixture increased. The spectra show that hydrogen bonds were formed between the oxygen on the phenolic hydroxyl group, the nitrogen on the imino group of paracetamol and the hydrogens on the hydroxyl groups in β-CD.

Therefore, it was likely that β-CD could include paracetamol in a short time in solution state.

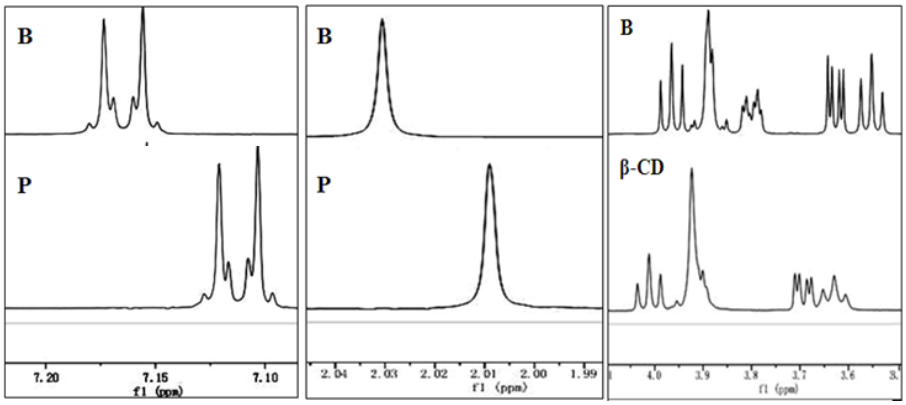

Figure 15 ^{1}H NMR spectra (left: the H-2, H-6 doublets of paracetamol; middle: the CH_3 singlet of paracetamol; right: multiple peaks of β-CD in 3.4 ppm-4.2 ppm) of β-CD, paracetamol (P), the physical mixture of βCD and paracetamol (B)

2.4.3.3 Dissolution test

The short term dissolution test (within 120s) was used to establish the release of free paracetamol from the formulations which would subsequently contribute the bitter taste experience (Figure 16). The release behaviour of paracetamol particle sized by the 160-200 mesh was tested. It was observed that paracetamol released rapidly under the sink conditions used, with 70% at 30 s and 100% within 120 s. In contrast, the paracetamol lipid microspheres exhibited sustained-release characteristics. When Eudragit E100 was added to the formulation, the release rate of paracetamol fell dramatically. Less than 2% paracetamol released at 30 s and approximately 35% at 300 s.

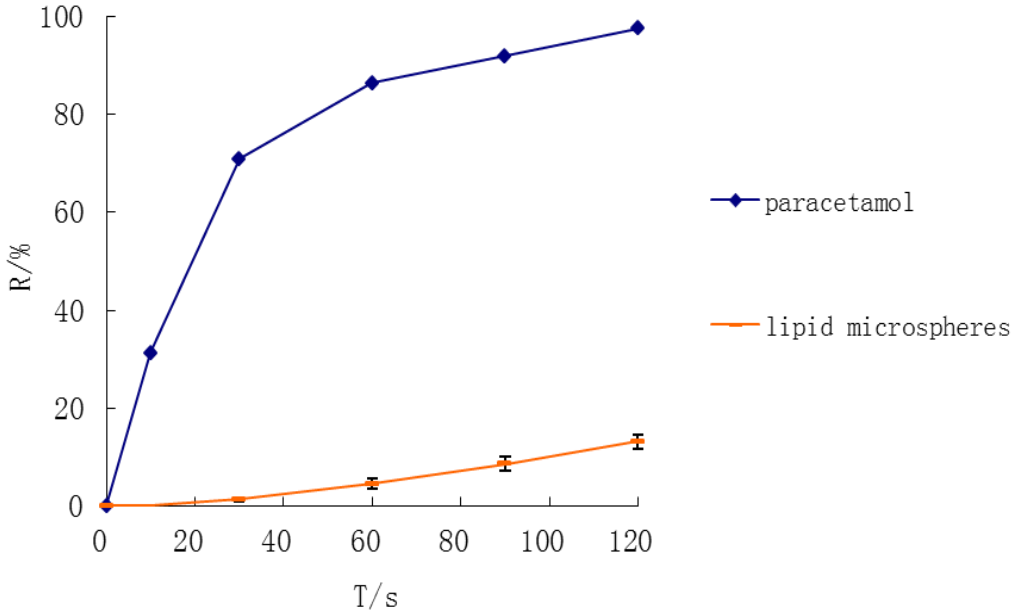

Figure 16 Drug release profile of paracetamol and paracetamol lipid microspheres prepared using octadecanol and Eudragit E100

2.4.3.4 In vitro taste masking evaluation (Astree electronic tongue)

The samples collected from the dissolution test at 30 s from paracetamol, paracetamol/β-CD complexes, lipid microspheres and lipid microspheres combined with β-CD were evaluated for taste masking using the electronic tongue. The taste maps were generated and analysed by PCA software.

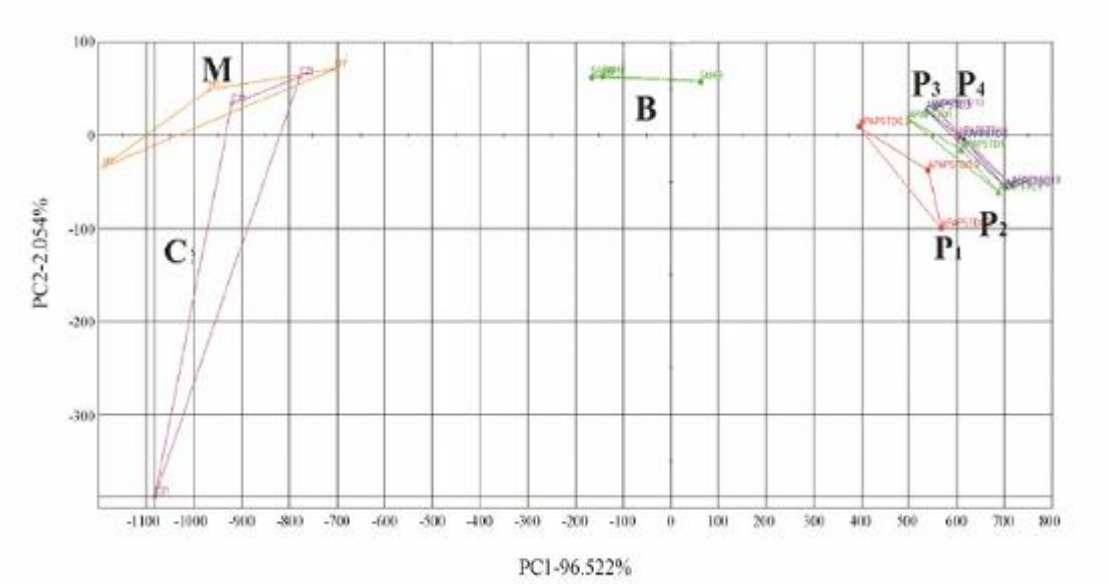

Figure 17 Electronic tongue ‘‘taste map’’: Global signal comparison (PCA analysis of the electrode responses) from paracetamol (P), paracetamol / β-CD inclusion complex (B); lipid microspheres (M); lipid microspheres combined with β-CD (C)

From the taste map of electronic tongue, it was clear that the taste of the paracetamol standard solutions (P1, P2, P3, P4), paracetamol included by β-CD (B) or lipid microspheres (M) were different. For paracetamol API standard solutions, triangles shifted from right to left as reduction of concentrations, indicating that samples with less bitterness should be on the left of taste map. Therefore, a noticeable taste masking effect was observed for paracetamol mixed with β-CD compared with paracetamol API standard solutions. A better taste masking effect was produced by lipid microspheres on the left of the taste map with larger distance to paracetamol API standard solutions than paracetamol mixed with β-CD. Lipid microspheres combined with β-CD showed an optimal taste masking effect for paracetamol although the lipid microspheres per se played a leading role in the total taste masking observed. The results for taste masking as evaluated by the electronic tongue were in accordance with

the kinetic model established previously established (see section 2.4), namely, the order of bitter intensity was paracetamol > paracetamol / β-CD inclusion complex > paracetamol lipid microspheres > paracetamol lipid microspheres combined with β-CD.

Paracetamol was used as a model bitter tasting drug to investigate the influence of lipid microspheres combined with β-CD inclusion as a method to mask the bitter taste of poorly soluble drugs. In order to optimize the formulation and minimise the amount of β-CD, a kinetic model was established. This could be used to calculate distribution of drug in medium, lipid microspheres and β-CD inclusion. It provided a basis to determine the optimal amounts of lipid microspheres and β-CD to reduce the concentration of bitter drug under the threshold perception concentration (35 μg/mL). Finally, the combination drug delivery systems were prepared and characterized by ^{1}HNMR and electronic tongue. The results tested by electronic tongue indicated that the paracetamol, paracetamol lipid microspheres, paracetamol-β-CD inclusion and combination drug delivery system showed different taste characteristics, with the order of low to high bitter perception; combination drug delivery systems < lipid microspheres < paracetamol / β-CD inclusion < paracetamol. It was proved that taste masking of bitter drug could be achieved using a combination of lipid microspheres and CD inclusion. The result of ^{1}HNMR also demonstrated that combination taste masking was jointly achieved through the inhibition of drug release by the lipid microspheres and the inclusion of the free paracetamol by β-CD.

In addition to the molecular basis of bitterness prevention, the microstructures of the formulations could also closely relate to effectiveness in taste masking,

especially for taste masking solid formulations, such as particles or granules. However, the taste masking characteristics of drug formulations have not been quantitatively correlated with the drug-in-formulation internal microstructure. Therefore, a quantitative method to correlate the detailed structural information along with the drug release behaviour will provide mechanistic and new knowledge for taste masking technologies to guide rational design of products.

Chapter 3 Fine Microstructure and Chemical Distribution of Taste Masking Microspheres Based on Synchrotron Radiation

The microencapsulation and microspheres are valuable techniques applicable to mask the unpleasant taste as well as to protect materials from volatilizing and oxidation [149]. Microencapsulation processes are generally based on the principle of solvent extraction or evaporation. However, residual organic solvents cause risk to safe use of pharmaceutical quality formulations. Therefore, other techniques such as spray drying and spray congealing are also utilized for microencapsulation [150]. It is well known that many properties of materials are determined by their particle structures. However, at the particle level, it seems that there is an absence of reports about the relationship between taste and particle microstructure.

From another perspective, in vitro drug release testing approaches have been widely used to predict or quantify the effectiveness of taste masking techniques used. Characterisation of bitter drug release under conditions that mimic the oral cavity fluid composition could effectively predict the taste masking effectiveness of a formulation designed to reduce contact between the bitter active pharmaceutical ingredient (API) and oral cavity taste bud regions [151, 152].

Moreover, the rate and mechanism of the drug release from solid dosage forms strongly depend upon morphology, such as shape and surface, of the dosage form. For example, ‘rough’ pellets showed a faster release rate than smooth or spherical pellets (after 2 h of release) [153]. Toshio Yajima et al prepared wax matrix of clarithromycin by different conditions. It was found that the morphology properties which were influenced by atomizer wheel speed affected the release behaviour of the matrix to control the taste properties [154].

The internal microstructure of pharmaceutical tablets not only influences the mechanical strength of the tablets but also impacts the release rate of APIs [155]. A good correlation has been also reported between the total porosity, mean pore diameter and drug release rate for erosion matrix drug loaded pellets, while these porosity parameters were important when evaluating the in vitro performance during the controlled release of an insoluble drug [156]. Recently, SR-μCT has been used for the microstructural investigation of pellets, and showed that the release profile of a single pellet correlated significantly with steric features such as drug loading, volume, and surface area [157]. These results suggest that the microstructure of particles or granules used to taste mask are closely relates to their effectiveness in this process. Moreover, characterization and evaluation of taste masked products are of significant interest. In addition to drug release testing, conventional methods have been employed for powders, including particle size analysis, porosity measurement, morphology analysis, differential scanning calorimetry (DSC) and x-ray diffraction (XRD) [158-164]. However, these methods are not able to directly investigate the internal fine structures and identify the roles in taste masking of the formulation ingredients. Therefore, a quantitative method to correlate the

detailed structural information with the drug release behaviour will provide mechanistic and new knowledge for taste masking technologies.

SR-μCT, a novel technique for investigation of the internal three dimensional (3D) structures of objects, shows great possibilities for quantitative evaluation and design for solid drug delivery systems. Our previous studies have shown that the interior porous channels and irregular structures can be quantified by the fractal dimensions, which were also well correlated with the drug release kinetics of felodipine osmotic pump tablets [165]. After the surface morphology and the internal 3D structure of felodipine osmotic pump tablets was visualized, the intrinsic drug release kinetics and 3D parameters, such as surface areas of the remaining core, were quantitatively elucidated using SR-μCT [166]. SR-μCT has also been used non-destructively to investigate the mixing and segregation of granular materials in three-dimensions combined with statistical methods [167]. Additionally, Shuji Noguchia applied CT using synchrotron X-ray radiation for the structural analysis of fine granules containing drugs prepared by melt granulation with irregular shape [168].

In this study, paracetamol was used as a model for bitter tasting drugs. Paracetamol lipid microspheres prepared by spray congealing were examined by SR-μCT to give quantitative analysis for the internal 3D structure and taste masking. The primary objectives were to study the micro-structural basis of lipid microspheres for taste masking by sustaining the release of drug and further to provide new knowledge and method for evaluation of taste masking formulations.

3.1 Fine Microstructure of Taste Masking Lipid Microsphere Based on SR-μCT

3.1.1 Materials

Paracetamol with purity of 99.45% was provided by Anhui Fengyuanlikang Pharmaceutical Co. Ltd., China. Octadecanol and Eudragit E100, as the excipients for taste masking were supplied by Hunan Erkang Pharmaceutical Co. Ltd. and Hanghai Chineway Pharmaceutical Tech. Co. Ltd., respectively. Sodium phosphate monobasic dehydrate, sodium hydrogen phosphate and phosphoric acid, used for dissolution test, were provided from Sinopharm Chemical Reagent Co., Ltd., China.

Taste masking microspheres were prepared using a spraying technique (Spray gun, W-71, Iwata, Japan). Inverted phase contrast microscopy (TS-100F, Nikon, Japan) and a particle sizing system (Camsizer XT, Retsch, Germany) were used for morphology characterization. Dissolution test was performed using a dissolution apparatus (ZRS-8G, Tianjin Haiyida Co., Ltd., China). The Synchrotron radiation X-ray microtomography scans were carried out at the Shanghai Synchrotron Radiation Facility (SSRF) in Shanghai Institute of Applied Physics, Chinese Academy of Sciences (Shanghai, China). Data were analyzed using the commercially available software VGStudio Max (Version 2.1, Volume Graphics GmbH, Germany) and Image Pro analyzer 3D (version 7.0, Media Cybernetics, Inc., Bethesda, MD, USA).

3.1.2 Methods

3.1.2.1 Preparation of paracetamol lipid microspheres

The preparation process was described in section 2.4.2.1.

The various formulations are shown in Table 6. The solid microspheres were sieved and the fraction sizes between 160-200 mesh (~75-96 μm) and 80-100 mesh (~150-180 μm) were collected for further study.

Table 6 Formulation of Microspheres

Ingredients	Formulation Codes and Compositions (%w/w)				
	F1	F2	F3	F4	F5
Paracetamol	33.3	32.3	31.7	30.8	30
Octadecanol	66.7	64.5	63.3	61.7	60
Eudragit E100	-	3.2	5.0	7.5	10

3.1.2.2 Morphology characterization of paracetamol lipid microsphere

The process of morphology characterization of paracetamol lipid microsphere was described in section 2.4.2.2.

The flowability of the microspheres was evaluated by pouring powder of microspheres onto a horizontal surface to form a conical heap. The angle of repose between the surface of the pile and the horizontal surface was measured.

3.1.2.3 Short term in vitro dissolution test

The process of short term in vitro dissolution test for paracetamol and paracetamol lipid microspheres (F1-F5) was described in section 2.4.2.4.

3.1.2.4 X-ray powder diffraction

Dissolution samples at 0, 5, 60 mins of microspheres with 10% Eudragit E100 (F5) and without Eudragit E100 (F1) were investigated by X-ray powder diffraction (XRD). The XRD patterns were measured on a Bruker D8-ADVANCE X-ray diffractometer using Cu–Kα radiation (λ = 1.5418 Å). The voltage and current were 40 kV and 40 mA, respectively. Reflection mode was used in the 2θ range of 3-40° with a scan speed of 15° min^{-1} (step size 0.025°, step time 0.1 s) by a LynxEye detector. All the data were acquired at ambient temperature (20 ^{o}C). The data were imaged and integrated with RINT Rapid and peak-analyzed with Jade 6.0 software from Rigaku. Calibration of the instrument was performed using a Corindon (Bruker AXS Korundprobe) standard.

3.1.2.5 SR-μCT

Microspheres were packed and set in polypropylene pipette tips with one end sealed and then measured by SR-μCT. For the structural investigation, microspheres containing 10% w/w Eudragit E100 and without Eudragit E100 were selected to determine the effect of Eudragit E100 on structural features and correlated with drug release. In consideration of the resolution of the X-ray image detector used in CT scans, paracetamol crystals and microspheres sieved between 80-100 mesh were selected for investigation. Drug dissolution test was also carried for this size fraction of microspheres. SR-μCT images

were acquired with beam line BL13W1 at Shanghai Synchrotron Radiation Facility (SSRF). In order to investigate the distribution of low Z materials (paracetamol and octadecanol) in the microsphere, the propagation-based imaging (PBI) method was used for the phase contrast imaging for the simplest experimental implementation. According to the preliminary experiments and also literature references, the imaging parameters were optimized [157, 169, 170]. The theoretical complex refractive index indicated that in order to enhance the phase contrast between paracetamol and octadecanol, the X-ray with a lower energy should be selected for the imaging. For the consideration of properties including composition, density and fractions, samples were scanned at 13.0 KeV for the higher flux to reduce the imaging times (according to the spectral flux profile of BL13W, the highest flux could be obtained near 13 KeV). In order to enhance the contrast to show the slight difference in density between paracetamol and octadecanol, the sample-to-detector distance was set at 12 cm after a series of confirmatory studies. After penetration through the sample, the X-rays were converted into visible light by a Lu_2SiO_5: Ce scintillator (10 μm thickness). Projections were magnified by diffraction-limited microscope optics (10×magnification) and digitized by a high-resolution 2048 pixel × 2048 pixel sCMOS camera (ORCA Flash 4.0 Scientific CMOS, Hamamatsu K.K, Shizuoka Pref., Japan). The pixel size was 0.65 μm and the exposure time was 1 s. For each acquisition, 900 projection images were captured. Flat-field and dark-field images were also collected during each acquisition procedure, in order to correct the electronic noise and variations in the X-ray source brightness.

The projected images for the samples at each time intervals (0, 5, 60 min) of drug dissolution test were reconstructed using the X-TRACT SSRF CWSx64

(CSIRO, Commonwealth Scientific and Industrial Research Organization, Australia, http://www.ts-imaging.net) to perform a direct filtered back projection algorithm. To enhance the quality of reconstructed slices, propagation-based phase contrast extraction was carried out. For the principle of phase contrast imaging, the amplitude and phase of X-ray were affected by the interaction of the wave with matter and the forward diffraction could formally be described by the complex refractive index (n) of the medium as

$$n = 1 - \delta + i\beta \tag{25}$$

The refractive index decrement δ results in a phase shift, and the absorption index β is linked to the linear absorption coefficient μ. The theoretical values of β and δ were calculated with the X-ray attenuation properties model of DCM (software for the data-constrained modeling and characterization of material compositional microstructure and properties, which was developed by CSIRO, http://research.csiro.au/dcm). At the beam energy of 13 KeV, the theoretical δ of octadecanol and paracetamol were 1.14e-6 and 1.68e-6, the corresponding β values were 6.75e-10 and 1.44e-9. As described in the paper [171], the larger sample-to-detector distances increased the contrast primarily due to the contribution from differences in the refractive properties across the sample in addition to the differential absorption. In combination with homogeneous Transport of Intensity equation (TIE-Hom) phase retrieval can achieve high quality reconstructed 3D images. But the value of β can be accurately reconstructed with TIE-Hom and conventional CT reconstruction from a single projection image per view angle. In contrast, the accuracy of reconstruction of δ depends strongly on the choice of the “regularization” (δ/β) parameter in TIE-Hom. During phase extraction, the parameter of δ/β was adjusted at 1200

according to the theoretical values. After phase retrieval and reconstruction, the calculated β of octadecanol and paracetamol were about 7.30e-10 and 1.10e-9 respectively. Then, for all samples the range of β values between 0 to 1.70e-9 in the images were truncated and rescaled to a grey value of 0 to 255 (8 bit grey level) [172]. The 3D rendered data were analyzed with commercially available software VGStudio Max (Version 2.1, Volume Graphics GmbH, Germany) and Image Pro Analyzer 3D (Version 7.0, Media Cybernetics, Inc., USA) to obtain qualitative and quantitative data, respectively.

3.1.3 Result and Discussion

3.1.3.1 Morphological characterization of paracetamol lipid microspheres

The result of morphological characterization of paracetamol lipid microspheres was described in section 2.4.3.1. In addition, the flowability of the microspheres was also found to be good, with the angle of repose at 29°.

3.1.3.2 Short term in vitro dissolution

The short term dissolution test within 120 s was used to indicate the availability of free paracetamol as an indication of bitter taste released from the formulations (Figure 18). The release behaviour of paracetamol powder passed through 160-200 mesh was also tested. It was observed that it released rapidly under the sink condition, with 70% at 30 s and 100% within 120 s. In contrast, the paracetamol lipid microspheres (Formulations F1-F5) exhibited sustained-release characteristics. When Eudragit E100 was added to the formulation, the release rate of paracetamol fell dramatically. However, as the Eudragit E100

concentration increased from 3.2% to 7.5% w/w in F2-F4, the release behaviours were similar, followed by a further decline at the 10% w/w level in F5.

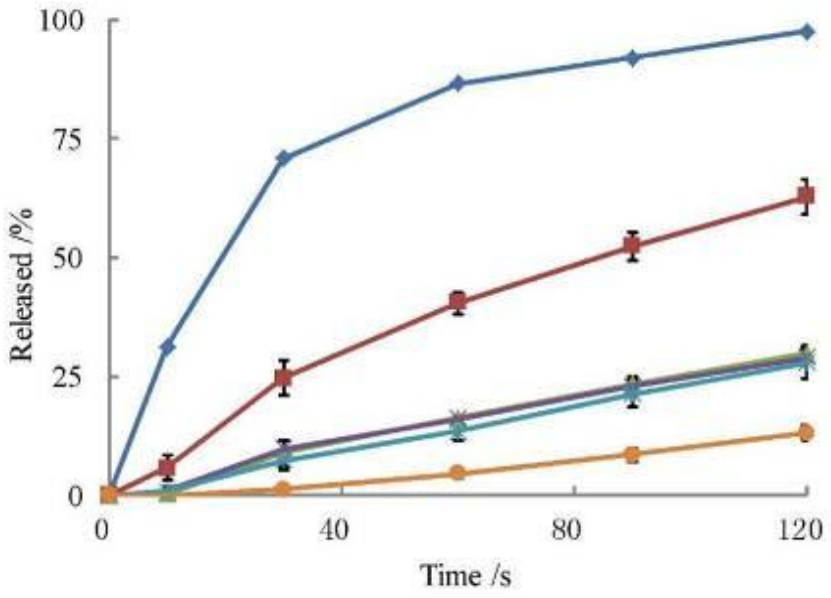

Figure 18 Results of in vitro dissolution test. Drug release profiles within 120 s of paracetamol lipid microspheres between 160-200 mesh with different contents of Eudragit E100 (◆: Paracetamol; ■: 0% Eudragit E100; ▲: 3.2% Eudragit E100; -: 5.0% Eudragit E100; ×: 7.5% Eudragit E100; ●: 10.0% Eudragit E100; n = 6)

Detailed data of percentage drug dissolution at 10 and 30 s were shown in Table 7. These time periods were selected according to the average swallowing time in humans, therefore the amount of drug released after 10 s and 30 s was a key factor when considering and comparing the taste masking potential of the test formulations. From this analysis, the microspheres (160-200 mesh) containing 10% w/w Eudragit E100 provided the optimal system in vitro, demonstrating a zero-order release model with less than 2% paracetamol released after 30 s.

Table 7 Results of dissolution test at 10 and 30 seconds Time (s)

	Drug Release Percentage of Different Formulations (%)					
	API	F1	F2	F3	F4	F5
10	31.2	5.8	0.3	0.9	0.8	0
30	70.9	24.7	8.9	9.7	9.7	1.2

API: paracetamol bulk drug; F1-F5: paracetamol taste masking lipid microspheres formulations described in Table 6

3.1.3.3 X-ray powder diffraction

In order to compare the XRD spectrum of various samples, the raw data of XRD were re-drawn by Excel (Version 2010, Microsoft, America). Figure 19A shows that the paracetamol and octadecanol were crystalline solids while Eudragit E100 was amorphous.

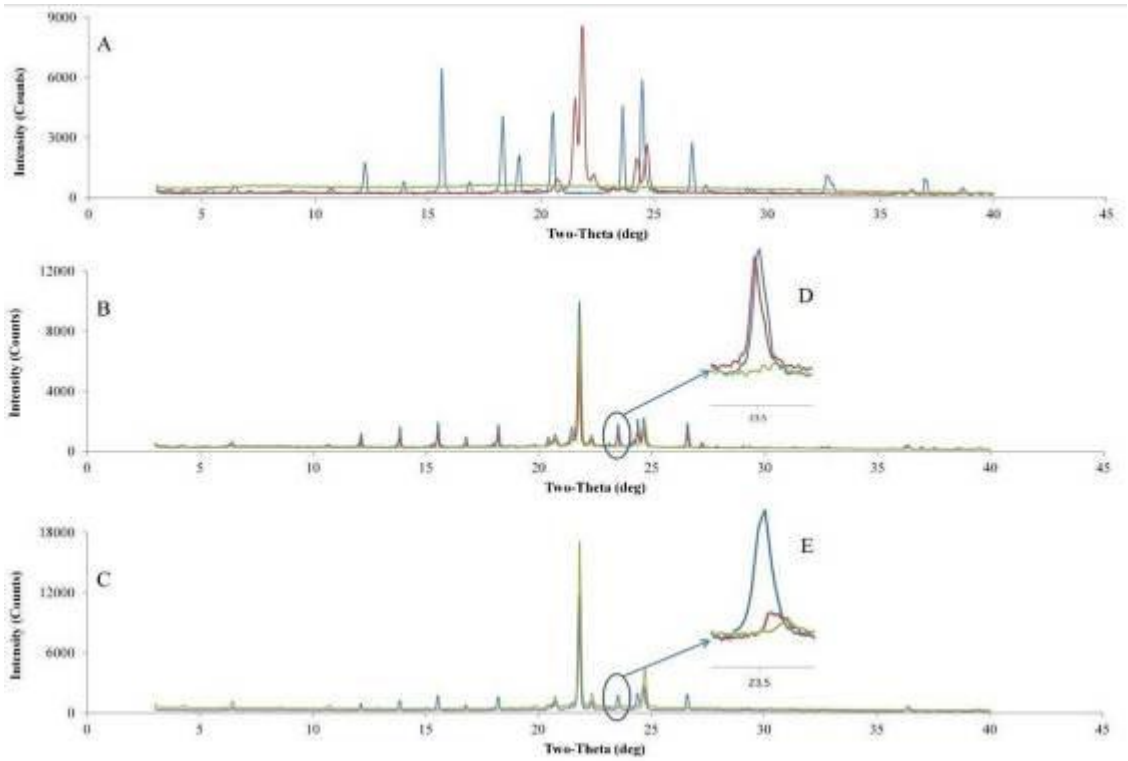

Figure 19 Results of XRD. 19A XRD spectrums of octadecanol (red), paracetamol (blue) and Eudragit E100 (green); 19B and 19D XRD spectrums of dissolution samples of F1 at 0 min (blue), 5 min (red), 60 min (green) and normalized spectrums of three samples at 2θ of 23.5°; 19C and 19E XRD spectrums of dissolution samples of F5 at 0 min (blue), 5 min (red), 60 min (green) and normalized spectrums of three samples at 2θ of 23.5°

The spectrums of samples after dissolution test at 0, 5, and 60 min of F1 and F5 are shown in Figure 19B and Figure 19C, respectively. It is well known that the intensities of XRD peaks are related to the loading amounts of samples. Therefore, the characteristic peaks for paracetamol were normalized to invariable peaks of octadecanol which was insoluble in the dissolution medium. The characteristic peaks at 2θ of 23.5° for paracetamol (Figure 19D and Figure 19E) was selected for relative quantification because the characteristic peak at 2θ of 24.5° overlapped with that of octadecanol.

The relative quantification showed that the paracetamol released rapidly from octadecanol based microspheres and Eudragit E100 significantly inhibited the release of paracetamol within 5 min, while the paracetamol almost completely released at 60 min from both formulations. The results of XRD test demonstrated the crystal forms of materials in the microspheres and illustrated the release behaviours of various formulations, which were in accordance with dissolution test and were supportive to the SR-μCT results from another perspective.

3.1.3.4 SR-μCT

During the drug dissolution test, three representative samples were selected for SR-μCT study, taken from the dissolution medium at 0, 5 and 60 min, which represented non-released, partly-released and completely-released drug samples, respectively.

Paracetamol of F1 without Eudragit E100 was released more rapidly than that of F5 with 10% Eudragit E100 and both F1 and F5 had completely released at 60 min (Figure 20). It is demonstrated that the release behaviour of microspheres with fraction size between 80-100 mesh was similar to those between 160-200 mesh. Therefore, the structural characteristics of both size fractions were also similar, which can be characterized by the SR-μCT investigation.

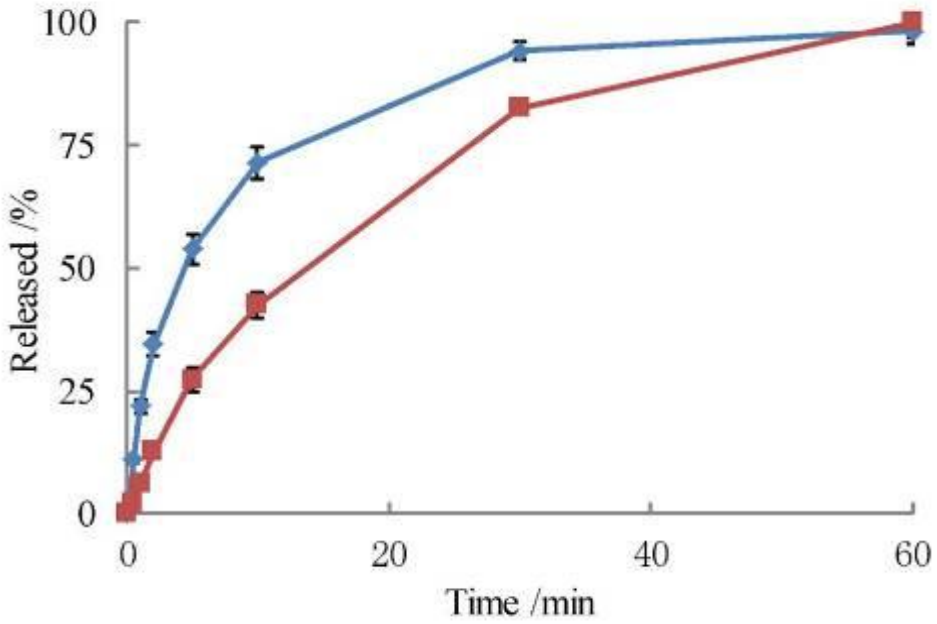

Figure 20 Results of in vitro dissolution test. Drug release profiles within 60 min of paracetamol lipid microspheres between 80-100 mesh with different contents of Eudragit E100 (◆: 0% Eudragit E100; ■: 10.0% Eudragit E100; n = 6)

3.1.3.4.1 2D monochrome X-ray CT images

Images were processed to reduce noise and enhance the contrast. All radiograph images were normalized based on the intensity within the selected rectangular reference region which was never occluded by the sample in any of the images for the correction of varied illumination, and a simple median smoothing filter was performed for the noise reduction. During the TIE-Hom phase retrieval, zingers filter has been applied to remove isolated pixels or small clusters of pixels in which the signal was much higher than that in the surrounding part of the input frame files or dark and flat field files for the correction of artefacts. Brightness, contrast and gamma settings were also adjusted for the contrast enhancement of reconstructed slices. After the optimization, the crystal particles of paracetamol could be distinguished from

the excipients due to the noise reduction and phase retrieval. The grey value of the background was closed to 0, while the excipients were between 60-140 and the crystal particles gave a grey value above 145. The bright/white areas in Figure 21 represented crystal particles and the octadecanol were seen as the grey areas.

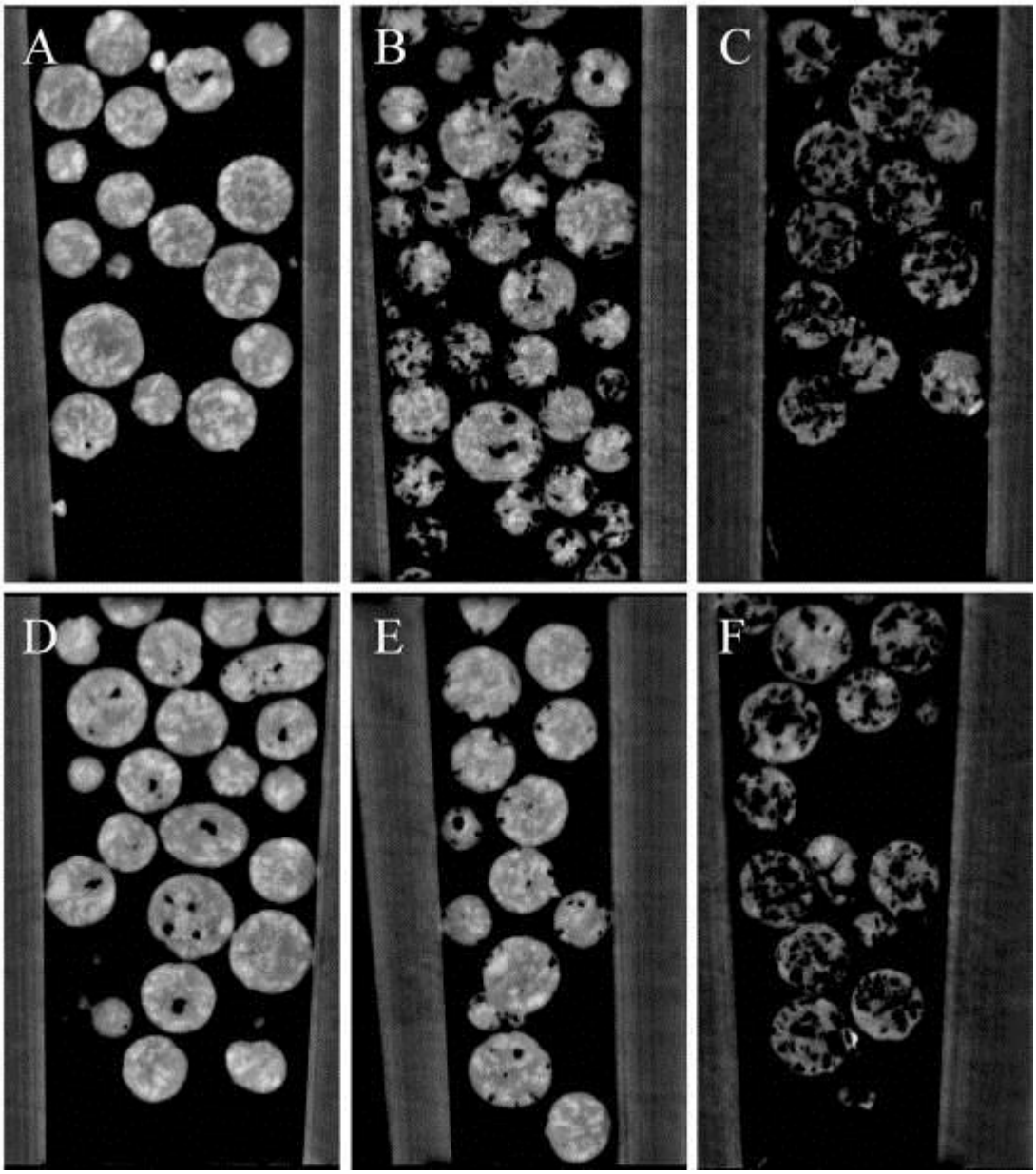

Figure 21 2D monochrome X-ray CT images of paracetamol microspheres (F1 and F5) at different sampling time (A, B and C are images of F1 at 0, 5 and 60 min; D ,E and F are images of F5 at 0, 5 and 60 min)

The 2D monochrome X-ray CT images of paracetamol lipid microsphere of F1 and F5 at different sampling time (0, 5 and 60 min) were shown in Figure 21. From Figure 21A and 21D, it was clear that the white zones, which were the paracetamol crystals, were randomly distributed in the microspheres. The size and shape of the paracetamol crystals were quite different from each other. A number of crystals had irregular or needle like shapes, and in some cases, a sharp segment partly exposed on the surface of microspheres. There were also some small voids within microspheres which were believed to be air bubbles resulting from the rapid stirring of the liquid phase prior to spraying in the microsphere formation process. The presence of the bubbles was more pronounced for the microspheres containing Eudragit E100 (Figure 21D) as a consequence of dramatically increased viscosity of the liquid phase during stirring, which retained the bubbles during further processing.

The voids, shown in Figure 21B and Figure 21E, demonstrated that the paracetamol crystals had been gradually dissolved. Most of these voids were located on the surface of the microspheres and in shape similar to those drug crystals, indicating that the sharp protuberances part of crystals might be well enveloped by octadecanol and the crystals exposed on the surface dissolved quickly after being soaked with the dissolution medium. Paracetamol in microspheres without Eudragit E100 dissolved faster than that with 10% Eudragit E100. It is well known that Eudragit E100 is water-insoluble with excellent film-coating function as a kind of coating material. Thus, it could inhibit the release of paracetamol from microspheres, which was the key factor to mask the bitter taste of paracetamol in the mouth for a period of time.

The images in Figure 21C and Figure 21F showed that all the paracetamol had been practically dissolved after 60 min regardless of the presence or absence of Eudragit E100 in the formulation. This finding demonstrated that the polymeric additive would not inhibit the release of the drug to such an extent that drug release and in vivo absorption would be inhibited whilst providing the potential of taste masking over a sufficient long period of time.

3.1.3.4.2 Visualization of the internal 3D structure

From analysis of grey values, X-ray CT data from all of the microspheres in the samples were examined. Highly resolved tomographic images of drug crystals and voids in the microspheres after different periods of dissolution test with high quality phase contrast were then derived after 3D reconstructions. Based on the difference of grey value, the matrix of octadecanol and paracetamol crystals in the microspheres had been segmented and extracted respectively. Then, the constructed 3D models of matrices and crystals were colored with different color maps (for matrices, autumn varied smoothly from red, through orange, to yellow; for crystals, jet ranges varied from blue to cyan, yellow, orange and red, indicating the density from low to high) and merged together to show the relative distributions. The morphology and changes over the release phase of all crystals had been shown with the extracted 3D models (Figure 22 and 23).

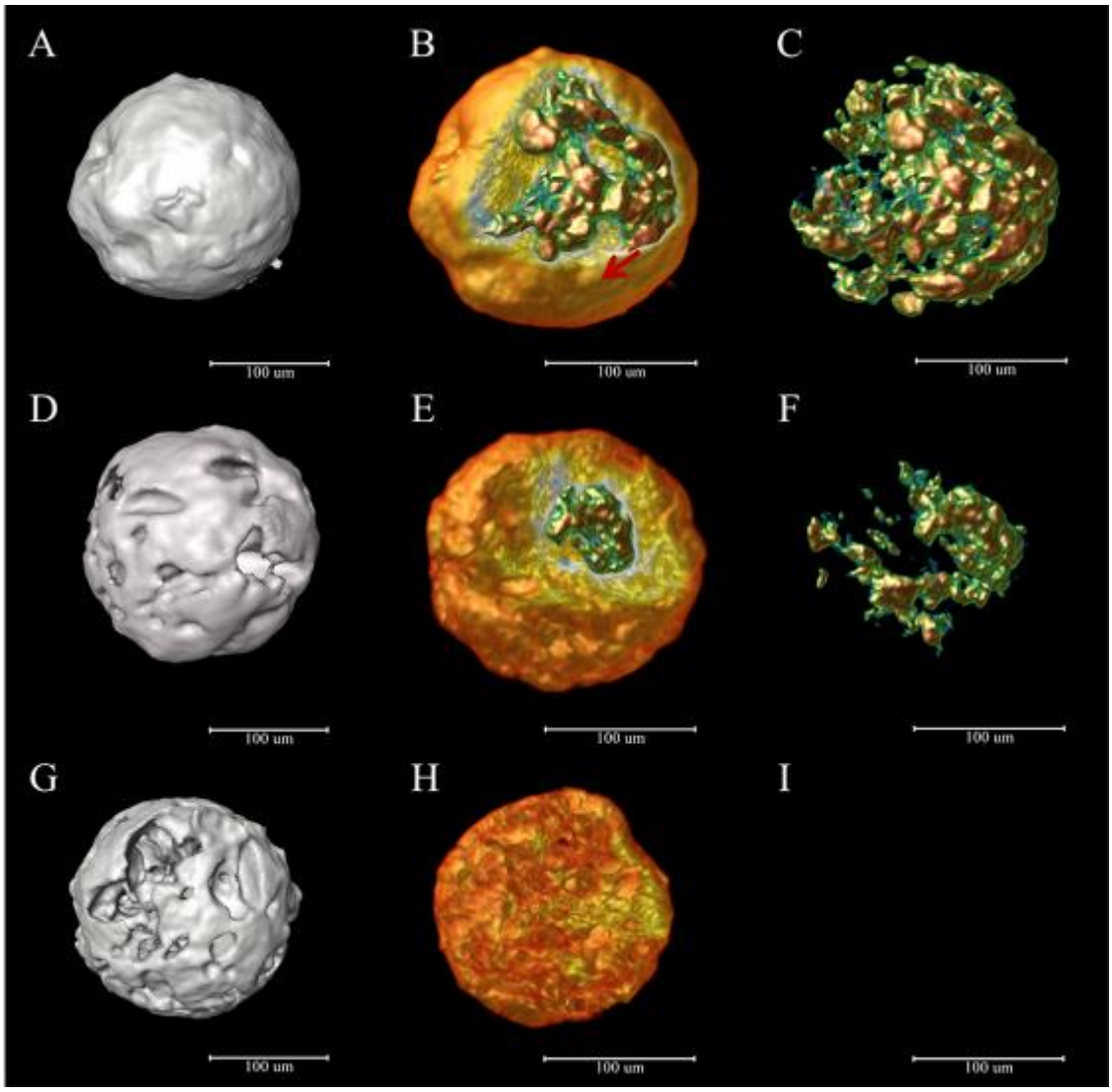

Figure 22 3D X-ray CT images of paracetamol microspheres (F1) at different sampling time (A, B and C are images of F1 at 0 min; D, E and F are images of F1 at 5 min; G, H and I are images of F1 at 60 min; A, D and G are ISO Surface images of complete microspheres; B, E and H are images of microspheres partly split; C, F and I are images of paracetamol crystals extracted from microspheres). Nothing could be seen in image I, because all of the drug crystals have dissolved.

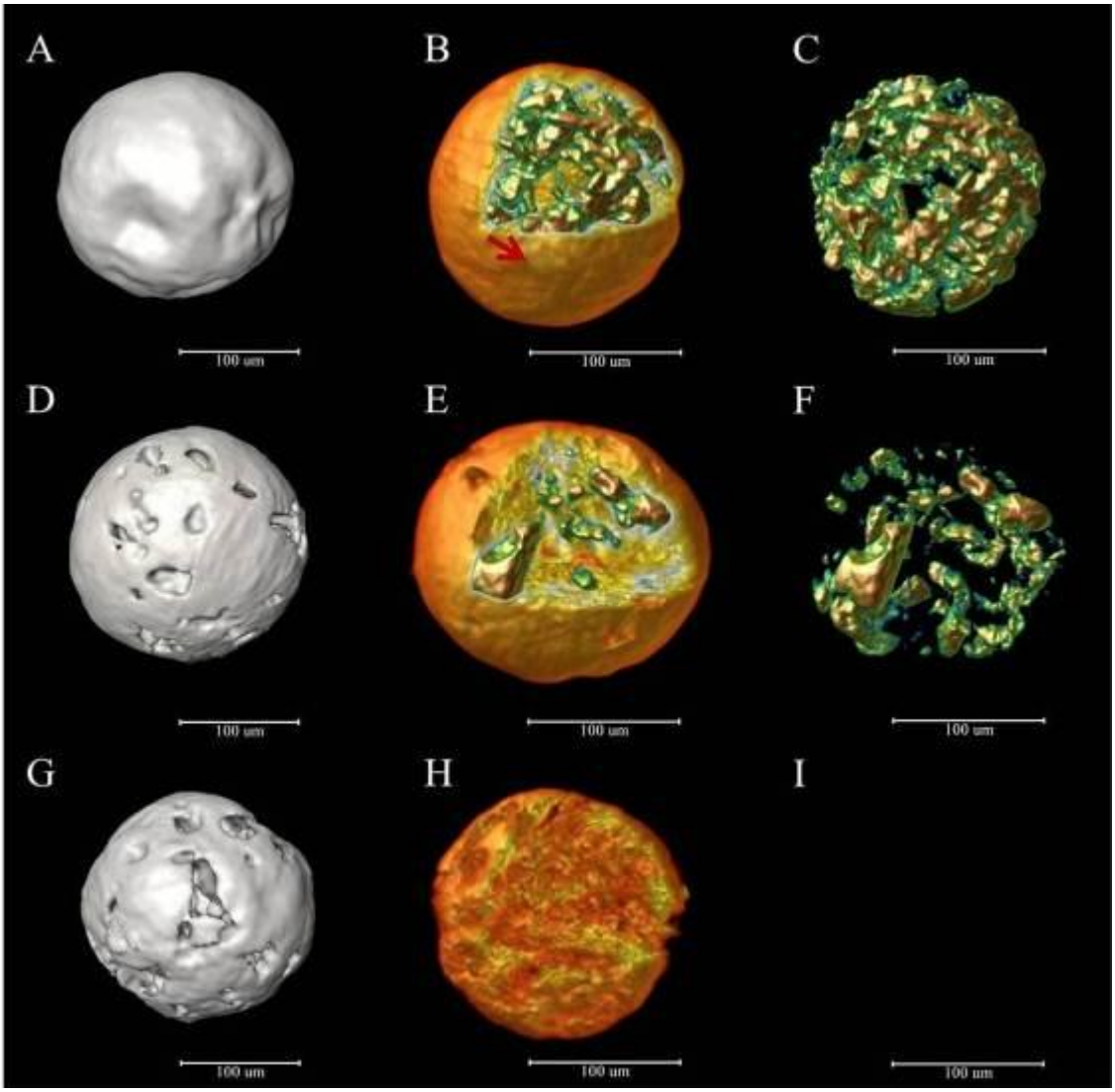

Figure 23 3D X-ray CT images of paracetamol microspheres (F5) at different sampling time (A, B and C are images of F5 at 0 min; D, E and F are images of F5 at 5 min; G, H and I are images of F5 at 60 min; A, D and G are ISO Surface images of complete microspheres; B, E and H are images of microspheres partly split; C, F and I are images of paracetamol crystals extracted from microspheres). Nothing could be seen in image I, because all of the drug crystals have dissolved.

The reconstructed 3D tomographic images of paracetamol microspheres demonstrated that the 3D morphology and distribution of paracetamol crystals embedded in the microsphere were highly variable (Figure 22 and Figure 23). Both irregular, small crystals and long needles were identified mostly embedded

in the microsphere. However, a few small particles and segments of several needle-shaped crystals exposed to the surface of microspheres. Therefore, some protuberances of paracetamol crystals were observed on the surface of microspheres as the red arrows indicated. Comparison between Figure 22A and Figure 23A indicated that before being soaked in the dissolution medium, the original surface of F5 microspheres was smoother than that of F1, due to more hollows and protuberances distributed on the surface of F1 microspheres. This should be the results of the addition of Eudragit E100 in the formulation to increase the viscosity of F5 mixture and influence the ejection process of droplets. The illustrations also showed the surface morphology and internal structural changes of different formulations of paracetamol microspheres after dissolution test. A number of voids distributed around the surface of microspheres and complex interconnecting tunnels were found throughout the microspheres (Figure 22D-I and Figure 23D-I). These findings provided a structural evidence to support the interpretations of drug release profiles discussed above. It was concluded that at the early stage of the dissolution process, exposed paracetamol crystals and segments of the needle crystals dissolved rapidly to leave voids, and then the voids gradually became larger and finally integrated with each other to generate interconnected tunnels. The images also showed that all of the paracetamol crystals had been dissolved or released from the tunnels at 60 min (Figure 22I and Figure 23I).

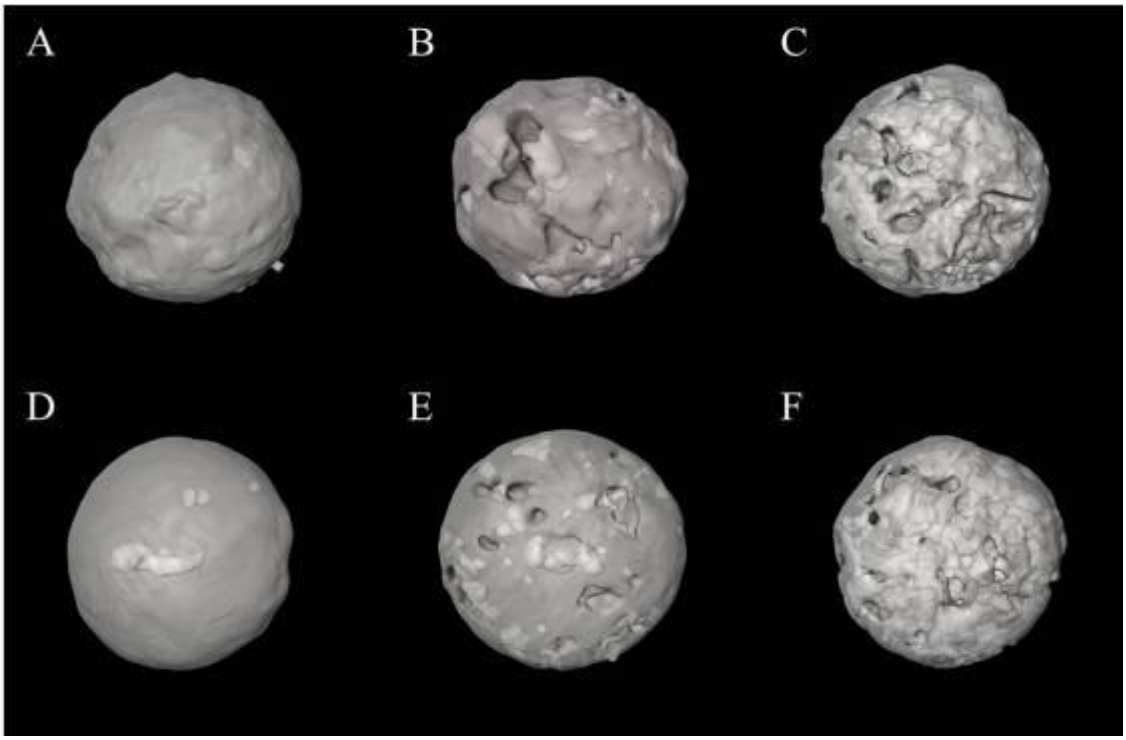

Figure 24 Transparent 3D ISO surface model of paracetamol microspheres at different sampling time (A is the image of F1 at 0 min; B is the image of F1 at 5 min; C is the image of F1 at 60 min; D is the image of F5 at 0 min; E is the image of F5 at 5 min; F is the image of F5 at 60 min)

The transparent 3D ISO surface models showed the surface morphology, the distribution of voids on the surface and the internal tunnels in the microspheres (Figure 24). The original surface of F5 exhibited a smoother surface and inner voids, which might result from the presence of Eudragit E100 with high viscosity and strong film-forming property (Figure 24A and Figure 24D). After 5 minutes dissolution, the crystals on the surface and crystals with protuberances exposed on the surface were dissolved and voids with different depths inside were generated. Compared with F1, the voids in F5 were separated with each other. It was hypothesized that small sized crystals and angular segments of larger crystals on the external surface were completely covered by the Eudragit E100

during processing. Voids formed tunnels and thus internally located and embedded crystals could contact with the dissolution medium.

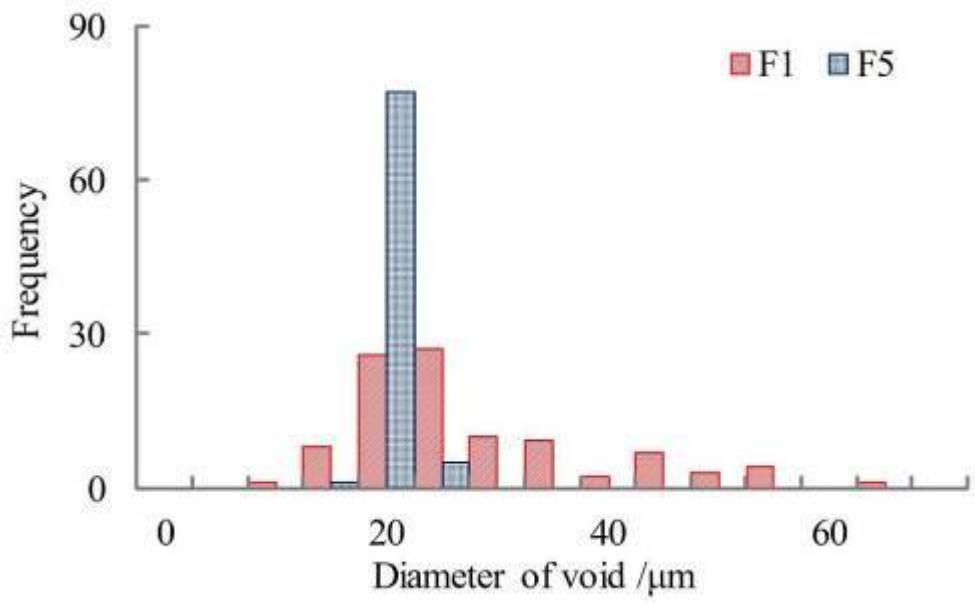

Figure 25 Size distributions of all the pores on the surface of microspheres after dissolution test for 60 minutes (three microspheres had been calculated for each formulation; dotted columns are F1; slashed columns are F5)

However, the voids on the surface of F1 microspheres were obviously larger than those of F5, which was also the same after 60 minutes dissolution with complete release of the paracetamol. In order to quantitatively evaluate the microstructure of the surface, the void diameter distributions have been calculated. All voids distributed on the surface were measured manually with the 3D reconstructed model (Figure 22G and Figure 23G) and three microspheres for each formulation had been calculated. The results showed significant difference between the two formulations (Figure 25), for which the mean void diameter of F5 had a smaller value of 30.81 μm, while the average void diameter of F1 was 39.51 μm. The wider distribution range of F1 indicated the higher morphological irregularity of the voids. This observation was

attributed to Eudragit E100, as the insolubility of Eudragit E100 would lead to a reduction in the degree of hydration and extent of erosion.

After 60 minutes in the dissolution medium, numerous tunnels in the microspheres were interconnected and reached to the surface. The total void volume of F1 and F5 were similar, but voids on the surface of F1 were larger in dimension than F5, indicating that without Eudragit E100 the erosion degree of octadecanol was higher.

These results indicated that an appropriate size of drug crystals is one of the important factors for taste masking for the hydrophobic matrix based microspheres. The oversize crystals of drug raw material are disadvantageous to the coating and coverage by octadecanol and Eudragit E100 generating large tunnels, while the undersized crystals have high dissolution rate, both of which increase free drug concentration in medium or saliva to bring about bitter taste. Besides, the addition of hydrophobic materials with high viscosity, such as Eudragit E100, could significantly benefit taste masking, which is helpful to coat the drug crystals as well as inhibits the release of drug because of its low hydration rate.

3.1.3.4.3 Correlation between structural parameters and drug release

Three microspheres were randomly selected for quantitative analysis of drug content by SR-μCT. The volume ratio of paracetamol in the microsphere had been calculated by segmenting and extracting different materials based on phase contrast images.

The tested volume ratio of paracetamol in microspheres before dissolution test (0 min), described as R_{V0}, which can be obtained from Eq. 26:

$$R_{V0} = \frac{M_{Ace} / \rho_{Ace}}{M_{Ace} / \rho_{Ace} + M_{Oct} / \rho_{Oct} + M_{Eud} / \rho_{Eud}} \quad (26)$$

where M is the mass of various materials in microspheres before dissolution test, and ρ is the density of materials (Ace: Paracetamol, Oct: Octadecanol, Eud: Eudragit E100).

After dissolution testing, the volume ratio of paracetamol in the released microsphere (R_{V1}) can be obtained from Eq. 27:

$$R_{V1} = V_{1Ace} / \left(V_{1Ace} + V_{1Oct} + V_{1Eud}\right) \quad (27)$$

where V1 is the volume of various materials in released microspheres, which could be calculated by Image Pro analyzer 3D.

Also, R_{V1} can be calculated from Eq. 28:

$$R_{V1} = \left(R_{V0} - R_{VR}\right) / \left(1 - R_{VR}\right) \quad (28)$$

where R_{VR} is the volume ratio between released paracetamol and the total volume of microsphere before dissolution test. Here, it is assumed that Eudragit E100 and octadecanol are insoluble in distilled water. Therefore, R_{VR} can be obtained by combining Eq. 27 with 28.

The tested volume ratio between volume of released paracetamol and volume of original paracetamol (R_{VT}) is equal to release percentage (R), which can be obtained from Eq. 29.

$$R = R_{VT} = R_{VR} / R_{V0} \quad (29)$$

Table 8 Comparison of tested and calculated values of drug content and release for F1 and F5 at 0, 5 and 60 min

Formulations		Drug content at 0 min (%)	Drug Release Percentage (%)	
			5 min	60 min
F1	Tested	23.9	53.8±3.0	98.2±2.5
	Calculated by SR-μCT	20.9±2.3	51.7±1.4	99.0±1.4
F5	Tested	21.2	27.3±2.3	99.6±3.0
	Calculated by SR-μCT	17.9±0.8	28.0±4.6	98.4±3.0

The “Calculated by by SR-μCT” drug release percentages for 5 and 60 min were measured by SR-μCT, while the “Tested” drug release percentages for 5 and 60 min were determined by dissolution test. Drug contents in the microspheres at 0 min for “Tested” and “Calculated by SR-μCT” are the volume ratio of the Paracetamol in the microspheres before dissolution test, which were obtained by formula and SR-μCT measurement, respectively. F1: paracetamol taste masking lipid microspheres without Eudragit E100; F5: paracetamol taste masking lipid microspheres with Eudragit E100 (10%, w/w).

From data in Table 8, it was clear that the drug content and release values measured by SR-μCT were in good agreement with experimentally determined data, which demonstrated that SR-μCT can distinguish various materials and accurately calculate their volume in multicomponent microspheres.

3.2 Chemical Distribution on Surface of Taste Masking Lipid Microspheres as Determined by SR-FTIR

In the pharmaceutical sciences, membranes play important roles in masking undesirable tastes. High coating weight is necessary for conventional coating technologies for taste masking, especially for small particles, such as microspheres. Layer-by-layer (LBL) is a flexible coating method to fabricate functional films with precise control of chemical composition and architecture on micro- and nanoscales [173, 174]. This method involves alternative adsorption of oppositely charged polyelectrolytes on substrates. The molecular and interactive multilayers might have important value in control release and taste masking for drugs. In my research, ibuprofen lipid microspheres prepared by octadecanol could mask the bitter taste of the drug to some extent, which were further coated with chitosan (cationic) and gelatin (anionic) by Layer-by-Layer method. LBL films will be applied in modification of the surface of lipid microspheres to obtain satisfactory taste masking effects.

Most reported research into membrane has used scanning electron microscopy (SEM) for observing the structural changes of membranes [175-177]. Combining SEM data with FTIR and differential scanning calorimeter (DSC) techniques, characterization of the effects of the membrane preparation methods on the in vitro release of theophylline through CA membranes has been attempted [178]. With the development of imaging and spectroscopic techniques for the quality control of pharmaceutical products, three-dimensional terahertz pulsed imaging and terahertz time-domain reflection signals have also been applied to investigate coating characteristics of membranes, detecting the

influence of internal physical alterations to the drug release kinetics and obtaining information on both the spatial distribution of the coating thickness and physical alterations impacting the drug release [179]. Magnetic resonance imaging and relaxometry have also been applied to study water transport mechanisms in a commercially available gastrointestinal therapeutic system tablet [180]. Quartz crystal microbalance (QCM) was used to investigate the interaction between anion and cation by measuring shift of crystal oscillator frequency among deposition of each layer to confirm the fabrication of LBL films [181]. However, these reported techniques for examining the structural changes of membranes failed to reveal the spatial chemical distribution simultaneously. FTIR spectroscopy is widely employed to determine the molecular structure and chemical composition of a given sample [182]. Compared with a conventional standard Globar IR source commonly used in an offline laboratory-based FTIR microspectroscopic instrument, the highly collimated synchrotron radiation based FTIR (SR-FTIR) beam essentially offers 100-1000 times higher brightness (defined as the photon flux or power emitted per source area and solid angle) [183]. The SR-FTIR microspectroscopy and imaging are able to provide a higher signal-to-noise ratio at high spatial resolutions and allow for smaller regions within a specimen to be analyzed [184]. Recently, SR-FTIR has been developed as a rapid, direct and non-destructive chemical microprobe with high flux and brightness, and high coherence. SR-FTIR has also been successfully used as a powerful tool to reveal internal chemical structure changes at a cellular or subcellular dimension among various food/ feed and plant/seed tissues [185-188], as well as the quantitative measurement of the distribution and localization of protein/peptide constituents within a single

microsphere made of poly-lactide-coglycolide [189]. Following a thorough literature search, no reports on the direct observation of the chemical distribution in the LBL membranes could be identified. Thus, the existence and distribution of the drug and material of coated film have been determined using SR-FTIR to provide deep understanding of LBL membranes.

3.2.1 Materials

Ibuprofen with purity of 99.9% was provided by Baikegelai Pharmaceutical Co., Ltd., China; chitosan and gelatin were purchased from Jinke Pharmaceutical Excipients Co., Ltd., China； paraffin was purchased from Sinopharm Chemical Reagent Co., Ltd., China. The Synchrotron radiation FTIR mapping scans were carried out at the Shanghai Synchrotron Radiation Facility (SSRF) in Shanghai Institute of Applied Physics, Chinese Academy of Sciences (Shanghai, China). Data were analyzed using the commercially available software OMINIC (9.2.86 Thermo Fisher Scientific, Inc.) and Matlab (R2012a， Math Works, Inc.).

3.2.2 Methods

3.2.2.1 Preparation of ibuprofen lipid microspheres

Ibuprofen lipid microspheres were prepared by the addition of an appropriate amount of Ibuprofen into octadecanol at 60 ^{o}C (1:2, w/w) whilst stirring the system at 1000 rpm to obtain a uniform fusion. The mixture was then immediately poured into the reservoir of a spray gun preheated to 70 ^{o}C in a drying oven and sprayed such that the air dried microspheres at room temperature were collected from stainless steel trays for further research.

3.2.2.2 Preparation of polyelectrolyte coated ibuprofen lipid microspheres

The ibuprofen lipid microspheres were coated with polyelectrolytes by layer-by-layer assembly using vacuum filtration system. The ibuprofen lipid microspheres were placed on gauze or filter paper with Buchner funnel. The Buchner funnel was stopped during the polyelectrolyte adsorption period to ensure consistent contact of polyelectrolyte solution and microspheres. Afterwards vacuum pumping was used to remove the polyelectrolyte solution.

Firstly, the chitosan layer was deposited with addition of chitosan 1% acetic acid solution (1% w/v) into the Buchner funnel. The mixture was then incubated for 0.5 min. Thereafter, the next layer of gelatin (type B with the isoelectric point about 4.5-5.6) water solution (1% w/v) was deposited using the same procedure. The above two steps were identified as ‘one cycle’. Subsequent alternating chitosan and gelatin layers were deposited in an identical way until the desired number of chitosan/gelatin cycles was achieved. Following this the coated samples were oven dried at 40 ºC for 2 h. Control samples were prepared that contained only chitosan or gelatin solutions (both 1% w/v) cycled with the same number of coating layers as used with the LBL method.

3.2.2.3 Short term in vitro drug release test

Short term in vitro drug release tests were conducted in an incubator shaker (ES-60+, Miu Instruments Co., Ltd., China). As a mimic of the microenvironment of the human oral cavity, the release medium selected was buffer (5mL, pH 7.2) and it was monitored at 15, 30 and 60 s. The temperature of the release medium was maintained at 37 ± 0.5 °C and the rotation speed of the incubator shaker was 100 rpm. Aliquots of samples (0.5 mL) were withdrawn at the set

times and replaced with equivalent volumes of fresh medium. The samples withdrawn were filtered (0.22 μm porous membrane filter) and analyzed using a high performance liquid chromatograph system (1260, Agilent, Palo Alto, USA) consisting of a binary pump (G1311C), an auto-sampler (G1329B) and a diode array detector (G4212B). The separation was achieved on a Diamonsil C18 column (5 μm, 150 mm × 4.6 mm) at 40 °C. The mobile phase consisted of sodium acetate buffer (7 mM, pH2.5): acetonitrile (40:60, v/v) and flow rate 1.0 mL/min. A calibration graph showed that the linear concentration range for was 0.5 - 75.0 μg/mL (R = 0.9999). Repeat in vitro experiments were carried out (n= 6).

3.2.2.4 Processing of membranes for SR-FTIR

The uncoated microspheres, microspheres coated with 80 layers of chitosan, microspheres coated with 80 layers of gelatin and microspheres coated with 80 cycles of chitosan and gelatin were poured into melting paraffin and then cooling. Paraffin-embedded samples were sectioned into 10-μm-thick sections.

The LBL membrane powder sample was peeled by gently scraping the surface of microspheres coated with 80 cycles of chitosan and gelatin (as described in section 3.2.2.2) using a razor blade.

3.2.2.5 SR-FTIR microspectroscopy and imaging

SR-FTIR microspectroscopy was performed with the BL01B beamline at SSRF (Shanghai Synchrotron Radiation Facility). Spectra of the samples were recorded on a Nicolet Continuμm XL microscope (ThermoFisher Scientific, Inc.) equipped with a 250× 250 μm^2 liquid nitrogen cooled MCT/A detector, a

32X/NA0.65 Schwarzschild objective, a motorized knife-edge aperture, and a Prior XYZ motorized stage and coupled with Nicolet 6700 spectrometer (Thermo Fisher Scientific, Inc.) equipped with a Michelson interferometer. Following sample preparation using KBr tableting, FTIR spectra of chitosan, gelatin, octadecanol and ibuprofen were recorded in transmission mode between 600 cm^{-1} and 4000 cm^{-1}, with 128 scans at 4 cm^{-1} resolution, and 10 μm × 10 μm aperture dimension.

The cross section of paraffin-embedded microspheres were mapped on the BaF_2 substrate and scanned in transmission mode between 600 cm^{-1} and 4000 cm^{-1}, with 64 scans at 4 cm^{-1} resolution, aperture dimension was set at 10 μm × 10 μm. With step size of 10 μm, totally spectra of 20 × 18 points were captured.

3.2.3 Results and discussion

3.2.3.1 Short term in vitro drug release

It could be observed that ibuprofen released more slowly from coated microspheres than uncoated microspheres. And the optimal sustained-release behaviour was observed for microspheres coated by 80 cycles of chitosan and gelatin, indicating unpleasant taste could be masked by microspheres coated by LBL membranes (Figure 26).

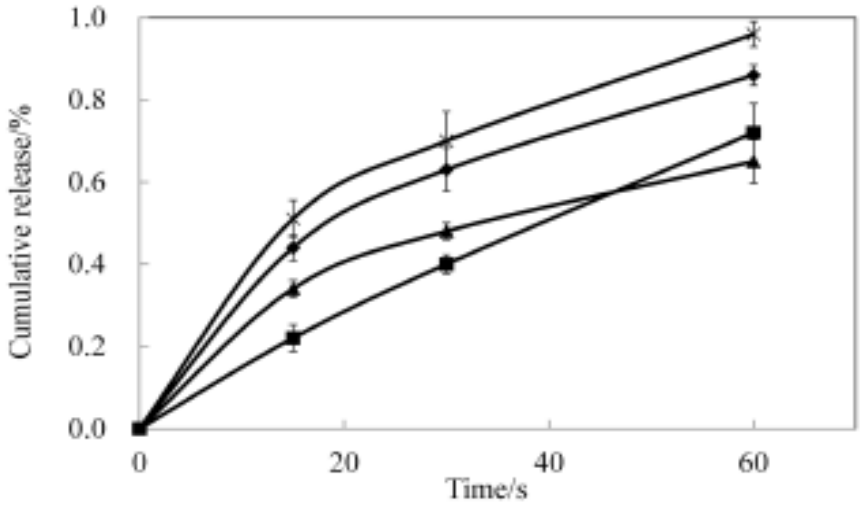

Figure 26 The release profiles of microspheres coated with different materials in PBS pH 7.2 (◆: Gelatin, ■: Gelatin and chitosan, ▲: Chitosan and ╳: Lipid microspheres without coating)

3.2.3.2 Specific bands of SR-FTIR spectra

Chitosan, gelatin, ibuprofen, octadecanol and the membranes powder samples were characterized by SR-FTIR (Figure 26). For the spectra of ibuprofen, the absorption peak at 1723 cm^{-1} corresponded to the C=O stretching vibration. For the spectra of octadecanol and chitosan, 1462 cm^{-1} and 1653 cm^{-1} were characteristic peaks of these compounds respectively. The band at 1548 cm^{-1} corresponded to the amide Ⅱ infrared band, which could be identified as a characteristic peak of gelatin.

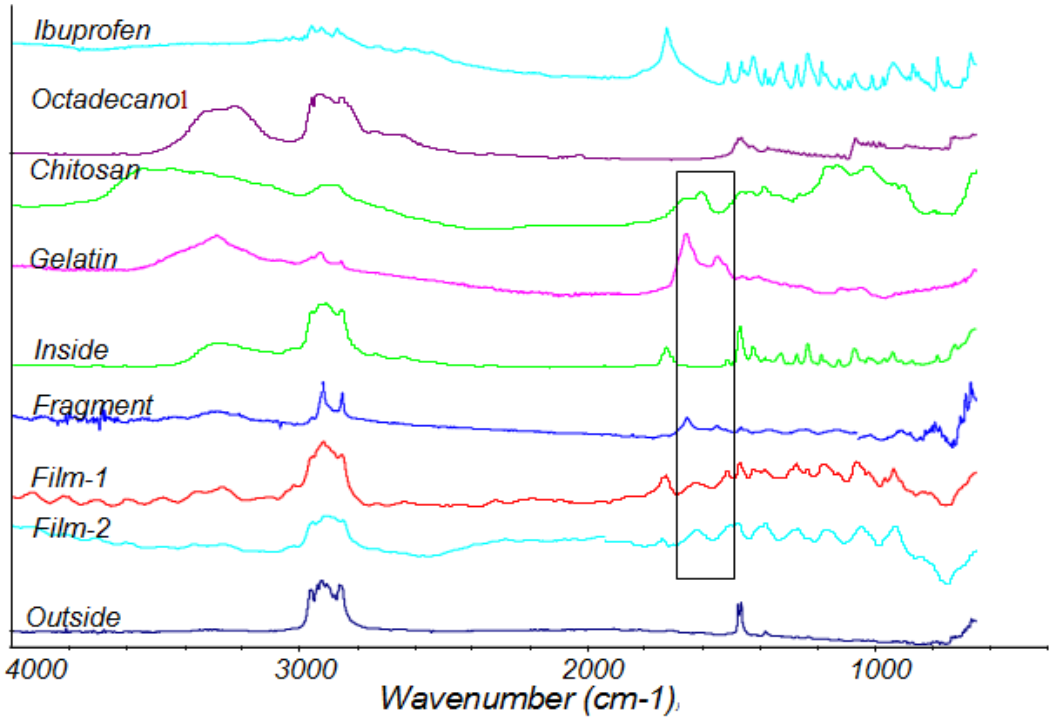

Figure 27 Following spectral bands were identified, ibuprofen, 1713-1733 cm^{-1} (C=O bond); octadecanol,1452-1472 cm^{-1} (-CH_2 bond); chitosan; 1590-1610 cm^{-1} and 1650-1670 cm^{-1}; gelatin, 1538-1558 cm^{-1} and 1643-1663 cm^{-1} (amide band).

The characteristic absorption of gelatin and chitosan could be observed in the membrane powder, from the surface of the particles and the film, which are primarily responsible for taste masking effect.

Absorption peaks at 1538-1558 cm^{-1} and 1650-1670 cm^{-1} were observed for the membrane peeled from the surface of LBL coated microspheres, which might indicated that gelatin and chitosan were deposited on the surface of microspheres by LBL coating.

3.2.3.3 Analysis of SR-FTIR mapping

Results in Figure 28 show that SR-FTIR scans reveal significant differences from inside to the outside surface of microsphere (1-14 scanning points). In

particular, specific peaks of gelatin and chitosan could not been observed in the interior of microspheres (1-12 scanning points). Data extracted from mapping image demonstrated that the absorptions of chitosan and gelatin existed on the surface of the coated microspheres. As the scanning progressed to the edge of the microsphere cross section (13 scanning points), specific intense peaks of gelatin and chitosan were observed (see Figure 28). At the 14 scanning point, specific peak (double peaks) of gelatin could be observed (Figure 28). It was confirmed that as scanning from the interior to the surface, the ibuprofen signature remained unchanged but decreased in intensity near the surface film. At the surface of the microspheres, both of drug and excipients can be distinguished, because the spatial resolution of mapping was 10 μm which was limited by the size of light spot (10 μm*10μm), while thickness of film might be less than 10 μm.

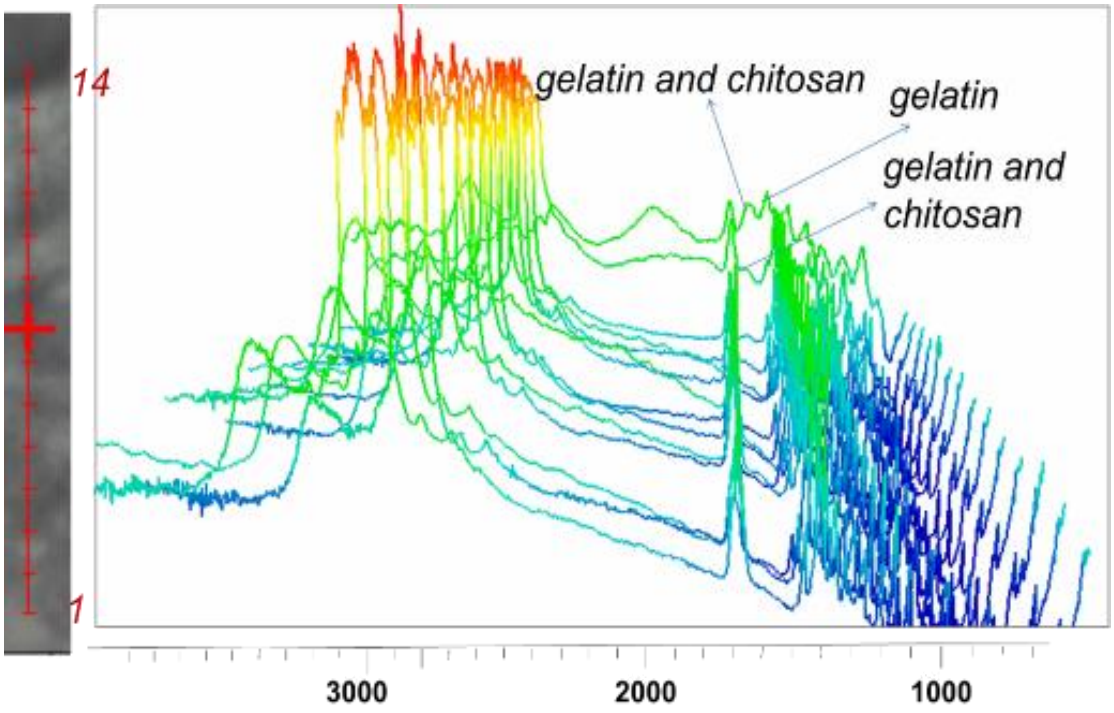

Figure 28 Synchrotron radiation-based Fourier-transform infrared spectra of 14 scanning points (numbered from inside to outside of microspheres as 1 to 14) gelatin

For the microspheres coated with 80 cycles of chitosan and gelatin, the mapping was analyzed using OMNIC software (ThermoFisher Scientific Company) to get the integral distribution of chitosan and gelatin. Integral distribution showed the evidence for existence and the location of chitosan (a) and gelatin (b) (Figure 29). The distribution of chitosan and gelatin characterized as a band absorption showing a section of the sliced film. Neither chitosan nor gelatin could be observed inside or outside of the microspheres, both compounds only appearing on the microsphere surface (Figure 29). The results show that chitosan and gelatin were deposited on the microsphere surface and formed a film to the benefit of taste masking the microsphere entrapped ibuprofen.

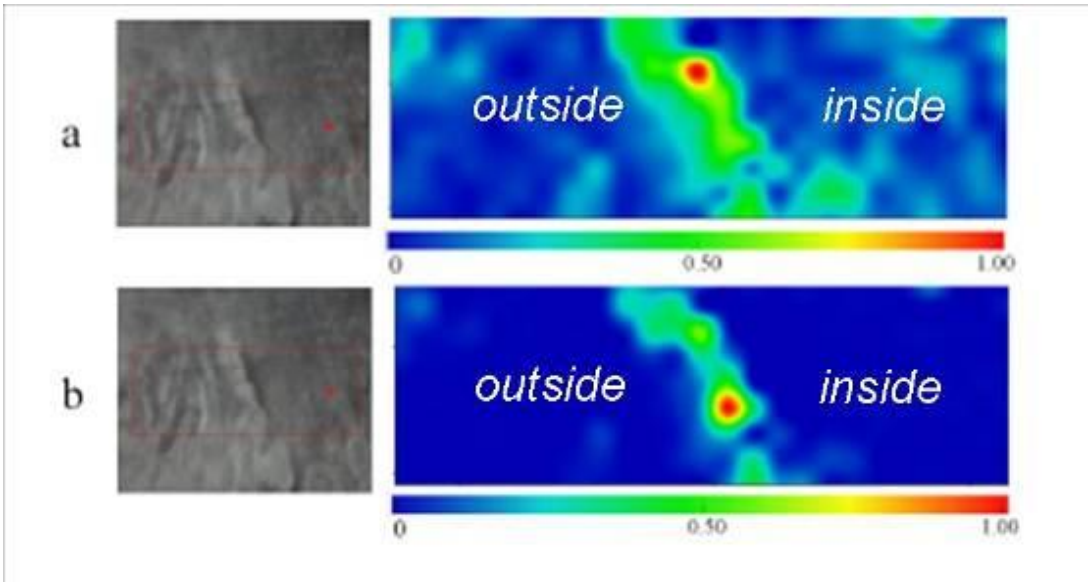

Figure 29 Distribution of chitosan and gelatin as determined by integral distribution map. a: The integral distribution map gained from the specific peak of chitosan in scanning area; b: The integral distribution map was obtained from the specific FT-IR peak of gelatin in the scanned area. The red outlined areas for (a) and (b) (left image) indicate the area imaged by synchrotron radiation-based. The Fourier-transform infrared spectromicroscopy integral distributions of chitosan or gelatin (right images)

After data smoothing and automatic baseline correction, the ratio map analysis was carried out by MATLAB. From ratio mapping of gelatin (1590-1610 cm^{-1}) / octadecanol (1452-1472 cm^{-1}) and chitosan (1643-1663cm^{-1}) / octadecanol (1452-1472cm^{-1}), the absorption band distributed along with the microsphere surface confirming the presence of gelatin and chitosan on the film (b and c). In contrast chitosan and gelatin could not been clearly observed in microspheres coated only by chitosan (d) or gelatin (e) (Figure 30). Further, for chitosan, the weak FT-IR absorbance in the map indicates a limited amount of adhesion on the surface probably as a result of the high viscosity of chitosan. The ionic interaction of ibuprofen with gelatin and chitosan made possible by the layer-by-layer coating procedure will facilitate entrapment of the bitter tasting drug within

the microsphere. The net result is prevention of ibuprofen release with concomitant masking of the unpleasant taste of ibuprofen formulated in this way.

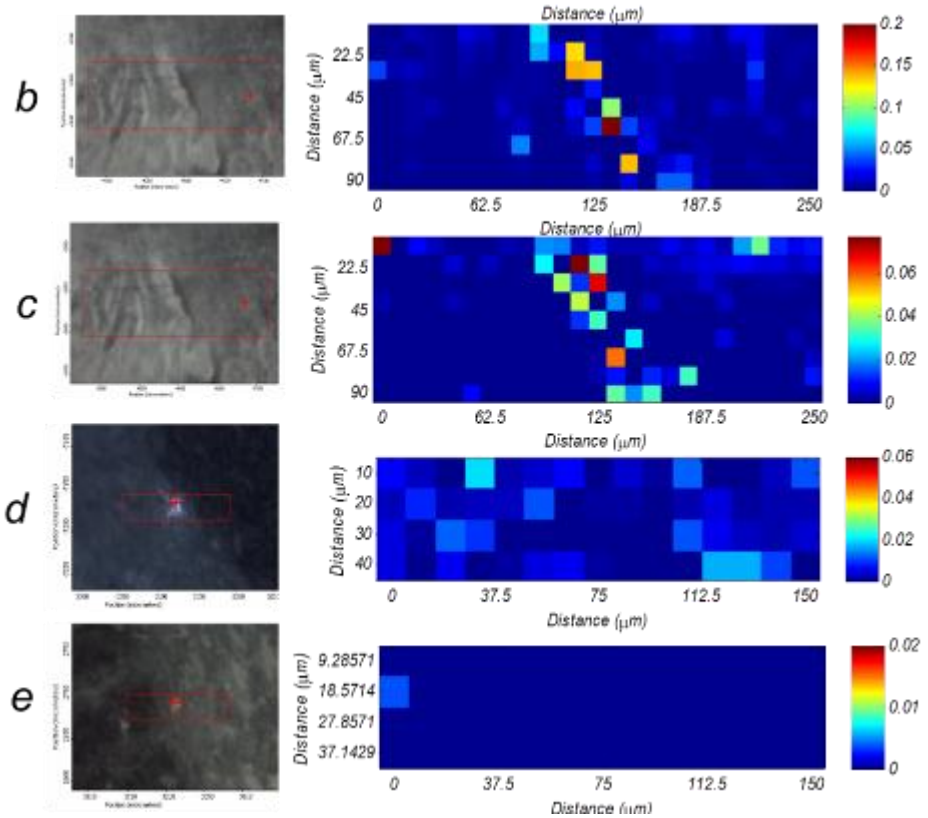

Figure 30 Chemical distributions by ratio analysis showing intensity map of gelatin and chitosan within microspheres (red most intense distribution, dark blue least intense distribution). b: Distribution of chitosan obtained by ratio between chitosan/octadecanol on the microspheres coated with gelatin and chitosan; c: Distribution of gelatin obtained by ratio between gelatin/octadecanol on the microspheres coated with gelatin and chitosan. d: Distribution of chitosan obtained by ratio between chitosan/octadecanol on the microspheres coated with chitosan. e: Distribution of chitosan obtained by gelatin / octadecanol on the microspheres coated with gelatin. The red boxes indicated the area imaged by synchrotron radiation-based Fourier-transform infrared spectromicroscopy (left); distributions of chitosan or gelatin (right).

The results indicate that ibuprofen formulated as lipid microspheres prepared by melting method (see section 3.2.2.1) does effectively entrap this drug and could

therefore help mask ibuprofen’s unpleasant taste. Coating the lipid microspheres with chitosan (cationic) and gelatin (anionic) using a layer-by-layer self-assembly (LBL) coating should further support entrapment of ibuprofen facilitating further a bitter taste masking effect. The release percentage of drugs in short time (1 min) was utilized as an indicator for the taste-masking, and it confirmed the LBL coating inhibited the release of model drug of ibuprofen.

Chapter 4 Conclusions

The presented research has established a relationship between association and dissociation rates (as measured by K_a and K_d respectively) and bitter taste masking of drugs complexed with cyclodextrins. Using both SPRi and HPAC methodologies to determine K_a, K_d and their derivative constants allowed the development of a model useful to the prediction of bitter taste masking. More specifically the results successfully established a relationship between the kinetic interactions of HP-β-CD complexed with a panel of drugs and generated model data which was proved sufficiently accurate by 10-fold cross-validation. The relationship model could be used to predict the bitter taste masking of drugs more generally. The model provided basis and strategy to taste masking formulation design by drug-CD inclusions. On the other hand, HPAC method was also used to investigate the relationship between taste masking effects and kinetic constants between drugs and cyclodextrins, by which the model was established and similar to that established by SPRi in a great extent. The results demonstrated that both of the two methods could be used to investigate and provide new vision that the molecular kinetic interaction between cyclodextrins and bitter drugs could be correlated with the taste masking effects. The model based on SPRi showed better accuracy and precision in comparison with HPAC due to the intrinsic and different properties of the two methods, namely, drugs or cyclodextrins immobilized on stationary phase influenced binding interactions. There were also other limits, such as organic solvents and flow rate of mobile phase, for the applications of HPAC. At the same time, the relationship of taste

masking and host-guest kinetic interaction of cyclodextrins and bitter drugs was further successfully applied to optimize formulation.

As for microstructure, SR-μCT and SR-FTIR were utilized to investigate the relationship of fine microstructure of microsphere and mechanism of taste masking. As a powerful structural characterization tool, SR-μCT was used to study the internal fine structure of the paracetamol loaded microspheres and the calculated amounts of drug released, revealing the primary influence of Eudragit E100 on particle morphology, structure and taste masking effects. Quantitative structure analysis indicated that precise evaluation of the changes in fine structure for particle formulations could contribute to explain the mechanism and illustrate the structural change during a short period of time to simulate the taste masking. Thus the analysis provided knowledge and deep understanding of the role of particle morphology and their structural assembly in microspheres for a rational design and manufacturing taste masking products. On the other hand, SR-FTIR has been applied to investigate the material distributions on the cross section of microspheres and film coating. Characteristic absorptions of the compositions were obtained by SR-FTIR single spectrum scanning. The distributions of the drug and materials in coated films were determined by SR-FTIR mapping. The FTIR absorptions of chitosan and gelatin on the surface of lipid microspheres were examined to verify the deposition of chitosan and gelatin on the surface and film formation using SR-FTIR ratio analysis. Whilst microspheres coated only by chitosan or gelatin did not show the characteristic absorption peaks, which confirmed the effects of ionic interaction on the film formation process. Therefore, the method of SR-FTIR established for the study of distribution of materials in coated film provided a new choice for researches

on membranes/films in taste masking drug delivery systems and pharmaceutical preparations.

In conclusion, this research illustrates the relationships between bitter taste and molecular interactions and structures from micro scales, namely, molecular kinetic basis of interaction between bitter drugs and CD as well as microstructural basis of particles formulation for taste masking. Novel methodologies and strategies based on SPRi and SR are provided to investigate bitter taste masking from molecular interactions and microstructures, deepening knowledge and view to understand and formulations design for taste masking.

Reference

[1] R.L. Rousseff, Bitterness in foods and beverages, in: Developments in food science, Elsevier, Amsterdam, 1990.

[2] J.G. Brand, Biophysics of taste, in: G.K.B. Beauchamp, L. (Ed.) Tasting and smelling. Handbook of perception and cognition, Academic Press, San Diego, 1997.

[3] S.S. Schiffman, Taste quality and neural coding: Implications from psychophysics and neurophysiology, Physiol Behav, 69 (2000) 147-159.

[4] H.T. Lawless, Evidence for neural inhibition in bitter-sweet taste mixtures, J Comp Physiol Psychol, 93 (1979) 538-547.

[5] W. Meyerhof, Beisiegel, U., Joost, H., Oral and Extraoral Bitter Taste Receptors, Sensory and Metabolic Control of Energy Balance, (2010) 88.

[6] P.A.S. Breslin, G.K. Beauchamp, Suppression of bitterness by sodium: Variation among bitter taste stimuli, Chem Senses, 20 (1995) 609-623.

[7] M.W. Behrens M., Chemosensory Systems in Mammals, Fishes, and Insects, Springer, Verlag Berlin Heidelberg, 2009.

[8] M. Behrens, W. Meyerhof, Bitter taste receptors and human bitter taste perception, Cell Mol Life Sci, 63 (2006) 1501-1509.

[9] E. Adler, M.A. Hoon, K.L. Mueller, J. Chandrashekar, N.J.P. Ryba, C.S. Zuker, A novel family of mammalian taste receptors, Cell, 100 (2000) 693-702.

[10] W. Meyerhof, Elucidation of mammalian bitter taste, Rev Physiol Bioch P, 154 (2005) 37-72.

[11] J. Chandrashekar, K.L. Mueller, M.A. Hoon, E. Adler, L.X. Feng, W. Guo, C.S. Zuker, N.J.P. Ryba, T2Rs function as bitter taste receptors, Cell, 100 (2000) 703-711.

[12] J.D. Boughter, S. Raghow, T.M. Nelson, S.D. Munger, Inbred mouse strains C57BL/6J and DBA/2J vary in sensitivity to a subset of bitter stimuli, Bmc Genet, 6 (2005).

[13] L.M. Bartoshuk, Comparing sensory experiences across individuals: Recent psychophysical advances illuminate genetic variation in taste perception, Chem Senses, 25 (2000) 447-460.

[14] B. Bufe, P.A.S. Breslin, C. Kuhn, D.R. Reed, C.D. Tharp, J.P. Slack, U.K. Kim, D. Drayna, W. Meyerhof, The molecular basis of individual differences in phenylthiocarbamide and propylthiouracil bitterness perception, Curr Biol, 15 (2005) 322-327.

[15] U. Kim, S. Wooding, D. Ricci, L.B. Jorde, D. Drayna, Worldwide haplotype diversity and coding sequence variation at human bitter taste receptor loci, Hum Mutat, 26 (2005) 199-204.

[16] U.K. Kim, E. Jorgenson, H. Coon, M. Leppert, N. Risch, D. Drayna, Positional cloning of the human quantitative trait locus underlying taste sensitivity to phenylthiocarbamide, Science, 299 (2003) 1221-1225.

[17] A.N. Pronin, H. Xu, H. Tang, L. Zhang, Q. Li, X. Li, Specific Alleles of bitter receptor genes influence human sensitivity to the bitterness of aloin and saccharin, Curr Biol, 17 (2007) 1403-1408.

[18] N. Soranzo, B. Bufe, P.C. Sabeti, J.F. Wilson, M.E. Weale, R. Marguerie, W. Meyerhof, D.B. Goldstein, Positive selection on a high-sensitivity allele of the human bitter-taste receptor TAS2R16, Curr Biol, 15 (2005) 1257-1265.

[19] S. Wooding, U.K. Kim, M.J. Bamshad, J. Larsen, L.B. Jorde, D. Drayna, Natural selection and molecular evolution in PTC, a bitter-taste receptor gene, Am J Hum Genet, 74 (2004) 637-646.

[20] Z.e.a. Ayenew, Trends in pharmaceutical taste masking technologies: a patent review, Recent Pat Drug Deliv Formul, 3 (2009) 26-39.

[21] J.R. Luber, Film coated tablet compositions having enhanced disintegration characteristics, US5807580, 1998.

[22] J.C. Chen, Bunick, F.J., McNally, G., Fast dissolving/disintegrating coating compositions, US8367104, 2013.

[23] P.E. Bertelsen, Olsen, P.M., Nielsen, C.M., Tolleshanaug, M.W., Melt granulation of a composition containing a calcium-containing compound, US2009068268, 2009.

[24] R. Dabre, Nagaprasad, V., Malik, R., Taste masked compositions of erythromycin a and derivatives thereof, EP1492504 , 2007.

[25] F. Stroppolo, Ciccarello, F., Milani, R., Bellorini, L., Oral pharmaceutical compositions containing cyclodextrins as taste masking agent. US20040115258 2004.

[26] S. Dehli, Ptricia, A., Taste masking of phenolics using citrus flavours, US6235267, 2001.

[27] B. Michael, Katharina, R., Jakob, L.D., Susanne, P., Specific vanillyl lignanes and their use as taste enhancers, EP2517574, 2012.

[28] H. Jaffe, Microencapsulation process, US4272398, 1981.

[29] S. Freitas, H.P. Merkle, B. Gander, Microencapsulation by solvent extraction/evaporation: reviewing the state of the art of microsphere preparation process technology, J Control Release, 102 (2005) 313-332.

[30] A. Berger, Mattern, C., Process for masking the taste of substances by microencapsulation, EP1362583, 2003.

[31] D. Bora, P. Borude, K. Bhise, Taste Masking by Spray-Drying Technique, Aaps Pharmscitech, 9 (2008) 1159-1164.

[32] X.L. Hu, Y.B. Li, E.J. Zhang, X.Z. Wang, M. Xing, Q. Wang, J. Lei, H. Huang, Preparation and Evaluation of Orally Disintegrating Tablets Containing Taste-Masked Microcapsules of Berberine Hydrochloride, Aaps Pharmscitech, 14 (2013) 29-37.

[33] U. Stange, C. Fuhrling, H. Gieseler, Taste masking of naproxen sodium granules by fluid-bed coating, Pharm Dev Technol, 19 (2014) 137-147.

[34] Y. Katsuragi, Y. Sugiura, C. Lee, K. Otsuji, K. Kunihara, Selective-Inhibition of Bitter Taste of Various Drugs by Lipoprotein, Pharmaceut Res, 12 (1995) 658-662.

[35] D. Felisaz, Jacquier, Y., Powder sweetener for human food, WO/1999/030573, 1999.

[36] E.J. Kim, M.K. Chun, J.S. Jang, I.H. Lee, K.R. Lee, H.K. Choi, Preparation of a solid dispersion of felodipine using a solvent wetting method, Eur J Pharm Biopharm, 64 (2006) 200-205.

[37] F.A. Cabrera, Solid phase dispersion of quinolone or naphthyridonecarboxylic acids, US7112336, 2006.

[38] P. Becourt, Chauvin, J., Schwabe, D., Pharmaceutical formulation having a masked taste and method for the production thereof, UA7138138, 2007.

[39] C.P. Yewale, M.N. Rathi, G.G. Kore, G.V. Jadhav, M.P. Wagh, Formulation and development of taste masked fast-disintegrating tablets (FDTs) of Chlorpheniramine maleate using ion-exchange resins, Pharm Dev Technol, 18 (2013) 367-376.

[40] V.K. Arora, Isloor, S., Kakumanu, V.K., Taste masked dosage forms of bitter tasting anti-retroviral drugs, EP2519264, 2012.

[41] D. Shukla, S. Chakraborty, S. Singh, B. Mishra, Fabrication and Evaluation of Taste Masked Resinate of Risperidone and Its Orally Disintegrating Tablets, Chem Pharm Bull, 57 (2009) 337-345.

[42] K. Bhise, S. Shaikh, D. Bora, Taste mask, design and evaluation of an oral formulation using ion exchange resin as drug carrier, Aaps Pharmscitech, 9 (2008) 557-

562.

[43] R.E. Tully, Oral liquid antidepressant solution, US6040301, 2000.

[44] J. Szejtli, L. Szente, Elimination of bitter, disgusting tastes of drugs and foods by cyclodextrins, Eur J Pharm Biopharm, 61 (2005) 115-125.

[45] P.P. Shah, R.C. Mashru, Palatable reconstitutable dry suspension of artemether for flexible pediatric dosing using cyclodextrin inclusion complexation, Pharm Dev Technol, 15 (2010) 276-285.

[46] N. Ono, Y. Miyamoto, T. Ishiguro, K. Motoyama, F. Hirayama, D. Iohara, H. Seo, S. Tsuruta, H. Arima, K. Uekama, Reduction of Bitterness of Antihistaminic Drugs by Complexation with beta-Cyclodextrins, J Pharm Sci-Us, 100 (2011) 1935-1943.

[47] M. Stojanov, R. Wimmer, K.L. Larsen, Study of the Inclusion Complexes Formed Between Cetirizine and alpha-, beta-, and gamma-Cyclodextrin and Evaluation on Their Taste-Masking Properties, J Pharm Sci-Us, 100 (2011) 3177-3185.

[48] H.T. Arima H, Motoyama K., Improvement of the bitter taste of drugs by complexation with cyclodextrins: Applications, evaluations and mechanisms, Ther Deliv, 3 (2012) 633-644.

[49] I. Ullah, G.J. Wyley, Palatable oral suspension and method, US7175856 2007.

[50] N. Kashid, Chouhan, P., Mukherji, G., Taste masked phamaceutical composition for oral solid dosage form and process for preparing the same using magnesium aluminium silicate, US20100226979, 2010.

[51] G. Crini, Review: A History of Cyclodextrins, Chem Rev, 114 (2014) 10940-10975.

[52] A. Rescifina, U. Chiacchio, D. Iannazzo, A. Piperno, G. Romeo, beta-Cyclodextrin and Caffeine Complexes with Natural Polyphenols from Olive and Olive Oils: NMR, Thermodynamic, and Molecular Modeling Studies, J Agr Food Chem, 58 (2010) 11876-11882.

[53] N.J. Gaudette, G.J. Pickering, The efficacy of bitter blockers on health-relevant bitterants, J Funct Foods, 4 (2012) 177-184.

[54] N. Funasaki, I. Uratsuji, T. Okuno, S. Hirota, S. Neya, Masking mechanisms of bitter taste of drugs studied with ion selective electrodes, Chem Pharm Bull, 54 (2006) 1155-1161.

[55] N. Funasaki, T. Sumiyoshi, S. Ishikawa, S. Neya, Solution structures of 1 : 1 complexes of oxyphenonium bromide with beta- and gamma-cyclodextrins, Mol

Pharmaceut, 1 (2004) 166-172.
[56] V. Anand, M. Kataria, V. Kukkar, V. Saharan, P.K. Choudhury, The latest trends in the taste assessment of pharmaceuticals, Drug Discov Today, 12 (2007) 257-265.
[57] Z.B. Chen, J.H. Wu, Y. Zhao, F. Xu, Y.Q. Hu, Recent advances in bitterness evaluation methods, Anal Methods-Uk, 4 (2012) 599-608.
[58] Y. Vlasov, A. Legin, A. Rudnitskaya, C. Di Natale, A. D'Amico, Nonspecific sensor arrays ("electronic tongue") for chemical analysis of liquids (IUPAC Technical Report), Pure Appl Chem, 77 (2005) 1965-1983.
[59] Q.S. Chen, J.W. Zhao, Z.M. Guo, X.Y. Wang, Determination of caffeine content and main catechins contents in green tea (Camellia sinensis L.) using taste sensor technique and multivariate calibration, J Food Compos Anal, 23 (2010) 353-358.
[60] D. Braeken, D.R. Rand, A. Andrei, R. Huys, M.E. Spira, S. Yitzchaik, J. Shappir, G. Borghs, G. Callewaert, C. Bartic, Glutamate sensing with enzyme-modified floating-gate field effect transistors, Biosens Bioelectron, 24 (2009) 2384-2389.
[61] A. Legin, A. Rudnitskaya, D. Clapham, B. Seleznev, K. Lord, Y. Vlasov, Electronic tongue for pharmaceutical analytics: quantification of tastes and masking effects, Anal Bioanal Chem, 380 (2004) 36-45.
[62] K. Woertz, C. Tissen, P. Kleinebudde, J. Breitkreutz, Performance qualification of an electronic tongue based on ICH guideline Q2, J Pharmaceut Biomed, 51 (2010) 497-506.
[63] K. Woertz, C. Tissen, P. Kleinebudde, J. Breitkreutz, A comparative study on two electronic tongues for pharmaceutical formulation development, J Pharmaceut Biomed, 55 (2011) 272-281.
[64] M. Maniruzzaman, D. Douroumis, An in-vitro-in-vivo taste assessment of bitter drug: comparative electronic tongues study, J Pharm Pharmacol, 67 (2015) 43-55.
[65] T. Uchida, M. Yoshida, M. Hazekawa, T. Haraguchi, H. Furuno, M. Teraoka, H. Ikezaki, Evaluation of palatability of 10 commercial amlodipine orally disintegrating tablets by gustatory sensation testing, OD-mate as a new disintegration apparatus and the artificial taste sensor, J Pharm Pharmacol, 65 (2013) 1312-1320.
[66] M. Yoshida, T. Haraguchi, T. Uchida, Bitterness Evaluation of Acidic Pharmaceutical Substances (NSAIDs) Using a Taste Sensor, Chem Pharm Bull, 62 (2014) 1252-1258.
[67] A. Fini, V. Bergamante, G.C. Ceschel, C. Ronchi, C.A.F. Moraes, Fast dispersible/slow releasing ibuprofen tablets, Eur J Pharm Biopharm, 69 (2008) 335-341.

[68] F.M. Mady, A.E. Abou-Taleb, K.A. Khaled, K. Yamasaki, D. Iohara, T. Ishiguro, F. Hirayama, K. Uekama, M. Otagiri, Enhancement of the Aqueous Solubility and Masking the Bitter Taste of Famotidine Using Drug/SBE-beta-CyD/Povidone K30 Complexation Approach, J Pharm Sci-Us, 99 (2010) 4285-4294.

[69] H. Tasaki, T. Yoshida, A. Maeda, M. Katsuma, K. Sako, Effects of physicochemical properties of salting-out layer components on drug release, Int J Pharm, 376 (2009) 13-21.

[70] T. Yoshida, H. Tasaki, A. Maeda, M. Katsuma, K. Sako, T. Uchida, Salting-out taste-masking system generates lag time with subsequent immediate release, Int J Pharm, 365 (2009) 81-88.

[71] T. Yoshida, H. Tasaki, A. Maeda, M. Katsuma, K. Sako, T. Uchida, Mechanism of controlled drug release from a salting-out taste-masking system, J Control Release, 131 (2008) 47-53.

[72] F.Q. Li, R.R. Ji, X. Chen, B.M. You, Y.H. Pan, J.C. Su, Cetirizine Dihydrochloride Loaded Microparticles Design Using Ionotropic Cross-linked Chitosan Nanoparticles by Spray-drying Method, Arch Pharm Res, 33 (2010) 1967-1973.

[73] J. Vaassen, K. Bartscher, J. Breitkreutz, Taste masked lipid pellets with enhanced release of hydrophobic active ingredient, Int J Pharm, 429 (2012) 99-103.

[74] D.A. Chiappetta, A.M. Carcaboso, C. Bregni, M. Rubio, G. Bramuglia, A. Sosnik, Indinavir-Loaded pH-Sensitive Microparticles for Taste Masking: Toward Extemporaneous Pediatric Anti-HIV/AIDS Liquid Formulations with Improved Patient Compliance, Aaps Pharmscitech, 10 (2009) 1-6.

[75] S. Mohammad, S.N.H. Shah, B. Nasir, Q. Khan, A. Aslam, R. Riaz, M. Sher, S. Karim, G. Murtaza, Efficacious formulation of anti-malarial dry suspension for pediatric use, Afr J Pharm Pharmaco, 6 (2012) 2629-2633.

[76] Q.Y. Tan, L. Zhang, L.K. Zhang, Y.Z. Teng, J.Q. Zhang, Design and Evaluation of an Economic Taste-Masked Dispersible Tablet of Pyridostigmine Bromide, a Highly Soluble Drug with an Extremely Bitter Taste, Chem Pharm Bull, 60 (2012) 1514-1521.

[77] R.K. Palmer, D. Long, F. Brennan, T. Buber, R. Bryant, F.R. Salemme, A High Throughput In Vivo Assay for Taste Quality and Palatability, Plos One, 8 (2013).

[78] J.K. Gore-Langton, S.M. Flax, R.L. Pomfrey, B.B. Wetzell, A.L. Riley, Measures of the aversive effects of drugs: A comparison of conditioned taste and place aversions,

Pharmacol Biochem Behav, 134 (2015) 99-105.

[79] A.C. Spector, S.L. Kopka, Rats fail to discriminate quinine from denatonium: implications for the neural coding of bitter-tasting compounds, J Neurosci, 22 (2002) 1937-1941.

[80] A.M. Torregrossa, G.C. Loney, J.C. Smith, L.A. Eckel, Examination of the perception of sweet- and bitter-like taste qualities in sucralose preferring and avoiding rats, Physiol Behav, 140 (2015) 96-103.

[81] Z.H. Wang, Z.X. He, L. Zhang, H.H. Zhang, M.M. Zhang, X.G. Wen, G.L. Quan, X.T. Huang, X. Pan, C.B. Wu, Optimization of a doxycycline hydroxypropyl-β-cyclodextrin inclusion complex based on computational modeling, Acta Pharmaceutica Sinica B, 3 (2013) 130-139.

[82] A. Atipairin, S. Sawatdee, Inclusion complexes between sildenafil citrate and cyclodextrins enhance drug solubility, Asian Journal of Pharmaceutical Sciences, 11 (2016) 104-105.

[83] E.M.M. Del Valle, Cyclodextrins and their uses: a review, Process Biochem, 39 (2004) 1033-1046.

[84] L. Szente, J. Szejtli, Cyclodextrins as food ingredients, Trends Food Sci Tech, 15 (2004) 137-142.

[85] G. Astray, C. Gonzalez-Barreiro, J.C. Mejuto, R. Rial-Otero, J. Simal-Gandara, A review on the use of cyclodextrins in foods, Food Hydrocolloid, 23 (2009) 1631-1640.

[86] A. Dahan, J.M. Miller, A. Hoffman, G.E. Amidon, G.L. Amidon, The Solubility-Permeability Interplay in Using Cyclodextrins as Pharmaceutical Solubilizers: Mechanistic Modeling and Application to Progesterone, J Pharm Sci-Us, 99 (2010) 2739-2749.

[87] H.Y. Li, J. Sun, Y.J. Wang, X.F. Sui, L. Sun, J.W. Zhang, Z.G. He, Structure-based in silico model profiles the binding constant of poorly soluble drugs with beta-cyclodextrin, Eur J Pharm Sci, 42 (2011) 55-64.

[88] K.A. Connors, The stability of cyclodextrin complexes in solution, Chemical reviews, 97 (1997) 1325-1357.

[89] G. Astray, J.C. Mejuto, J. Morales, R. Rial-Otero, J. Simal-Gandara, Factors controlling flavors binding constants to cyclodextrins and their applications in foods, Food Res Int, 43 (2010) 1212-1218.

[90] T. Loftsson, S.B. Vogensen, M.E. Brewster, F. Konradsdottir, Effects of cyclodextrins on drug delivery through biological membranes, J Pharm Sci-Us, 96 (2007) 2532-2546.
[91] T. Loftsson, M.E. Brewster, Pharmaceutical applications of cyclodextrins: effects on drug permeation through biological membranes, J Pharm Pharmacol, 63 (2011) 1119-1135.
[92] R.A. Copeland, D.L. Pompliano, T.D. Meek, Opinion - Drug-target residence time and its implications for lead optimization, Nat Rev Drug Discov, 5 (2006) 730-739.
[93] R.M. Zhang, F. Monsma, Binding kinetics and mechanism of action: toward the discovery and development of better and best in class drugs, Expert Opin Drug Dis, 5 (2010) 1023-1029.
[94] M. Novo, D. Granadero, J. Bordello, W. Al-Soufi, Host-guest association studied by fluorescence correlation spectroscopy, J Incl Phenom Macro, 70 (2011) 259-268.
[95] C. Bohne, Supramolecular dynamics studied using photophysics, Langmuir, 22 (2006) 9100-9111.
[96] W. Al-Soufi, B. Reija, S. Felekyan, C.A.M. Seidel, M. Novo, Dynamics of supramolecular association monitored by fluorescence correlation spectroscopy, Chemphyschem, 9 (2008) 1819-1827.
[97] G.G. Mironov, V. Okhonin, S.I. Gorelsky, M.V. Berezovski, Revealing Equilibrium and Rate Constants of Weak and Fast Noncovalent Interactions, Anal Chem, 83 (2011) 2364-2370.
[98] H.Y. Li, J.W. Ge, T. Guo, S. Yang, Z.G. He, P. York, L.X. Sun, X. Xu, J.W. Zhang, Determination of the kinetic rate constant of cyclodextrin supramolecular systems by high performance affinity chromatography, Journal of Chromatography A, 1305 (2013) 139-148.
[99] V. Singh, Z. Li, X.T. Zhou, X.N. Xu, J.H. Xu, A. Nand, H.J. Wen, H.Y. Li, J.S. Zhu, J.W. Zhang, High-throughput measurement of drug-cyclodextrin kinetic rate constants by a small molecule microarray using surface plasmon resonance imaging, Rsc Adv, 6 (2016) 3213-3218.
[100] J. Homola, S.S. Yee, G. Gauglitz, Surface plasmon resonance sensors: review, Sensor Actuat B-Chem, 54 (1999) 3-15.
[101] S. Scarano, M. Mascini, A.P.F. Turner, M. Minunni, Surface plasmon resonance imaging for affinity-based biosensors, Biosens Bioelectron, 25 (2010) 957-966.

[102] E.J. Jeong, Y.S. Jeong, Y. Park, S.Y. Yi, J. Ahn, S.J. Chung, M. Kim, B.H. Chung, Directed immobilization of DNA-binding proteins on a cognate DNA-modified chip surface, J Biotechnol, 135 (2008) 16-21.

[103] B.H. Garcia, R.M. Goodman, Use of surface plasmon resonance imaging to study viral RNA : protein interactions, J Virol Methods, 147 (2008) 18-25.

[104] W. Liu, Y. Chen, M.D. Yan, Surface plasmon resonance imaging of limited glycoprotein samples, Analyst, 133 (2008) 1268-1273.

[105] C.F. Grant, V. Kanda, H. Yu, D.R. Bundle, M.T. McDermott, Optimization of Immobilized Bacterial Disaccharides for Surface Plasmon Resonance Imaging Measurements of Antibody Binding, Langmuir, 24 (2008) 14125-14132.

[106] N.O. K. Abe, H. Nagase, T. Endo, H. Ueda, Evaluation of the abilities of γ-cyclodextrin to form complexes by surface plasmon resonance with a Biacore ® system, J. Inclusion Phenom. Macrocyclic Chem, 70 (2011) 385-388.

[107] A.N. V. Singh, Sarita, J. Zhang, J. Zhu, Non-specific adsorption of serum and cell lysate on 3D biosensor platforms: A comparative study based on SPRi, Arab J Chem, 25 (2015) DOI: 10.1016/j.arabjc.2015.1006.1037.

[108] N. Kanoh, M. Kyo, K. Inamori, A. Ando, A. Asami, A. Nakao, H. Osada, SPR imaging of photo-cross-linked small-molecule arrays on gold, Anal Chem, 78 (2006) 2226-2230.

[109] V. Singh, A. Nand, Sarita, Universal screening platform using three-dimensional small molecule microarray based on surface plasmon resonance imaging, Rsc Adv, 5 (2015) 87259-87265.

[110] A. Legin, A. Rudnitskaya, L. Lvova, Y. Vlasov, C. Di Natale, A. D'Amico, Evaluation of Italian wine by the electronic tongue: recognition, quantitative analysis and correlation with human sensory perception, Anal Chim Acta, 484 (2003) 33-44.

[111] Y. Kobayashi, M. Habara, H. Ikezazki, R.G. Chen, Y. Naito, K. Toko, Advanced Taste Sensors Based on Artificial Lipids with Global Selectivity to Basic Taste Qualities and High Correlation to Sensory Scores, Sensors-Basel, 10 (2010) 3411-3443.

[112] D.S. Dyminski, L.G. Paterno, H.H. Takeda, H.M.A. Bolini, L.H.C. Mattoso, L.M.B. Candido, Correlation between human panel and electronic tongue responses on the analysis of commercial sweeteners, Sens Lett, 4 (2006) 403-408.

[113] J.H. Thorngate, A.C. Noble, Sensory Evaluation of Bitterness and Astringency of 3r(-)-Epicatechin and 3s(+)-Catechin, J Sci Food Agr, 67 (1995) 531-535.

[114] H. Hotelling, Analysis of a complex of statistical variables into principal components, J Educ Psychol, 24 (1933) 498-520.

[115] M.N. Nounou, B.R. Bakshi, P.K. Goel, X.T. Shen, Bayesian principal component analysis, J Chemometr, 16 (2002) 576-595.

[116] R. L.Rouseff, Bitterness in Foods and Beverages (Developments in Food Science), 25 (1990).

[117] P.P. Shah, R.C. Mashru, Formulation and Evaluation of Taste Masked Oral Reconstitutable Suspension of Primaquine Phosphate, AAPS PharmSciTech, 9 (2008) 1025-1030.

[118] A.R. Patel, P.R. Vavia, Preparation and evaluation of taste masked famotidine formulation using drug/beta-cyclodextrin/polymer ternary complexation approach, AAPS PharmSciTech, 9 (2008) 544-550.

[119] Y. Wei, M.P. Nedley, S.B. Bhaduri, X. Bredzinski, S.H. Boddu, Masking the bitter taste of injectable lidocaine HCl formulation for dental procedures, AAPS PharmSciTech, 16 (2015) 455-465.

[120] M.A. Khan, K.S. Wu, A. Gupta, FDA: Contribution to developing pediatric formulations and transatlantic collaboration, Int J Pharmaceut, 435 (2012) 146-148.

[121] B. Basu, K.R. Aviya, A. Bhattacharya, Development and characterization of mouth dissolving tablets of prednisolone, Journal of Pharmaceutical Investigation, 44 (2014) 79-102.

[122] M. Tomita, S. Shimamura, K. Kawase, Y. Fukuwatari, M. Takase, W. Bellamy, K. Yamauchi, H. Wakabayashi, Y. Tokita, B. Uein, W.R. Bellamy, Antibacterial agent comprising decomposition products of lactoferrin with chelate e.g. EDTA alcohol and/or antibiotic e.g. penicillin, also useful against yeast and fungi - with chelate e.g. EDTA alcohol and/or antibiotic e.g. penicillin, also useful against yeast and fungi, in, Morinaga Milk Ind Co Ltd (Morg-C) Morinaga Milk Ind Co Ltd (Morg-C), pp. 629347-A629341:.

[123] K.V. Rao, J.C. Pati, A. Gupta, A. Kumar, K. Dondilkar, Oral pharmaceutical composition used as antibiotic highly active against a wide range of gram-positive and gram-negative micro-organisms, comprises cefuroxime axetil, cyclodextrin or its derivative, and excipients, in, NECTAR LIFESCIENCES LTD (NECT-Non-standard), pp. 25.

[124] M. Preis, C. Eckert, O. Hausler, J. Breitkreutz, A comparative study on solubilizing

and taste-masking capacities of hydroxypropyl-beta-cyclodextrin and maltodextrins with high amylose content, Sensor Actuat B-Chem, 193 (2014) 442-450.

[125] B. Loun, D.S. Hage, Chiral separation mechanisms in protein-based HPLC columns. 2. Kinetic studies of (R)- and (S)-warfarin binding to immobilized human serum albumin, Anal Chem, 68 (1996) 1218-1225.

[126] J. Yang, D.S. Hage, Effect of mobile phase composition on the binding kinetics of chiral solutes on a protein-based high-performance liquid chromatography column: interactions of D- and L-tryptophan with immobilized human serum albumin, J Chromatogr A, 766 (1997) 15-25.

[127] A.M. Talbert, G.E. Tranter, E. Holmes, P.L. Francis, Determination of drug-plasma protein binding kinetics and equilibria by chromatographic profiling: exemplification of the method using L-tryptophan and albumin, Anal Chem, 74 (2002) 446-452.

[128] J.E. Schiel, C.M. Ohnmacht, D.S. Hage, Measurement of drug-protein dissociation rates by high-performance affinity chromatography and peak profiling, Anal Chem, 81 (2009) 4320-4333.

[129] Z. Tong, J.E. Schiel, E. Papastavros, C.M. Ohnmacht, Q.R. Smith, D.S. Hage, Kinetic studies of drug-protein interactions by using peak profiling and high-performance affinity chromatography: examination of multi-site interactions of drugs with human serum albumin columns, J Chromatogr A, 1218 (2011) 2065-2071.

[130] Z. Tong, D.S. Hage, Characterization of interaction kinetics between chiral solutes and human serum albumin by using high-performance affinity chromatography and peak profiling, J Chromatogr A, 1218 (2011) 6892-6897.

[131] J. Chen, J.E. Schiel, D.S. Hage, Noncompetitive peak decay analysis of drug-protein dissociation by high-performance affinity chromatography, J Sep Sci, 32 (2009) 1632-1641.

[132] M.J. Yoo, D.S. Hage, Use of peak decay analysis and affinity microcolumns containing silica monoliths for rapid determination of drug-protein dissociation rates, J Chromatogr A, 1218 (2011) 2072-2078.

[133] M.J. Yoo, D.S. Hage, High-throughput analysis of drug dissociation from serum proteins using affinity silica monoliths, J Sep Sci, 34 (2011) 2255-2263.

[134] M.A. Nelson, A. Moser, D.S. Hage, Biointeraction analysis by high-performance affinity chromatography: Kinetic studies of immobilized antibodies, J Chromatogr B

Analyt Technol Biomed Life Sci, 878 (2010) 165-171.
[135] E. Pfaunmiller, A.C. Moser, D.S. Hage, Biointeraction analysis of immobilized antibodies and related agents by high-performance immunoaffinity chromatography, Methods, 56 (2012) 130-135.
[136] D.S. Hage, R.R. Walters, H.W. Hethcote, Split-peak affinity chromatographic studies of the immobilization-dependent adsorption kinetics of protein A, Anal Chem, 58 (1986) 274-279.
[137] H. Li, J. Ge, T. Guo, S. Yang, Z. He, P. York, L. Sun, X. Xu, J. Zhang, Determination of the kinetic rate constant of cyclodextrin supramolecular systems by high performance affinity chromatography, J Chromatogr A, 1305 (2013) 139-148.
[138] C. Wang, J. Ge, J. Zhang, T. Guo, L. Chi, Z. He, X. Xu, P. York, L. Sun, H. Li, Multianalyte determination of the kinetic rate constants of drug-cyclodextrin supermolecules by high performance affinity chromatography, J Chromatogr A, 1359 (2014) 287-295.
[139] H.Y.L. J.W. Zhang, L.X. Sun, C.F Wang, Determination of the kinetic rate constant of cyclodextrin supramolecular systems by high-performance affinity chromatography, in: S. Reichelt (Ed.) Affinity Chromatography, Methods. Mol. Biol, Springer, New York, 2015.
[140] F.C. Denizot, M.A. Delaage, Statistical theory of chromatography: new outlooks for affinity chromatography, Proc Natl Acad Sci U S A, 72 (1975) 4840-4843.
[141] J.E. Schiel, D.S. Hage, Kinetic studies of biological interactions by affinity chromatography, J Sep Sci, 32 (2009) 1507-1522.
[142] R.L. Carrier, L.A. Miller, I. Ahmed, The utility of cyclodextrins for enhancing oral bioavailability, J Control Release, 123 (2007) 78-99.
[143] R.A. Copeland, D.L. Pompliano, T.D. Meek, Drug-target residence time and its implications for lead optimization, Nat Rev Drug Discov, 5 (2006) 730-739.
[144] H. Lu, P.J. Tonge, Drug-target residence time: critical information for lead optimization, Curr Opin Chem Biol, 14 (2010) 467-474.
[145] R. Zhang, F. Monsma, Binding kinetics and mechanism of action: toward the discovery and development of better and best in class drugs, Expert Opin Drug Discov, 5 (2010) 1023-1029.
[146] Y. Nitanai, Y. Agata, Y. Iwao, S. Itai, A novel mathematical model considering change of diffusion coefficient for predicting dissolution behavior of acetaminophen

from wax matrix dosage form, Int J Pharm, 428 (2012) 82-90.
[147] K. Shiino, Y. Iwao, A. Miyagishima, S. Itai, Optimization of a novel wax matrix system using aminoalkyl methacrylate copolymer E and ethylcellulose to suppress the bitter taste of acetaminophen, Int J Pharm, 395 (2010) 71-77.
[148] F. Podczeck, S.R. Rahman, J.M. Newton, Evaluation of a standardised procedure to assess the shape of pellets using image analysis, Int J Pharmaceut, 192 (1999) 123-138.
[149] Z. Ayenew, V. Puri, L. Kumar, A.K. Bansal, Trends in pharmaceutical taste masking technologies: a patent review, Recent patents on drug delivery & formulation, 3 (2009) 26-39.
[150] M.N. Singh, K.S. Hemant, M. Ram, H.G. Shivakumar, Microencapsulation: A promising technique for controlled drug delivery, Research in pharmaceutical sciences, 5 (2010) 65-77.
[151] R. Sheshala, N. Khan, Y. Darwis, Formulation and optimization of orally disintegrating tablets of sumatriptan succinate, Chemical & pharmaceutical bulletin, 59 (2011) 920-928.
[152] D. Shukla, S. Chakraborty, S. Singh, B. Mishra, Fabrication and evaluation of taste masked resinate of risperidone and its orally disintegrating tablets, Chemical & pharmaceutical bulletin, 57 (2009) 337-345.
[153] C.A. Lorck, P.C. Grunenberg, H. Junger, A. Laicher, Influence of process parameters on sustained-release theophylline pellets coated with aqueous polymer dispersions and organic solvent-based polymer solutions, European Journal of Pharmaceutics and Biopharmaceutics, 43 (1997) 149-157.
[154] T. Yajima, N. Umeki, S. Itai, Optimum spray congealing conditions for masking the bitter taste of clarithromycin in wax matrix, Chemical & pharmaceutical bulletin, 47 (1999) 220-225.
[155] P.A.C. Gane, C.J. Ridgway, E. Barcelo, Analysis of pore structure enables improved tablet delivery systems, Powder Technol, 169 (2006) 77-83.
[156] K.A. Mehta, M.S. Kislalioglu, W. Phuapradit, A.W. Malick, N.H. Shah, Effect of formulation and process variables on porosity parameters and release rates from a multi unit erosion matrix of a poorly soluble drug, Journal of Controlled Release, 63 (2000) 201-211.

[157] S. Yang, X.Z. Yin, C.F. Wang, H.Y. Li, Y. He, T.Q. Xiao, L.X. Sun, J.S. Li, P. York, J. He, J.W. Zhang, Release Behaviour of Single Pellets and Internal Fine 3D Structural Features Co-define the In Vitro Drug Release Profile, Aaps J, 16 (2014) 860-871.

[158] M. Tange, Y. Hattori, M. Otsuka, M. Yoshida, J. Haginaka, T. Uchida, Comparison of the dissolution rate of ceftriaxone sodium preparations for injection, Chemical & pharmaceutical bulletin, 61 (2013) 1121-1129.

[159] S. Shah, S. Madan, S. Agrawal, Formulation and evaluation of microsphere based oro dispersible tablets of itopride hcl, Daru : journal of Faculty of Pharmacy, Tehran University of Medical Sciences, 20 (2012) 24.

[160] L. Hu, J. Pan, C. Liu, H. Xu, L. Luo, Preparation, characterization and taste-masking properties of microspheres containing azithromycin, The Journal of pharmacy and pharmacology, 61 (2009) 1631-1635.

[161] K. Malik, G. Arora, I. Singh, Taste masked microspheres of ofloxacin: formulation and evaluation of orodispersible tablets, Scientia pharmaceutica, 79 (2011) 653-672.

[162] Y.D. Yan, J.S. Woo, J.H. Kang, C.S. Yong, H.G. Choi, Preparation and evaluation of taste-masked donepezil hydrochloride orally disintegrating tablets, Biological & pharmaceutical bulletin, 33 (2010) 1364-1370.

[163] J. Xu, L.L. Bovet, K. Zhao, Taste masking microspheres for orally disintegrating tablets, Int J Pharmaceut, 359 (2008) 63-69.

[164] S. Qi, D. Deutsch, D.Q.M. Craig, An investigation into the mechanisms of drug release from taste-masking fatty acid microspheres, Journal of pharmaceutical sciences, 97 (2008) 3842-3854.

[165] X. Yin, H. Li, R. Liu, J. Chen, J. Ji, J. Chen, Q. Shao, T. Xiao, P. York, Y. He, J. Zhang, Fractal structure determines controlled release kinetics of monolithic osmotic pump tablets, J Pharm Pharmacol, 65 (2013) 953-959.

[166] H. Li, X. Yin, J. Ji, L. Sun, Q. Shao, P. York, T. Xiao, Y. He, J. Zhang, Microstructural investigation to the controlled release kinetics of monolith osmotic pump tablets via synchrotron radiation X-ray microtomography, Int J Pharm, 427 (2012) 270-275.

[167] R. Liu, X. Yin, H. Li, Q. Shao, P. York, Y. He, T. Xiao, J. Zhang, Visualization and quantitative profiling of mixing and segregation of granules using synchrotron radiation X-ray microtomography and three dimensional reconstruction, Int J Pharm, 445 (2013) 125-133.

[168] S. Noguchi, R. Kajihara, Y. Iwao, Y. Fujinami, Y. Suzuki, Y. Terada, K. Uesugi, K. Miura, S. Itai, Investigation of internal structure of fine granules by microtomography using synchrotron X-ray radiation, Int J Pharmaceut, 445 (2013) 93-98.

[169] Y.Q. Ren, C. Chen, R.C. Chen, G.Z. Zhou, Y.D. Wang, T.Q. Xiao, Optimization of image recording distances for quantitative X-ray in-line phase contrast imaging, Opt Express, 19 (2011) 4170-4181.

[170] P. Spanne, C. Raven, I. Snigireva, A. Snigirev, In-line holography and phase-contrast microtomography with high energy x-rays, Phys Med Biol, 44 (1999) 741-749.

[171] T. Gureyev, S. Mohammadi, Y. Nesterets, C. Dullin, G. Tromba, Accuracy and precision of reconstruction of complex refractive index in near-field single-distance propagation-based phase-contrast tomography, J Appl Phys, 114 (2013).

[172] Y.D. Wang, Y.S. Yang, I. Cole, A. Trinchi, T.Q. Xiao, Investigation of the microstructure of an aqueously corroded zinc wire by data-constrained modelling with multi-energy X-ray CT, Mater Corros, 64 (2013) 180-184.

[173] J. Hernandez-Montelongo, V.F. Nascimento, D. Murillo, T.B. Taketa, P. Sahoo, A.A. de Souza, M.M. Beppu, M.A. Cotta, Nanofilms of hyaluronan/chitosan assembled layer-by-layer: An antibacterial surface for Xylella fastidiosa, Carbohydr Polym, 136 (2016) 1-11.

[174] N. Xiang, Lyu, Y, Narsimhan G, Characterization of fish oil in water emulsion produced by layer by layer deposition of soy b-conglycinin and high methoxyl pectin, Food Hydrocoll, 52 (2016) 678-689.

[175] A.A. Ali, Sayed, O.M., Development and characterization of ketorolac tromethamine osmotic pump tablets, J. Drug Delivery Sci. Technol, 23 (2013) 275-281.

[176] Z.A. Khan, R. Tripathi, B. Mishra, Design and evaluation of enteric coated microporous osmotic pump tablet (ECMOPT) of quetiapine fumarate for the treatment of psychosis, Acta Pol Pharm, 69 (2012) 1125-1136.

[177] R.B. Patel, G.N. Patel, H.R. Patel, M.M. Patel, Inlay osmotic pump tablets containing metformin and glipizide, Drug Dev Ind Pharm, 37 (2011) 1244-1252.

[178] G. Asman, Akcay, E., Effect of membrane preparation methods on the release of theophylline through CA membranes at in-vitro conditions, J. Macromol. Sci. A, 51 (2014) 326-338.

[179] V. Malaterre, M. Pedersen, J. Ogorka, R. Gurny, N. Loggia, P.F. Taday, Terahertz

pulsed imaging, a novel process analytical tool to investigate the coating characteristics of push-pull osmotic systems, Eur J Pharm Biopharm, 74 (2010) 21-25.

[180] A.L. Broadbent, R.J. Fell, S.L. Codd, K.A. Lightley, S. Konagurthu, D.G. Koehler-King, J.D. Seymour, Magnetic resonance imaging and relaxometry to study water transport mechanisms in a commercially available gastrointestinal therapeutic system (GITS) tablet, Int J Pharm, 397 (2010) 27-35.

[181] A.C. Pinheiro, A.I. Bourbon, M.A. Cerqueira, E. Maricato, C. Nunes, M.A. Coimbra, A.A. Vicente, Chitosan/fucoidan multilayer nanocapsules as a vehicle for controlled release of bioactive compounds, Carbohydr Polym, 115 (2015) 1-9.

[182] C. Petibois, M. Piccinini, M.C. Guidi, A. Marcelli, Facing the challenge of biosample imaging by FTIR with a synchrotron radiation source, Journal of synchrotron radiation, 17 (2010) 1-11.

[183] W.D. Duncan, G.P. Williams, Infrared synchrotron radiation from electron storage rings, Appl Opt, 22 (1983) 2914.

[184] G.L. Carr, Reffner, J.A.,Williams, G.P., Performance of an infrared microspectrometer at the Nsls, Rev. Sci. Instrum, 66 (1995) 1490-1492.

[185] H.Y.N. Holman, Martin, M.C., McKinney, W.R, Tracking chemical changes in a live cell: biomedical applications of SR-FTIR spectromicroscopy, Spectrosc. Int. J, 17 (2003) 139-159.

[186] A. Marcelli, A. Cricenti, W.M. Kwiatek, C. Petibois, Biological applications of synchrotron radiation infrared spectromicroscopy, Biotechnol Adv, 30 (2012) 1390-1404.

[187] L.M. Miller, P. Dumas, Chemical imaging of biological tissue with synchrotron infrared light, Biochimica et biophysica acta, 1758 (2006) 846-857.

[188] L.M. Miller, Q. Wang, R.J. Smith, H. Zhong, D. Elliott, J. Warren, A new sample substrate for imaging and correlating organic and trace metal composition in biological cells and tissues, Analytical and bioanalytical chemistry, 387 (2007) 1705-1715.

[189] Wang, M., Lu, X., Yin, X., Tong, Y., Peng,W., Wu, L., Li, H., Yang, Y., Gu, J., Xiao, T., Chen, M., Zhang, J., Synchrotron radiation-based Fourier-transform infrared spectromicroscopy for characterization of the protein/peptide distribution in single microspheres, Acta. Pharm. Sin. B 5 (2015) 270–276.

Appendix

SPRi Data of interactions between 485 drugs and HP-β-CD

Drug name	K_a(1/Ms)	K_d(1/s)	K(1/M)
Azaguanine-8	4810	1.03E-05	4.69E+08
Meticrane	7660	1.94E-04	3.95E+07
Minoxidil	1290	4.57E-05	2.82E+07
Khellin	5960	1.06E-04	5.63E+07
Zimelidine	3980	4.01E-05	9.93E+07
Azacyclonol	2800	8.34E-05	3.35E+07
Lynestrenol	1690	3.63E-05	4.66E+07
Guanabenz	54.6	1.62E-04	337000
isulfiram	1330	1.29E-04	1.04E+07
Acetylsalicylsalicylic acid	569	1.00E-04	5.68E+06
Amoxapine	1130	5.12E-05	2.20E+07
Cyproheptadine	67.7	1.17E-04	577000
Danazol	1230	1.39E-04	8.85E+06
Pioglitazone	1470	1.54E-04	9.54E+06
Dizocilpine	8470	2.93E-05	2.89E+08
Triamterene	54.5	1.39E-04	391000
Dapsone	61	9.04E-05	675000
Pyrimethamine	218	1.49E-04	1.46E+06
Diflunisal	1360	1.70E-04	8.01E+06
Niclosamide	1500	8.69E-05	1.73E+07
Metolazone	8.61	5.29E-05	163000
Naproxen	337	7.24E-05	4.66E+06
Ticlopidine	1880	6.18E-05	3.05E+07
Dicyclomine	39.3	7.05E-05	558000
Amyleine	1600	2.97E-05	5.38E+07

Amfepramone	102	1.26E-04	813000
Dehydrocholic acid	7120	9.63E-05	7.39E+07
Tioconazole	718	8.26E-05	8.69E+06
Perphenazine	437	1.33E-04	3.30E+06
Isoconazole	4940	9.49E-05	5.20E+07
Spironolactone	37.2	1.65E-04	226000
Dexamethasone	735	1.72E-04	4.26E+06
Carbamazepine	89.2	1.25E-04	717000
Trifluprомazine	134	1.54E-04	869000
Mefenamic acid	3820	1.21E-04	3.15E+07
Acetohexamide	575	1.25E-04	4.62E+06
Chlorpromazine	1100	0.00172	640000
Diphenhydramine	115	0.00172	66900
Miconazole	2.55	0.00175	1460
Isoxsuprine	2680	0.00171	1.57E+06
Tolnaftate	3740	0.00165	2.26E+06
Verapamil	17800	0.00168	1.06E+07
Nicergoline	2170	1.03E-04	2.11E+07
Dihydroergotamine	4450	3.96E-05	1.12E+08
Riluzole	2450	3.12E-05	7.86E+07
Flavoxate	5380	1.63E-05	3.31E+08
Norethindrone	502	1.27E-05	3.96E+07
Nortriptyline	2370	1.00E-04	2.37E+07
Niflumic acid	110	3.79E-06	2.91E+07
Isotretinoin	80.1	2.07E-05	3.87E+06
Antazoline	151	1.92E-05	7.83E+06
Ethacrynic acid	240	1.94E-05	1.24E+07
Praziquantel	1310	2.78E-05	4.70E+07
Levamisole	612	2.41E-05	2.54E+07

Catharanthine	1220	8.34E-06	1.47E+08
Nimesulide	1460	3.38E-06	4.31E+08
Vincamine	432	9.57E-06	4.51E+07
Indomethacin	125	3.80E-05	3.29E+06
Cortisone	574	1.74E-06	3.31E+08
Prednisolone	200	2.06E-05	9.72E+06
Fenofibrate	342	1.63E-05	2.10E+07
Bumetanide	636	5.73E-07	1.11E+09
Labetalol	312	1.90E-05	1.64E+07
Flufenamic acid	1850	4.16E-05	4.44E+07
Tolfenamic acid	1890	3.48E-05	5.44E+07
Perhexiline	317	1.00E-04	3.17E+06
Mebendazole	865	1.11E-04	7.78E+06
Ketoprofen	2690	1.11E-04	2.42E+07
Indapamide	1870	1.05E-05	1.78E+08
Dantrolene	346	9.96E-05	3.47E+06
Trazodone	21.3	1.04E-04	205000
Glafenine	2660	9.63E-05	2.76E+07
Acemetacin	4340	6.29E-05	6.89E+07
Benzydamine	1230	5.78E-05	2.12E+07
Fipexide	87.4	5.08E-05	1.72E+06
Mifepristone	909	7.96E-05	1.14E+07
Diperodon	4290	6.43E-05	6.67E+07
Gestrinone	1360	3.64E-05	3.75E+07
Etomidate	1180	4.11E-05	2.87E+07
Prednicarbate	6460	3.23E-05	2.00E+08
Iopanoic acid	1860	7.24E-06	2.57E+08
Propoxycaine	1870	4.02E-06	4.66E+08
Norgestimate	1890	1.61E-05	1.17E+08

Chlormadinone	2150	8.34E-06	2.58E+08
Fluticasone propionate	107	1.25E-04	860000
Proguanil	71.1	1.13E-04	629000
Lymecycline	379	8.70E-05	4.36E+06
Cyproterone acetate	119	9.52E-05	1.25E+06
(R)-Propranolol	512	9.83E-05	5.20E+06
Ciprofibrate	1180	7.66E-05	1.55E+07
Formestane	230	9.67E-05	2.38E+06
Benzylpenicillin	422	1.18E-04	3.57E+06
Chlorambucil	241	9.21E-05	2.62E+06
Homosalate	266	6.92E-05	3.84E+06
Trapidil	48.3	5.54E-05	872000
Tribenoside	3820	3.35E-05	1.14E+08
Rimexolone	5870	5.90E-05	9.95E+07
Misoprostol	3430	1.31E-05	2.62E+08
Sulfadoxine	6700	3.14E-05	2.13E+08
Perindopril	1670	2.20E-05	7.60E+07
Clonixin Lysinate	1510	3.11E-05	4.85E+07
Rifabutin	2700	2.13E-05	1.26E+08
Parbendazole	2610	1.99E-05	1.31E+08
Halofantrine	2800	2.33E-05	1.20E+08
Articaine	2610	2.01E-05	1.30E+08
Nomegestrol	2410	1.66E-05	1.45E+08
Methyldopate	216	2.17E-06	9.93E+07
Levocabastine	211	2.37E-06	8.94E+07
Pyrvinium pamoate	319	3.80E-06	8.40E+07
Saquinavir	1890	2.01E-05	9.41E+07
Nadifloxacin	1890	1.51E-05	1.25E+08
Buspirone	1880	2.55E-05	7.39E+07

Estradiol Valerate	2610	9.04E-06	2.88E+08
Etodolac	1580	7.84E-06	2.02E+08
Fadrozole	895	7.06E-05	1.27E+07
Dilazep	584	7.23E-05	8.08E+06
Ofloxacin	530	5.47E-05	9.70E+06
Lomefloxacin	405	8.52E-05	4.76E+06
Orphenadrine	1520	6.38E-05	2.39E+07
Melengestrol	30.5	3.98E-05	766000
Bromhexine	478	3.18E-05	1.50E+07
Anethole-trithione	204	4.26E-05	4.77E+06
Amcinonide	142	3.57E-05	3.99E+06
Trifluoperazine	490	3.55E-05	1.38E+07
Cefdinir	836	2.71E-05	3.09E+07
Celecoxib	649	3.07E-05	2.11E+07
Cladribine	2230	2.06E-05	1.08E+08
Hexetidine	2360	2.57E-05	9.21E+07
Pentamidine	2300	2.44E-05	9.43E+07
Gliclazide	1140	1.59E-05	7.19E+07
Prenylamine	2410	2.04E-05	1.18E+08
Dipivefrin	30.4	6.65E-05	457000
Dexfenfluramine	401	1.00E-04	4.00E+06
Clofibrate	3050	8.99E-05	3.39E+07
Aripiprazole	9.35	7.71E-05	121000
Ethinylestradiol	2220	1.92E-05	1.16E+08
Sparfloxacin	15.8	7.98E-05	198000
Tripelennamine	427	1.14E-04	3.75E+06
Reserpine	886	8.34E-05	1.06E+07
Bicalutamide	39	6.19E-05	631000
Telmisartan	383	4.18E-05	9.16E+06

Nalmefene	545	2.95E-05	1.85E+07
Bifonazole	63.9	3.59E-05	1.78E+06
Tyloxapol	348	3.18E-05	1.09E+07
Florfenicol	9.88	3.72E-05	266000
Deoxycorticosterone	1660	1.71E-05	9.76E+07
Urosiol	10400	1.20E-04	8.68E+07
Proparacaine	2560	2.27E-05	1.13E+08
Gatifloxacin	2760	2.25E-05	1.23E+08
Bosentan	2490	1.60E-05	1.56E+08
Olmesartan	2420	1.73E-05	1.40E+08
Montelukast	2210	7.73E-06	2.86E+08
Alfuzosin	2780	2.07E-05	1.34E+08
Chlorpropamide	2720	1.97E-05	1.38E+08
Cefoperazone	357	6.94E-05	5.14E+06
Tacrine	1480	4.45E-05	3.33E+07
Testosterone	3590	3.86E-05	9.31E+07
Haloprogin	114	8.15E-05	1.39E+06
Thyroxine (L)	119	7.43E-05	1.60E+06
Idebenone	2720	8.15E-05	3.34E+07
Pepstatin A	5050	3.92E-05	1.29E+08
Butoconazole	2100	8.35E-05	2.52E+07
Chlormezanone	301	7.29E-05	4.14E+06
Androsterone	232	5.44E-05	4.26E+06
Erlotinib	3920	5.80E-05	6.76E+07
Furosemide	298	2.64E-05	1.13E+07
Methapyrilene	2060	7.21E-05	2.86E+07
Desipramine	395	6.32E-05	6.25E+06
Clorgyline	4990	1.06E-04	4.71E+07
Thioguanosine	2270	2.61E-05	8.70E+07

Chlorprothixene	1460	7.78E-05	1.88E+07
Clozapine	41.9	2.66E-05	1.57E+06
Zotepine	7.12	2.66E-05	268000
Cisapride	3450	5.22E-06	6.60E+08
Pemirolast	395	2.74E-05	1.44E+07
Droperidol	256	2.86E-05	8.96E+06
Pefloxacine	701	2.36E-05	2.97E+07
Corticosterone	753	2.39E-05	3.15E+07
Cefadroxil	725	3.38E-05	2.14E+07
Digoxin	1090	2.68E-05	4.08E+07
Doxorubicin	933	2.94E-05	3.17E+07
Epiandrosterone	962	2.90E-05	3.32E+07
Betamethasone	844	3.20E-05	2.64E+07
Colchicine	1170	2.59E-05	4.50E+07
Metergoline	173	1.42E-05	1.21E+07
Brinzolamide	239	1.45E-05	1.65E+07
Ambroxol	95.5	1.27E-05	7.52E+06
Benfluorex	520	1.49E-05	3.50E+07
Cyclobenzaprine	3850	2.97E-06	1.30E+09
Ketotifen	249	3.20E-05	7.80E+06
Amethopterin (R,S)	738	2.29E-05	3.22E+07
Methiothepin	532	2.78E-05	1.91E+07
Clofazimine	906	2.06E-05	4.40E+07
Nafronyl	702	2.39E-05	2.94E+07
Bezafibrate	5220	0.0767	68000
Nefazodone	20700	0.0721	287000
Clebopride	18900	0.0538	351000
Stanozolol	15500	0.0546	284000
Calcipotriene	18200	0.0472	386000

Meclocycline sulfosalicylate	182000	0.0757	2.41E+06
Meclozine	463000	0.0802	5.77E+06
Butalbital	181000	0.0496	3.65E+06
Lidoflazine	168000	0.0686	2.45E+06
Betaxolol	138000	0.0546	2.53E+06
Nicardipine	39600	0.0551	718000
Fusidic acid	14500	5.62E-05	2.58E+08
Indatraline	1210	1.31E-04	9.22E+06
Ketanserin	1010	7.71E-05	1.31E+07
Etoposide	65800	0.0612	1.07E+06
Clomiphene citrate (Z,E)	70300	0.0704	998000
Prochlorperazine	46800	0.0699	669000
Hesperidin	213000	0.0787	2.71E+06
Vatalanib	124000	0.0791	1.57E+06
Cefotetan	936	6.94E-05	1.35E+07
Fentiazac	4330	7.69E-05	5.63E+07
Brompheniramine	23.6	4.80E-05	492000
Primaquine	1790	4.76E-05	3.76E+07
Progesterone	220	6.50E-05	3.38E+06
Felodipine	94.1	6.94E-05	1.36E+06
Raclopride	267000	0.0743	3.60E+06
Benperidol	229000	0.0701	3.26E+06
Cefaclor	359000	0.0692	5.19E+06
Pyridostigmine	497	3.37E-05	1.48E+07
Pentobarbital	1140	2.52E-05	4.54E+07
Metixene	537	2.57E-05	2.09E+07
Nitrofural	268	2.85E-05	9.38E+06
Omeprazole	14.6	3.16E-05	462000
Terconazole	571	2.55E-05	2.24E+07

Tiaprofenic acid	172	2.93E-05	5.89E+06
Vancomycin	242	2.87E-05	8.44E+06
Propafenone	621	8.44E-05	7.36E+06
Tetracaine	2040	2.56E-05	7.98E+07
Mometasone furoate	58.2	5.45E-05	1.07E+06
Troglitazone	4340	4.39E-05	9.90E+07
Ropinirole	1000	6.78E-06	1.47E+08
Argatroban	1000	3.39E-06	2.95E+08
Acenocoumarol	1820	3.36E-05	5.41E+07
Bromperidol	1840	3.53E-05	5.20E+07
Reboxetine	1820	2.92E-05	6.25E+07
Camylofine	1830	3.42E-05	5.34E+07
Papaverine	1820	3.13E-05	5.79E+07
Yohimbine	1690	3.49E-05	4.84E+07
Voriconazole	1840	3.22E-05	5.72E+07
Alfacalcidol	1790	3.15E-05	5.67E+07
Cilostazol	1740	3.35E-05	5.20E+07
Azelastine	1680	3.76E-05	4.47E+07
Etretinate	1750	3.52E-05	4.98E+07
Fluoxetine	1660	3.20E-05	5.18E+07
Norcyclobenzaprine	449	4.34E-05	1.04E+07
Lovastatin	159	7.49E-05	2.13E+06
Budesonide	2750	2.55E-05	1.08E+08
Zaleplon	5440	6.72E-06	8.09E+08
Diclofenac	1210	1.82E-05	6.62E+07
Exemestane	2650	7.70E-07	3.44E+09
Xylazine	5250	4.96E-05	1.06E+08
Celiprolol	5340	3.18E-05	1.68E+08
Zopiclone	6130	5.09E-05	1.21E+08

Lofexidine	4000	9.12E-05	4.39E+07
Zafirlukast	733	9.52E-05	7.70E+06
Rimantadine	91.9	1.08E-04	854000
Ipsapirone	260	3.11E-05	8.37E+06
Hydroxychloroquine	303	3.10E-05	9.79E+06
Thiocolchicoside	1800	9.15E-06	1.97E+08
Clorsulon	2670	9.46E-06	2.82E+08
Diosmin	500	7.97E-05	6.27E+06
Diflorasone	609	5.62E-05	1.08E+07
Ciclopirox ethanolamine	1570	7.21E-05	2.17E+07
Tetramisole	45.9	0.0624	736
Chloroquine	7330	0.0364	201000
Mizolastine	981	9.22E-06	1.06E+08
Amisulpride	949	1.02E-05	9.30E+07
Althiazide	943	1.46E-05	6.46E+07
6-Furfurylaminopurine	980	2.75E-05	3.57E+07
Flumethasone	741	2.21E-05	3.36E+07
Loratadine	623	8.25E-05	7.55E+06
Nisoldipine	1970	5.45E-05	3.61E+07
Zonisamide	2440	6.15E-05	3.96E+07
Irsogladine	562	1.02E-04	5.49E+06
Sulfamethizole	395	7.18E-05	5.50E+06
Medrysone	2780	1.22E-04	2.27E+07
Monensin	3100	3.72E-05	8.35E+07
Dydrogesterone	4370	3.63E-05	1.20E+08
Opipramol di	9940	1.48E-05	6.74E+08
Pranoprofen	1080	2.11E-05	5.09E+07
Estropipate	2320	8.73E-06	2.66E+08
Irinotecan	3150	7.54E-05	4.18E+07

Furaltadone	2330	1.21E-06	1.92E+09
Ethoxyquin	51.4	1.36E-04	378000
Alclometasone	1910	3.86E-05	4.96E+07
Norgestrel-(-)-D	2700	2.26E-05	1.20E+08
Fluocinonide	3160	1.61E-05	1.97E+08
Alexidine di	1470	2.38E-05	6.16E+07
Proadifen	1010	9.53E-05	1.06E+07
Trihexyphenidyl-D,L	322	1.24E-04	2.59E+06
Succinylsulfathiazole	336	1.12E-04	3.00E+06
Famprofazone	702	9.69E-05	7.25E+06
Bromopride	131	1.32E-04	993000
Chlorcyclizine	1400	1.59E-04	8.77E+06
Diphenylpyraline	1600	1.03E-04	1.55E+07
Sulfachloropyridazine	245	9.73E-05	2.52E+06
Cefuroxime	1070	1.70E-05	6.26E+07
Dienestrol	1130	7.14E-05	1.58E+07
Digoxigenin	140	2.67E-05	5.25E+06
Clioquinol	241	3.31E-05	7.28E+06
Bucladesine	2680	2.04E-05	1.31E+08
Suprofen	2050	1.04E-05	1.97E+08
Deflazacort	1160	6.57E-05	1.77E+07
Benzthiazide	310	4.10E-06	7.56E+07
S-(+)-ibuprofen	30.4	4.18E-05	728000
Cefoxitin	420	3.47E-05	1.21E+07
Carbenoxolone	2350	5.45E-06	4.31E+08
Iocetamic acid	2350	1.12E-05	2.10E+08
Nitrendipine	303	8.54E-05	3.55E+06
Trimeprazine	188	5.44E-05	3.45E+06

Rolipram	1580	2.30E-05	6.85E+07
Idazoxan	1140	1.38E-05	8.23E+07
Quinapril	3300	1.80E-05	1.83E+08
Ketorolac tromethamine	315	9.53E-05	3.31E+06
Nylidrin	1670	3.93E-05	4.25E+07
Doxazosin	2090	1.13E-05	1.85E+08
S(-)Eticlopride	3260	1.80E-05	1.81E+08
Baclofen	302	6.49E-05	4.65E+06
Pindolol	2480	1.41E-04	1.75E+07
Hydroflumethiazide	3080	1.45E-04	2.13E+07
Sulfathiazole	4.11	1.73E-04	23700
Idoxuridine	3390	1.47E-05	2.30E+08
Captopril	809	1.96E-05	4.12E+07
Antipyrine, 4-hydroxy	676	4.82E-05	1.40E+07
Famotidine	899	8.93E-05	1.01E+07
Nomifensine	927	1.72E-04	5.40E+06
Chloramphenicol	3310	1.23E-04	2.68E+07
Naloxone	3620	2.48E-05	1.46E+08
Lidocaine	2260	1.31E-04	1.73E+07
Pirenzepine	132	1.02E-04	1.29E+06
Minaprine	2930	0.00178	1.65E+06
Acebutolol	5130	0.00183	2.81E+06
Dipyridamole	1780	0.00151	1.18E+06
Dihydrostreptomycin	390	4.18E-05	9.33E+06
Pentylenetetrazole	2280	2.30E-05	9.89E+07
Chlorzoxazone	2600	3.47E-05	7.49E+07
Ornidazole	2290	2.45E-05	9.32E+07
Hydralazine	2390	2.85E-05	8.41E+07

Mexiletine	5200	9.21E-05	5.64E+07
Glutethimide, para-amino	2750	1.47E-05	1.87E+08
Prilocaine	434	2.92E-06	1.49E+08
Camptothecine (S,+)	89.6	7.87E-06	1.14E+07
Mefexamide	1700	5.32E-05	3.19E+07
Tiapride	4890	7.97E-05	6.13E+07
Pramipexole	2360	2.73E-06	8.64E+08
Deptropine	1110	7.57E-05	1.46E+07
Moxonidine	1910	6.49E-05	2.94E+07
Ranolazine	1060	1.41E-05	7.52E+07
Cyclopentolate	1390	7.38E-05	1.88E+07
Meropenem	1650	2.03E-05	8.14E+07
Ramipril	2750	2.24E-05	1.23E+08
Mephenytoin	2740	2.21E-05	1.24E+08
Molindone	2780	2.35E-05	1.19E+08
Mecamylamine	96.3	1.94E-06	4.95E+07
Mepivacaine	3190	9.82E-06	3.25E+08
Hyoscyamine (L)	371	5.67E-05	6.54E+06
Proglumide	188	7.25E-05	2.59E+06
Mirtazapine	2310	2.63E-05	8.79E+07
Tulobuterol	266	6.29E-05	4.22E+06
Iopamidol	214	4.81E-05	4.46E+06
Theobromine	3420	4.57E-05	7.47E+07
Modafinil	2490	7.48E-05	3.34E+07
Lamivudine	1340	5.42E-05	2.48E+07
Ritodrine	236	2.54E-05	9.31E+06
Carisoprodol	449	3.05E-05	1.47E+07
Debrisoquin	579	2.68E-05	2.16E+07
Melatonin	183000	0.061	3.01E+06

Oxantel	81300	0.0541	1.50E+06
Itopride	154000	0.0874	1.77E+06
Atropine	587	4.98E-05	1.18E+07
Eserine hemisulfate	639	3.14E-05	2.04E+07
Cetirizine	1790	3.16E-05	5.66E+07
Cyclizine	1810	4.26E-05	4.24E+07
Fomepizole	2880	4.67E-06	6.18E+08
Phenacetin	329	3.00E-05	1.10E+07
Parthenolide	20700	0.0411	504000
Isopyrin	2040	1.01E-05	2.03E+08
Sulfamethoxypyridazine	1560	1.49E-05	1.04E+08
Deferoxamine	1330	5.89E-05	2.26E+07
Spiramycin	813	1.07E-04	7.58E+06
Tramadol	238	6.78E-05	3.51E+06
Eucatropine	1670	9.66E-06	1.73E+08
Nadolol	1250	8.19E-05	1.52E+07
Moxalactam	6.68	1.02E-04	65500
Tetrahydroxy-1,4-quinone	3100	1.69E-05	1.83E+08
Allantoin	2040	1.06E-05	1.94E+08
Sulfacetamide sodic hydrate	1530	1.59E-04	9.60E+06
Antipyrine	88	5.07E-05	1.74E+06
Trichlorfon	346	1.34E-04	2.58E+06
Ethosuximide	2280	2.30E-05	9.92E+07
Mafenide	2450	2.95E-05	8.31E+07
Ampyrone	1290	2.71E-05	4.77E+07
Methocarbamol	19.1	1.97E-05	971000
Dimaprit di	1700	1.44E-05	1.18E+08
Alcuronium	2420	1.66E-05	1.46E+08
Zalcitabine	77.6	2.11E-06	3.67E+07

Acetylcysteine	181	7.59E-05	2.39E+06
Caffeine	72.1	3.43E-05	2.10E+06
5-fluorouracil	503	2.03E-05	2.48E+07
(R)-(+)-Atenolol	724	2.68E-05	2.71E+07
Gemcitabine	3210	1.78E-05	1.80E+08
Phenylpropanolamine	635	8.22E-05	7.72E+06
Carbimazole	996	2.91E-05	3.42E+07
Carteolol	1900	7.55E-06	2.51E+08
Alizapride	14700	0.0702	210000
Terbutaline	76.2	6.94E-05	1.10E+06
Serotonin	1.05E+06	0.252	4.17E+06
Acarbose	455	2.72E-05	1.67E+07
Iohexol	1750	3.35E-05	5.22E+07
Trimethadione	302	8.96E-05	3.37E+06
Benfotiamine	189	1.27E-04	1.49E+06
Metoprolol-(+,-)	1520	2.31E-05	6.57E+07
Penicillamine	3900	8.29E-05	4.71E+07
Acefylline	1290	7.82E-05	1.64E+07
Secnidazole	1260	7.15E-05	1.76E+07
Pempidine	1140	7.52E-05	1.51E+07
Clodronate	292	1.22E-04	2.39E+06
Guaifenesin	3420	1.19E-05	2.88E+08
Dipyrone	1870	7.36E-06	2.54E+08
Aminophylline	1500	1.62E-04	9.21E+06
Aminohippuric acid	4380	1.02E-04	4.29E+07
N-Acetyl-L-leucine	2760	2.19E-07	1.26E+10
Xamoterol	15100	4.29E-05	3.51E+08
Thonzonium	2530	1.08E-05	2.34E+08
Diprophylline	89.5	1.33E-04	672000

Isoniazid	2390	2.71E-05	8.84E+07
Dropropizine (R,S)	2600	1.78E-05	1.46E+08
Metaraminol	1050	2.09E-06	5.04E+08
Ethamsylate	323	4.85E-05	6.64E+06
Spaglumic acid	361	4.91E-05	7.35E+06
(-)-Isoproterenol	3900	1.86E-05	2.10E+08
Dirithromycin	5890	4.31E-05	1.37E+08
Iopromide	1370	8.36E-05	1.64E+07
Theophylline	273	6.03E-05	4.52E+06
Racepinephrine	2180	7.24E-06	3.01E+08
Ascorbic acid	1100	8.14E-05	1.36E+07
Methyldopa (L,-)	1020	2.61E-05	3.91E+07
Cyclosporin A	1080	2.75E-05	3.94E+07
Bambuterol	1060	2.80E-05	3.79E+07
Kanamycin A	181000	0.072	2.51E+06
Amikacin	48200	0.0692	696000
Galanthamine	1750	3.72E-05	4.70E+07
Carbidopa	1040	6.15E-05	1.69E+07
Acipimox	915	6.81E-05	1.34E+07
Trimetazidine	32.9	0.0596	552
Tetraethylenepentamine penta	2710	4.75E-05	5.72E+07
Mevalonic-D, L acid lactone	1150	1.80E-05	6.38E+07
Ribostamycin	120	5.43E-05	2.20E+06
Thimerosal	1490	5.13E-05	2.91E+07
Amiprilose	1730	5.59E-05	3.09E+07
Thioperamide	3080	1.32E-05	2.34E+08
Flucytosine	275	1.38E-04	1.99E+06